Summer 2016

Structural analysis and fluid flow modeling of the Kapuni Field, New Zealand

Jarret Taylor Baldwin

Department:

STRUCTURAL ANALYSIS AND FLUID FLOW MODELING OF THE KAPUNI FIELD, NEW ZEALAND

By

JARRET TAYLOR BALDWIN

A THESIS

Presented to the Faculty of the Graduate School of the

MISSOURI UNIVERSITY OF SCIENCE AND TECHNOLOGY

In Partial Fulfillment of the Requirements for the Degree

MASTER OF SCIENCE IN GEOPHYSICS

2016

Approved by

Dr. Kelly Liu, Advisor
Dr. Stephen Gao
Dr. Neil Anderson

ABSTRACT

The Taranaki Basin is the largest hydrocarbon producing basin in New Zealand. A total area of over 330,000 km^2, the basin contains numerous oil and gas fields, but only a select few are accessible on-shore plays. One such gas field is the one of the largest (some 25 km^2) and oldest gas field discovered in New Zealand, the Kapuni gas/gas condensate field. Located in the Taranaki peninsula, this on-shore, deep anticline has been conventionally drilled since 1959 due to the successive terrestrial and marginal marine cycles of the Kapuni Group sediments which allow for multiple high porosity reservoirs. A large 350 km^2 3D survey of the Kapuni Field allows for a detailed structural interpretation of the petroleum system. Multiple faults, horizons, and a gas chimney were identified and tracked to produce a structural interpretation as well as a fluid flow model. Faults and horizons were identified based on the visible displacement of reflected and continuous layers within each vertical and horizontal seismic section. Through investigation and manipulation of the seismic data, a gas chimney structure was discovered which incorporated several interpreted faults and horizons. This structure proved a prominent candidate for fluid migration tracking. Through use of the structural interpretation and resulting digital elevation models, a complete and accurate fluid flow model was constructed which utilizes GIS based hydrogeologic software. The result is the construction of a baseline empirical layer which easily accommodates corrections and is readily exportable to almost any software platform.

ACKNOWLEDGEMENTS

This thesis was possible due to the combine efforts of the Geology and Geophysics program as well as the many esteemed advisors and colleagues who provided their wisdom, support, and friendship. I would like to express my gratitude to Aamer Alhakeem for his knowledge and support which was greatly appreciated during the processing of the data. I would also like to extend my sincere gratitude to Dr. Kelly Liu, my advisor, who provided continued support throughout my research and classes here at Missouri University of Science and Technology. Additionally I divulge my pedestalled appreciation and respect to my committee members Dr. Stephen Gao and Dr. Neil Anderson who provided precise advice and patience which led to the creation of a complete and profound thesis.

TABLE OF CONTENTS

LIST OF ILLUSTRATIONS

LIST OF TABLES

1. INTRODUCTION

1.1. AREA OF STUDY

Distribution of hydrocarbons within the Taranaki Basin of New Zealand is commonly correlated to tectonic activities which dominate the evolution of its petroleum systems. The basin stretches across the western coast of New Zealand's northern island and spans an area of over 330,000 km^2 (Reilly et al., 2015; NZ Petroleum & Minerals, 2014; Higgs et al., 2013; King & Thrasher, 1996). The region is divided by an east-west tectonic division and a north-south fault distinction. The southern region has become the focus of increasingly extensive research in recent years as the offshore reservoir potential has peaked great interest due to prime lithology and structural trap dissemination (Figure 1.1). Initial estimates of hydrocarbon production of the basin suggested over 332 million barrels of oil and more than 5.2 trillion cubic feet of gas (King & Thrasher, 1996; NZ Petroleum & Minerals, 2014). However, this 1970's estimate only considered a portion of the basin as well as exclusion of unconventional extraction methods. Since 2003, eight new gas/oil fields have been discovered within the basin, increasing the total production of the Taranaki Basin to 418 MMbbl of oil and 6.19 tcf of gas by December of 2011 (New Zealand Petroleum & Minerals, 2014).

The Taranaki Basin as a whole is incredibly complex, which has prompted many 2-D and 3-D seismic surveys with accompanied exploration wells. Figures 1.1 and 1.2 display the modern Taranaki Basin along with the active regional scale tectonics and recent exploration endeavors. The southern region of the Taranaki Basin, which is the more studied region, currently contains the majority of exploration wells (over 262) and 12 regional 2-D seismic surveys (see Figure 1.2) (Strogen et al., 2013; Reilly et al.,

2015). Including the northern Graben of the Taranaki Basin, over 500 exploration and production wells have been drilled as of 2015 (New Zealand P&M, 2014; Reilly et al., 2015).

One of the largest gas/gas condensate fields, and the focus of this study, is the Kapuni Field and anticline in the northernmost tip of the Manaia Fault. The Kapuni Field was first discovered in 1959 by Shell BP Todd (which today is Shell Todd Oil Services Limited) and started producing gas and gas condensate by 1969. Though it is the oldest gas producing field in New Zealand, it is the second largest in size at approximately 25 km^2 (stos…c2015). The Kapuni Field has been imaged within several 2D seismic lines since the 1970's, but a 350 km^2 3D survey was conducted in 1989 (see Fig. 1.1) (Voggenreiter, 1993). STOS owns and currently operates 18 wells within the field and to date has generated over 64.4 mmbbls of liquid hydrocarbons and 1238.5 Bcf of gas (stos…c2015; toddenergy…c2012). The 3D seismic survey reveals the anticlinal structure of the Kapuni play which, in tandem with well reports, has revealed to be an exceptional prospect over the last 55 years and continues to provide interest. Despite this, challenges induced by the tectonic regime and petrology of the system have reduced the economic feasibility of unconventional and deeper conventional extraction for this petroleum system.

1.2. PREVIOUS STUDIES

The Taranaki Basin has received a great deal of attention and study since the first hydrocarbon discoveries in the 1950's. The structural evolution, tectonics, and geologic influence of the area have been previously discussed and researched by Schmidt &

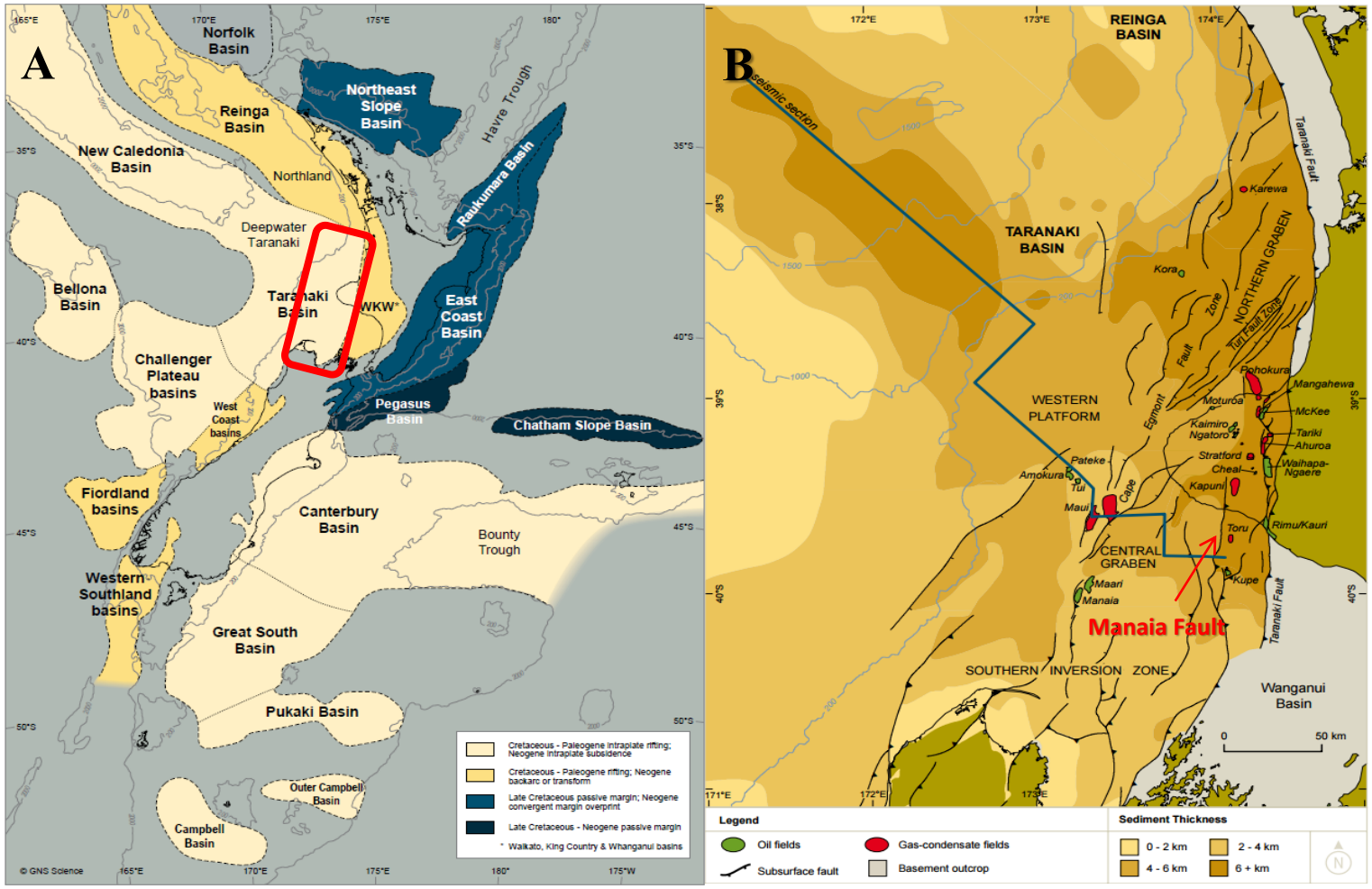

Figure 1.1. Map of the study area and surrounding New Zealand. (A) the whole of New Zealand along with all known basins surrounding the country. The red highlighted area indicates the zoomed in area in map (B). (B) the major faults and tectonic regimes. The red highlight box outlines the 3D Kapuni Survey location. Modified from NZ Petroleum & Minerals (2014).

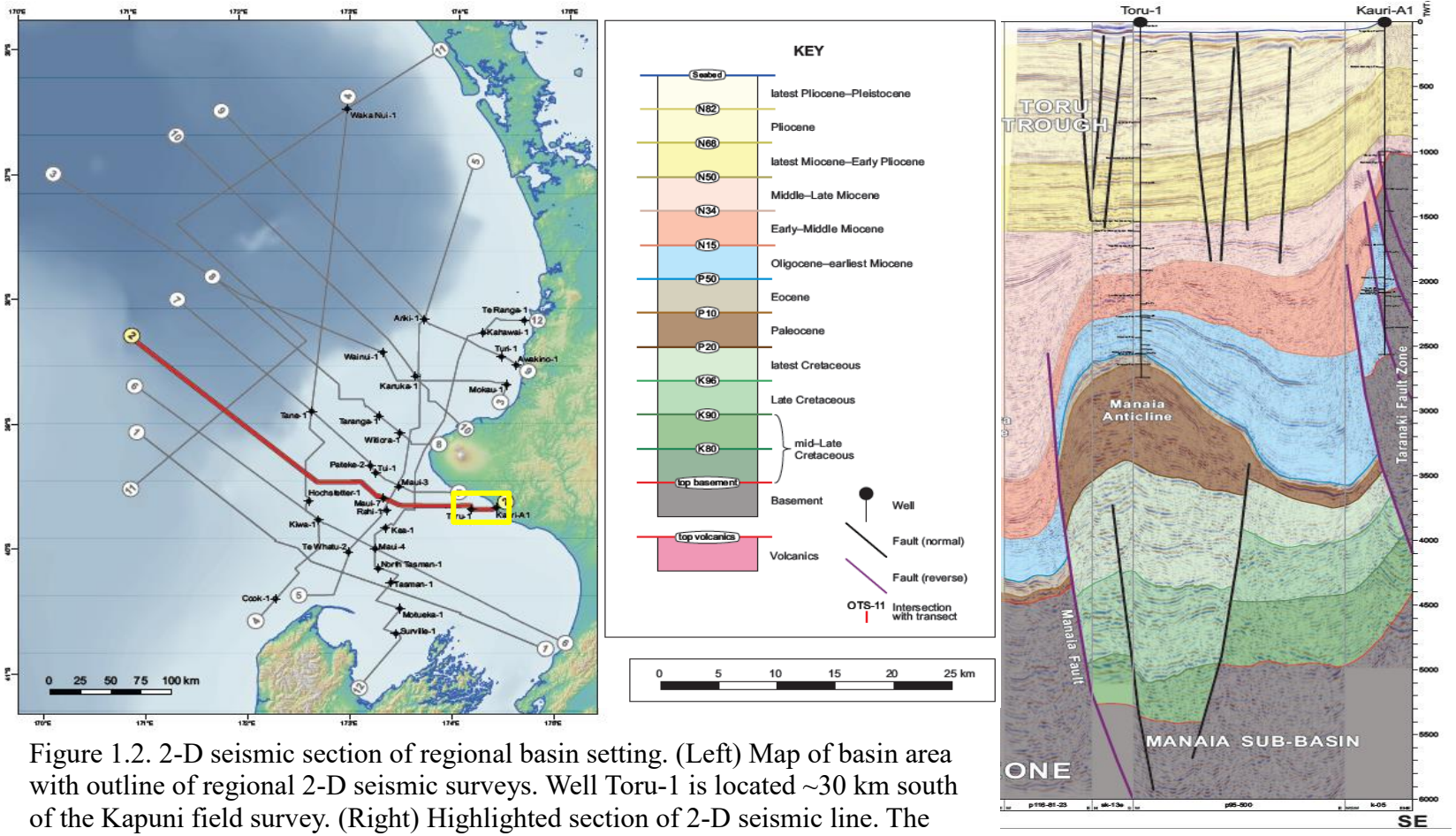

Figure 1.2. 2-D seismic section of regional basin setting. (Left) Map of basin area with outline of regional 2-D seismic surveys. Well Toru-1 is located ~30 km south of the Kapuni field survey. (Right) Highlighted section of 2-D seismic line. The seismic character below Toru-1 is representative of the general setting of the 3-D Kapuni survey. The thickness of late Miocene to latest Pleistocene deposits display a northward shallowing trend from Toru-1 to the 3D-Kapuni survey. This image is modified from Strogen & Bland et al. , 2014.

Robinson (1990), Muir et al. (2000), Reilly et al. (2015), Higgs et al. (2007), and King & Thrasher (1996). This extensive and continuing research has resulted in a well-defined off and on-shore geologic, tectonostratigraphic, and structural evolution.

The majority of current hydrocarbon exploration for the Taranaki Basin is concentrated on offshore and deep marine surveys. Many recent studies such as Johnston et al. (1991), Smale et al. (1999), Higg et al. (2007), and Bache et al. (2014) have been conducted to track the Kapuni group sediments. In addition to these studies, a recent initiative named 4D Taranaki conducted by GNS Science in New Zealand aims to fully map and understand the Taranaki and surrounding basins while giving immediate access of consolidated data to the petroleum industry (Fohrmann, 2012). In spite of this plethora of information regarding the Taranaki Basin, comparatively few studies such as Voggenreiter (1993), Hulston et al. (2001), and Higgs et al. (2013) have been conducted over the structure and petroleum geology of the Kapuni Field specifically.

1.3. OBJECTIVE

The objective of this study is to identify and analyze various faults within the northern half of the 3D Kapuni Field, as well as track fluid flow within the system as it flows from source to reservoir.

This study examines a graben formed within the Mangatoki fault zone of the Kapuni Field and debates the existence of a detachment surface. The identification and analysis of the faults is conducted using both Kingdom and Petrel software. Petrel is used for generating volume and surface attributes which aid in the identification of structures, hydrocarbons, and stratigraphic anomalies. The Kingdom software acts as the base software for the study as it provides better format conversion widgets, user friendly

fault picking and delineation, and preferred project organization. The fluid flow modeling utilizes RiverTools (a GIS based hydrologic software used by the USGS and other companies/agencies with hydrogeological interests) as opposed to an “in house” modeling software provided through seismic interpretation software such as Petrel and Kingdom. In using this study’s method and formats of calculation, it may be possible to easily add additional variables to fluid flow models and generate products which can be easily reformatted for use in the ever expanding GIS environment. This can be useful to petroleum extraction companies as it allows for layered, GIS formatted, scientific data to be compiled together in other software (such as ArcGIS) which are often used for land management by companies and governments alike.

2. REGIONAL GEOLOGY & TECTONICS

2.1. BASIN BACKGROUND AND EVOLUTION

The Taranaki and other large regional scale basins surrounding the New Zealand islands are accumulated in a submerged mini-continent commonly designated "Zealandia". Recent studies of Zealandia have suggested that 90% of the landmass was submerged around the Late Oligocene to Early Miocene, after the majority of the Taranaki Basin's deposition. This sinking of Zealandia could potentially be attributed to the rise of the New Zealand land mass during convergence of the Australian-Pacific plate boundaries in the early Cenozoic (Strogen et al., 2014; Reilly et al., 2015; Nicol et al., 2007; Wallace et al., 2007). The convergent tectonics gave rise to the back-are regime seen within the region today (Figures 2.1 and 2.2).

The entire Taranaki Basin overlays continental crust ("basement" in Figure 2.1), with westernmost portions of the basin sitting atop remnants of the Gondwana craton and the eastern edge of the basement being bordered by accreted terrane formed during the Late Paleozoic to Cretaceous. According to King and Thrasher (1996), the Taranaki Basin is divided into a passive margin called the "Western Stable Platform", and the active margin named the "Eastern Mobile Belt" (Figure 1.1). The segregation of the Taranaki Basin and its tectonic history can be broken into three major periods of development.

2.1.1. Early Period. The first period occurred in the latter of the Cretaceous and early Paleocene around 80 Ma. This period is associated with the extensional tectonics of Gondwana's rifting which resulted in the growth of the Tasman Sea, syn-rift

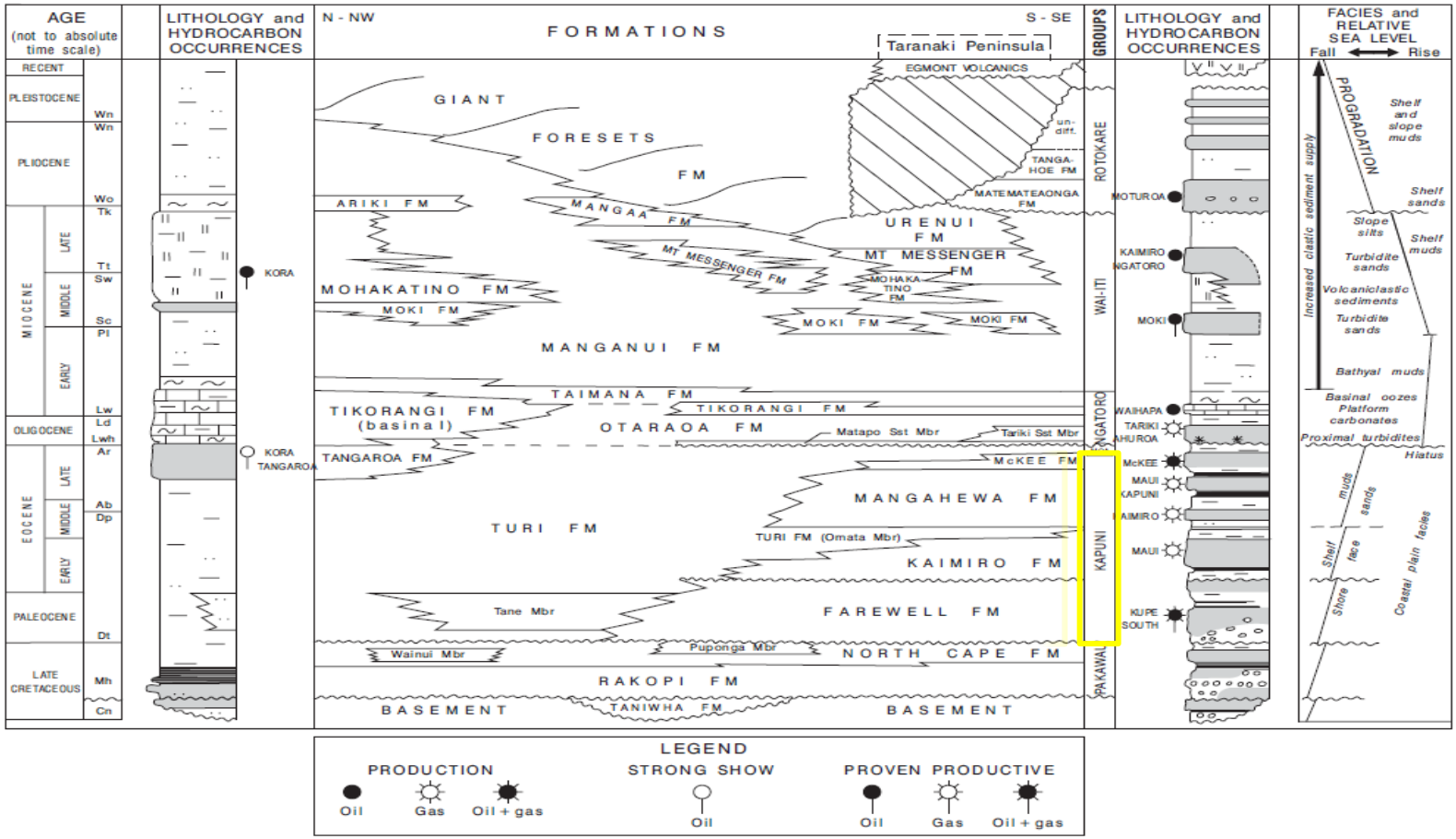

Figure 2.1. General stratigraphic layout of the greater Taranaki Basin. The basin's complex tectonic history has resulted in inconsistent layering and unconformities. Within the Kapuni group, formations such as the Farewell (a popular hydrocarbon target) can have a thickness ranging from 500-750 m. Note that most of the Kapuni group formations contain some amounts of coal deposits, which are believed to be the main source for gas and gas condensate found in many on-land wells and the Kapuni Field (Modified from King & Thrasher, 1996.

spreading of the New Caledonia basin, and initial Taranaki Basin deposition on the pacific plate.The deposition of strata occurred mainly within *en echelon*, half graben, sub-basins which contain accumulated deposits up to 4 km thick (King & Thrasher, 1996; Reilly et al., 2015; Strogen et al., 2014).

2.1.2. Middle Period. The second period of Taranaki Basin's evolution concerns its passive margin phase and extensive deposition. During the Eocene to early Oligocene, the area's tectonic stability and subsidence allowed for multiple transgressive and regressive cycles to occur, resulting in the deposition of many modern hydrocarbon targets. During the early Oligocene, the basin began to transition from quiescence to an active margin due to the collision of the Pacific and Australian plates and residual thrusting of the Taranaki fault (Reilly et al., 2015; King & Thrasher, 1996). This passive to active transition during the Oligocene generated an unconformity between the second and third period deposits which defines the start of the active convergent margin (King & Thrasher, 1996). This unconformity is defined in Figure 2.1.

2.1.3 Late-Current Period. The third period of evolution involves the formation and continuation of the contemporary tectonic regime of active margin uplift and back-arc volcanism. These Cenozoic sub-basin tectonics split the Taranaki Basin into the Eastern Mobile Belt, in which most hydrocarbon plays have been discovered, and the Western Stable Platform. This large multi-fault boundary is known to have started in the early Cenozoic and accompanies specific deformation restricted to the southern half (aka, Southern Inversion Zone) of the basin (King & Thrasher, 1996). The earliest record of uplift is found in the Manaia anticline and Kapuni Field which coincides with the Oligocene paraconformity (Figures 1.2 & 2.1). This event dates the end of the

southern region's peneplanation and the start of residual Alpine transpressional effects. The majority of tectonic activity which currently shapes the region however, is believed to have occurred during the Miocene when the Taranaki Fault began thrusting westward (King & Thrasher, 1992; King & Thrasher, 1996; Reilly et al., 2015; Strogen et al., 2014).

Once sufficient subduction of the pacific plate had occurred in the late Miocene, a series of submarine stratovolcanoes in the northeast of the basin erupted, starting the back-arc volcanism seen in the area today. These first volcanoes, called the Mohakatino volcanics, are only located in the northern half (Northern Graben) of the Taranaki Basin. Mohakatino volcanoes experienced extrusive volcanism for approximately 6 million years until ceasing activity around 8 Ma (King & Thrasher, 1996). Indirect evidence suggested by King and Thrasher (1992) and Adams and Ware (1977) infers a brief halt to active volcanism in the area until the Plio-Pleistocene, when modern back-arc volcanoes such as Mount Taranaki/Egmont began to form as shown in Figure 2.1.

2.2. THE MANAIA FAULT

Directly south east of the andesitic Pleistocene extrusives lays one of several active reverse faults, the Manaia Fault (Figures 1.1 & 2.4). The Manaia Fault has been imaged as far north as the 3D Kapuni Field and expires at the northernmost edge of the Kapuni anticline, where the fault alters from a north-south to a northeasterly trend. It has been observed to have a high angle dip with an easterly strike and displacement of approximately 900 m at its northernmost edge (Voggenreiter, 1993). Due in part to the extensive antiform folding throughout the hanging wall of the Manaia Fault, the system is often referred to as the Manaia anticline. The hanging wall of the fault, due to its

antiform nature, has become a prime target for hydrocarbon exploration and contains several active gas and gas-condensate fields (NZ Petroleum & Minerals, 2014).

The Manaia Fault originated in the Cretaceous to early Eocene as a normal fault which acted as a control to subsidence during the basin's transitional passive/active margin phase. The fault was inverted during the start of Alpine and Taranaki transpression and continues to be one of several compressional regimes within the Southern Inversion Zone (Voggenreiter, 1993; King & Thrasher, 1996; Pilaar & Wakefield, 1978). Through extensive mapping over time, it has been postulated that the Manaia Fault is actually the northernmost extension of the major Waimea Fault, and that this northern segment acts as a major terrane boundary where sediment thickness and seismic event incidence is distinct on the eastern and western sectors (Johnstone, 1996; King & Thrasher, 1996; NZ Petroleum & Minerals, 2014).

- **Kapuni Field.** The largest of the Manaia's hydrocarbon plays, and the focus of this study, is the Kapuni Field/anticline in the northernmost tip of the Manaia Fault (NZ Petroleum & Minerals, 2014; Voggenreiter, 1993). Most of the structural aspects of the Kapuni Field have been observed by Voggenreiter (1993), who described a layered system which provided the capability for both a compressional and extensional regime. A detachment surface was proposed for the Mangatoki Fault zone and graben which has apparent evidence within the seismic data, but no evidence in the well logs. This detachment surface which lies on the top of section B (Figure 2.4), cannot be proven due to lack of well log coverage and an inability to properly enhance the poor seismic character of unit B (Voggenreiter, 1993).

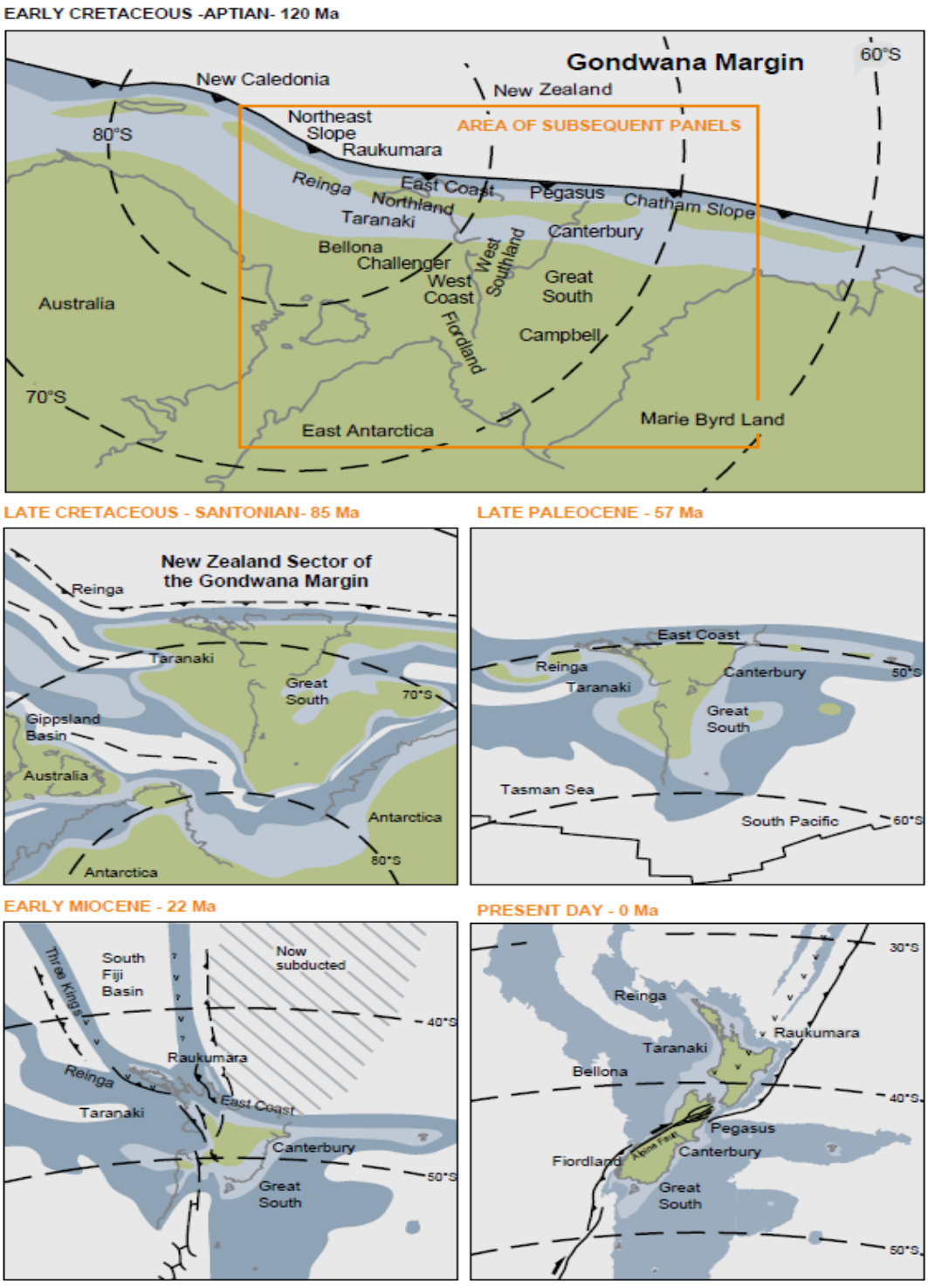

Figure 2.2. Stages of Taranaki Basin development. Large dashed circular lines represent various latitudes. Green coloration represents areas which were/are considered land while blue represents water and/or submerged continent. (Modified from NZ Petroleum & Minerals, 2014).

This proposed detachment along the mid-Miocene Moki Formation may exist as not a single detachment surface, but as a buffer zone for the extensional regime above, which could be overcome by transtentional forces, fluid inundation, and overpressure, leading to normal/oblique faulting.

Below the complexity of seismic section B lies the main source for petroleum in the system, the Kapuni Group (section C, Figures 2.3). These hydrocarbon rich formations have suffered great tectonic stresses since their deposition, and as a result are inundated with a complex system of faults which show both normal and reverse sense of evolution (Voggenreiter, 1993). Figure 2.4 displays some of these faults in cross section, but it does not cover all of the faults as many are undetectable due to poor character, resolution, and that some faults are discontinuous. It is likely that due the age of this lithology, these faults are a part of an ancient extensional fault complex and were consequently reactivated as reverse faults during marginal transition.

2.3. STRATIGRAPHY

The Taranaki Basin contains a famous section of stratigraphic column which has provided a great deal of hydrocarbons to many of the active plays within the Southern Inversion Zone (Figure 1.1), the Kapuni Group.

The Kapuni Group consists of a series of Paleocene and Eocene transgressive sequences which have been subject to both extensional and compressional tectonic stresses. This stratigraphic “Texas tea pot” of the region stretches across the southern basin and varies greatly in depth. In some areas the accumulations can reach an average of 2000 m (King & Thrasher, 1996; Higgs et al., 2007; NZ Petroleum & Minerals, 2014).

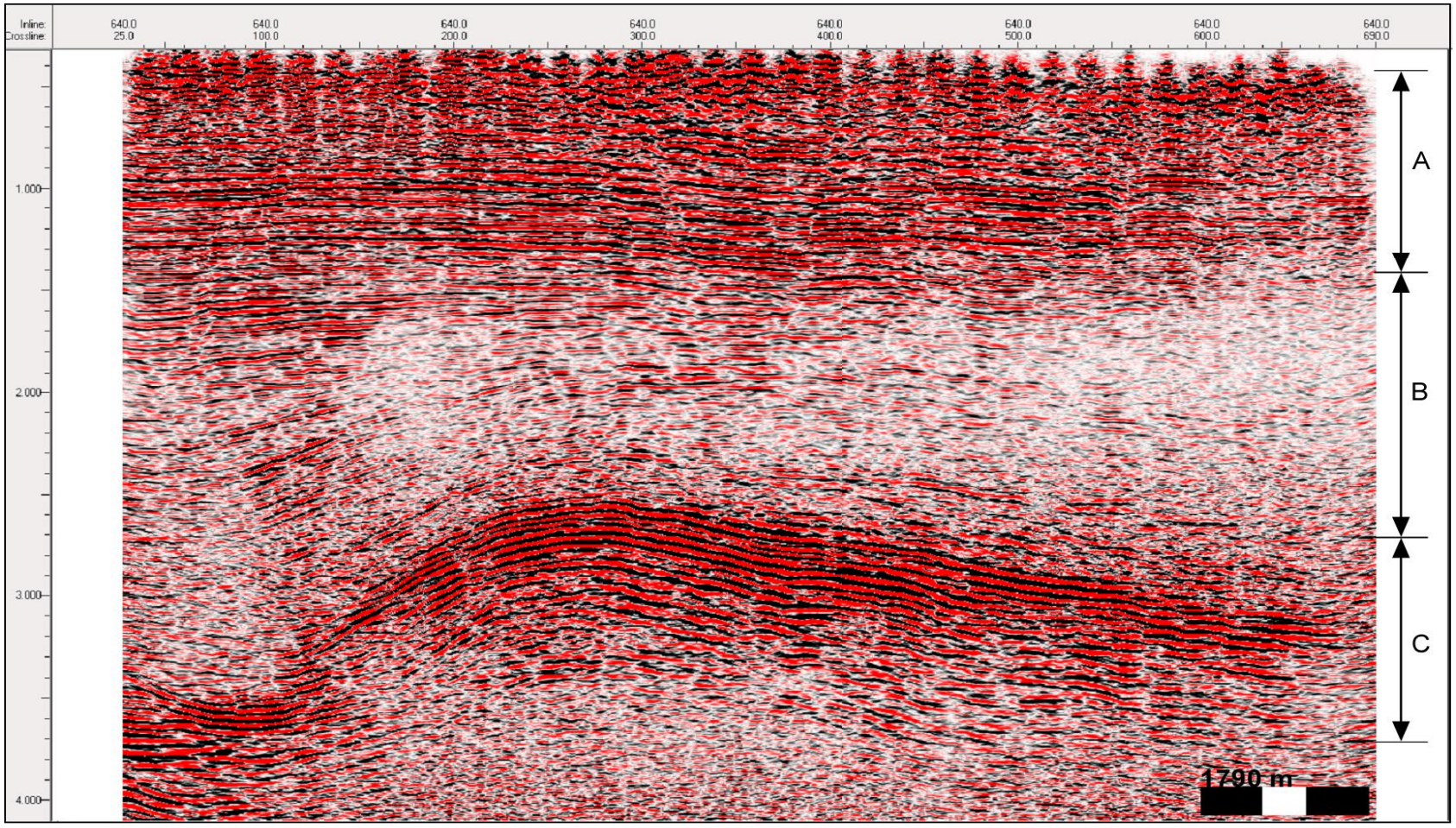

Figure 2.3. Time-amplitude seismic inline 640. There are three notable sections within the data; Section A boasts high seismic character and middle- Miocene to Quaternary sediments; Section B consists of very low seismic character and is comprised of late Eocene to early Miocene deposits; Section C which retains high reflectivity but fair seismic character, constitutes the target Kapuni Formation of early Eocene to Oligocene deposits.

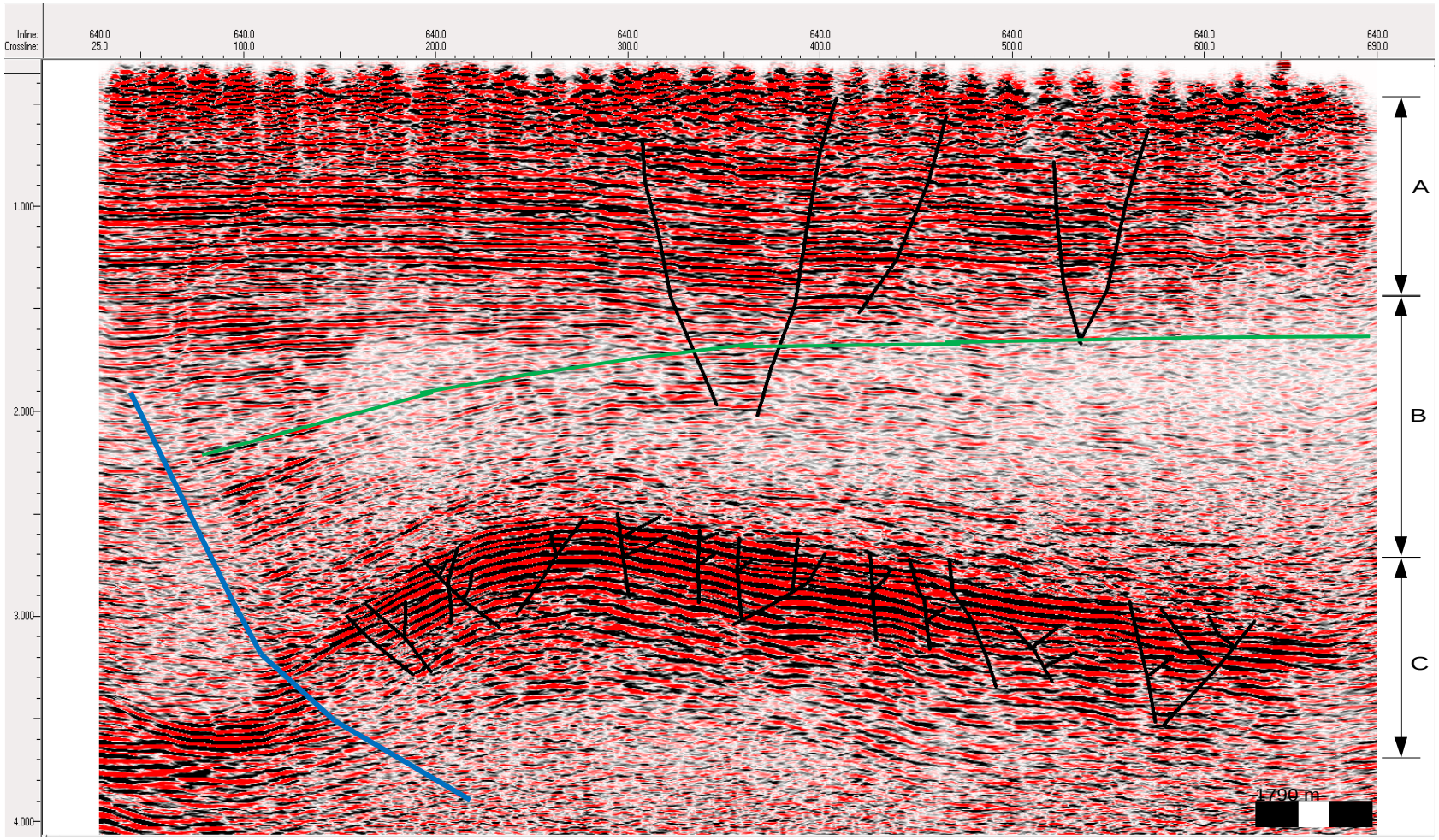

Figure 2.4. Inline 640 Interpreted. Note the extensive faulting within seismic section C. These faults show potential for being part of a normal fault system which may have formed before the Manaia uplift in the Oligocene. The majority of these faults have converted to minor reverse faults. Some of these reverse faults are thought to act as traps. Faults extending into section B are more recent normal/oblique faults.

The main hydrocarbon source within the Kapuni Group is a series of shaley coals which generate generous amounts of gas condensate within the system that migrates into surrounding terrestrial/marginal marine sandstones and carbonaceous mudstones (Higgs, 2013). Predictions by Beggs and Cook (1993) suggest over 79 MMBOE are still recoverable from this group of formations alone. Three significant formations make up the Kapuni Group, which includes the Mangahewa, Kaimiro, and Farewell (Figure 2.1).

2.3.1 Farewell Formation. The earliest deposition of the Kapuni Group sediments and the deepest source formation, the Farewell, has recently received more attention for its conventional and unconventional potential. The age of the Farewell Formation has been debated since its discovery, with original establishment as a Late Cretaceous deposition. However, studies in the 1980's have corrected this misplacement and reassigned the Farewell as a Paleocene age, eminently coarse grained, interbedded transgressive coal series which periodically contain conglomerates. This formation is often characterized by coarse grained sandstones with mudstone tops which can reach a thickness of 25 m (King & Thrasher, 1996).

The deepest well in the Kapuni Field, Kapuni Deep-1, managed to penetrate this early cyclical formation but was unable to reach the base. Samples from this formation have shown upwards of 40 plus percent hydrocarbon saturation including oil shows within the lowest cuts in the well. Conventional extraction has not been prevalent however, due to kaolinitic cements which have reduced porosity in some sands to less than 3% (Shell BP, 1984).

2.3.2. Kaimiro Formation. Above the Farewell, another source and reservoir bearing formation, the Kaimiro, has received much attention for its conventional use in

its upper sand strata, but has recently shown potential within the formation's lower source section. The Kaimiro Formation, like those formations above and below, consists of a cycled series of terrestrial, coastal plain, and marginal marine lithofacies. This series, compared to other cycles, was deposited between the Early and Middle Eocene (King & Thrasher, 1996).

Though this formation has seen great use and is examined for future potential, it contains many complex faults which hinder further exploration. This is due to the understanding that many of these faults act as pathways for hydrocarbon migration, and the bulk of such hydrocarbons may have already been recovered or lost. However, some groups of faults are known to act as traps due to their solid, compressional nature and are likely candidates for pocket hydrocarbons (Voggenreiter, 1993; Higgs, 2013). The Kaimiro Formation in the Kapuni Field lies between 3680 – 4553 m and through exploration and production wells have shown to be mostly water bearing in lower section sandstones (Higgs, 2014; Shell BP, 1984).

2.3.3. Mangahewa Formation. In the past, there were three target reservoirs that have been coveted within the Kapuni Field, all of which lay inside the Mangahewa Formation at depths between 3260 and 3680 m. Within the Kapuni Field and Taranaki Peninsula, this formation prevails at a thickness between 400 – 830 m. The Mangahewa Formation was segregated from other similar cyclical lithofacies in the Kapuni Group by its Middle to Late Eocene age (NZ Petroleum & Minerals, 2014; Higgs et al., 2013; King & Thrasher, 1996).

The last of the Kapuni Group to be deposited, this formation consists of the characteristic cyclical lithofacies of coals, sands, silt, and mudstones. The top of the

Mangahewa is capped by coals and mudstones, which are underline by its gas and gas condensate filled sandstone sequences. These reservoirs are characterized by estuarine channel sandstones with porosities ranging from 1-25% which cluster in adjoined 5-10 m thick deposits. The range of attributes is due to the existence of heterolithic intervals in the formation which cause irregular bright spots and along with its capping coal sequence, consequently contains poor image character within the 3D data set (Higgs, 2013; NZ Petroleum & Minerals, 2014; King & Thrasher, 1996).

3. DATA

3.1. SEISMIC DATA

The data used in this study was provided by New Zealand Petroleum and Minerals. The Kapuni Field survey is a 3D seismic data set which covers a total area of 350 km^2, records to a time depth of 6.59 seconds, and contains 22 wells. This 3D dataset contained a total of 945 inlines and 621 crosslines, each with a spacing of 25 m (Figure 3.1). The datum used for the survey was NZGD2000 and was projected in New Zealand Trans Mercator.

The entire 3D Kapuni survey is captured in Figures 3.1-3.4. The transition of the Kapuni anticline from bottom to top is displayed in Figure 3.2. These time slices display all 350 km^2 of the survey and range in depth from roughly 615 to 4975 m. Though the survey extends to 6.59 seconds (in TWTT), slices below 3.04 s begin to display total chaotic and undiscernible reflections with the exemption of one small section of Manaia foot wall which is better visualized in Figures 2.3, 2.4, and 3.4.

- **Caveat/Artifact.** Upon importation of the data into the Kingdom 2015 software, a large artifact zone in the northern section (henceforth the northern artifact zone, NAZ) of the data cube was discovered (Figures 3.2 and 3.3). The effects of this artifact are as such; a decrease in total number of colors within the color bar (<190/200) which additionally resulted in even more deficient seismic section B, a direct cut off point at inline 701, and an occasional inversion of the amplitude polarity color scheme in specific high character 2D displays. This artifact is decidedly apparent but caused little issue with structural interpretation for this study as the high character of the Kapuni Group was easily identifiable within the artifact zone. The large faults within this zone

are likewise clearly discernible, notably while implementing several seismic attributes. The cause of this artifact was due to the necessity of the considerable graphical processing power required, but was surely lacked by the computer(s) used for this research. Quality graphic cards which could handle such intensive requirements as Petrel and Kingdom were obtainable but were incompatible with the system(s) at hand. Another potential reason for this artifact zone is the original processing and stitching of data sets. It is probable that great emphasis and care was placed into the processing of the more southern portion of the data set as it contains the majority of the anticline where conventional extraction methods would be most prevalent. As the artifact zone is not within the coveted conventional play hot spot, it could have been processed separately and accreted subsequently for the sake of fluid dynamic comprehension.

3.2. WELL LOG DATA

The 3D Kapuni dataset included 18 wells which were drilled into the anticline and 4 wells which were clustered in the north-easternmost corner of the data set, for a total of 22 wells. Though there was sufficient well coverage of the Kapuni anticline's peaks, there is little to no coverage through the saddle structure and north eastern portion where the Tuikonga fault zone and potential gas chimney lay. The closest wells to the proposed seep was the Cardiff well cluster which is approximately 3.3 km to the north east. The distribution of wells within the anticline can be seen in Figure 3.5.

The majority of the wells contained an adequate number of usable logs, but many did not contain Time/Depth (henceforth known as TD) charts which limited their use for this study. The three highlighted logs in Table 3.1 were the main wells used in this study

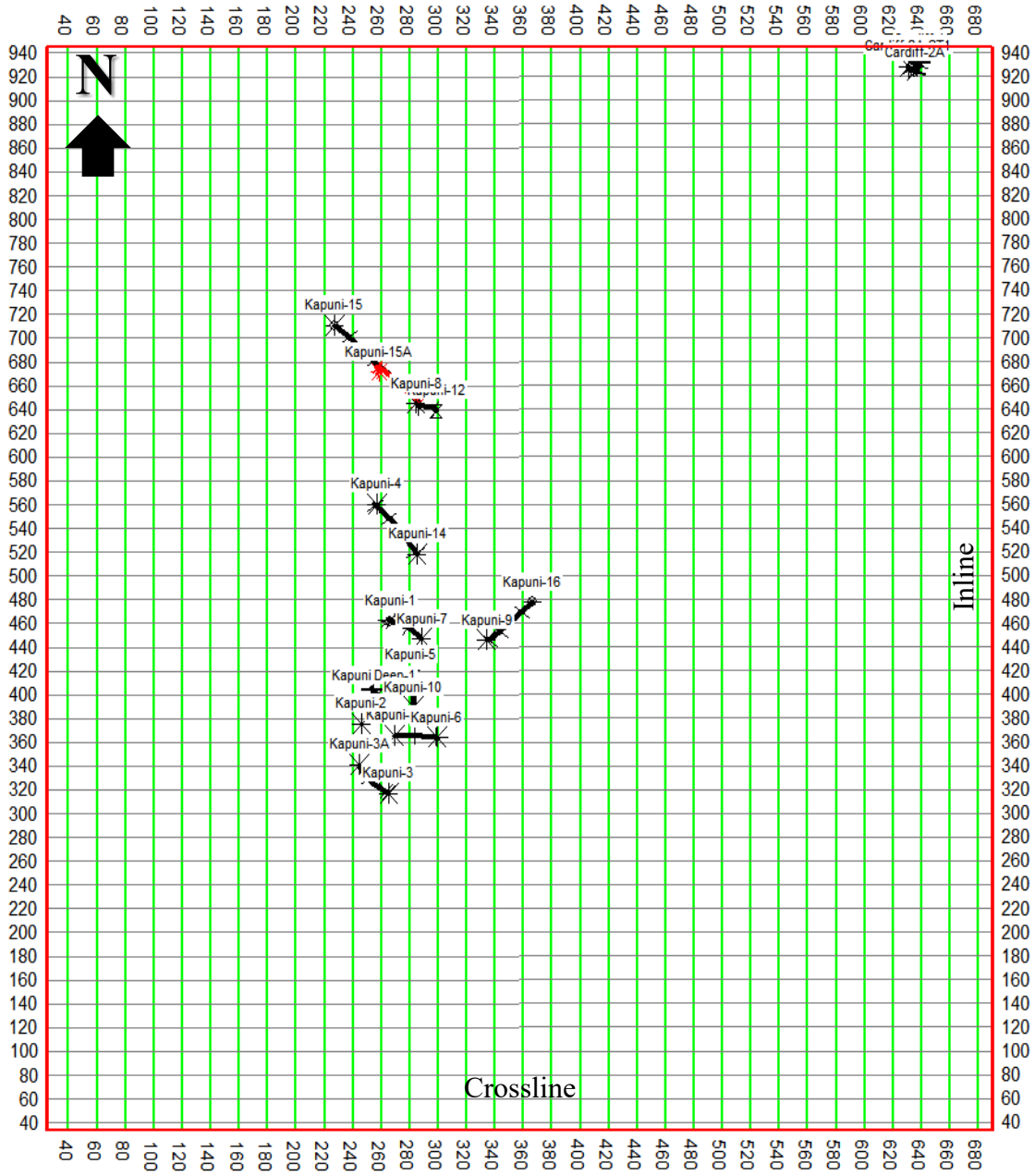

Figure 3.1. 3D Kapuni survey with all wells. Note that the majority of wells are located in the southern half of the survey. Most wells were drilled for gas and gas condensate extraction. Inline and crossline interval displayed is 20.

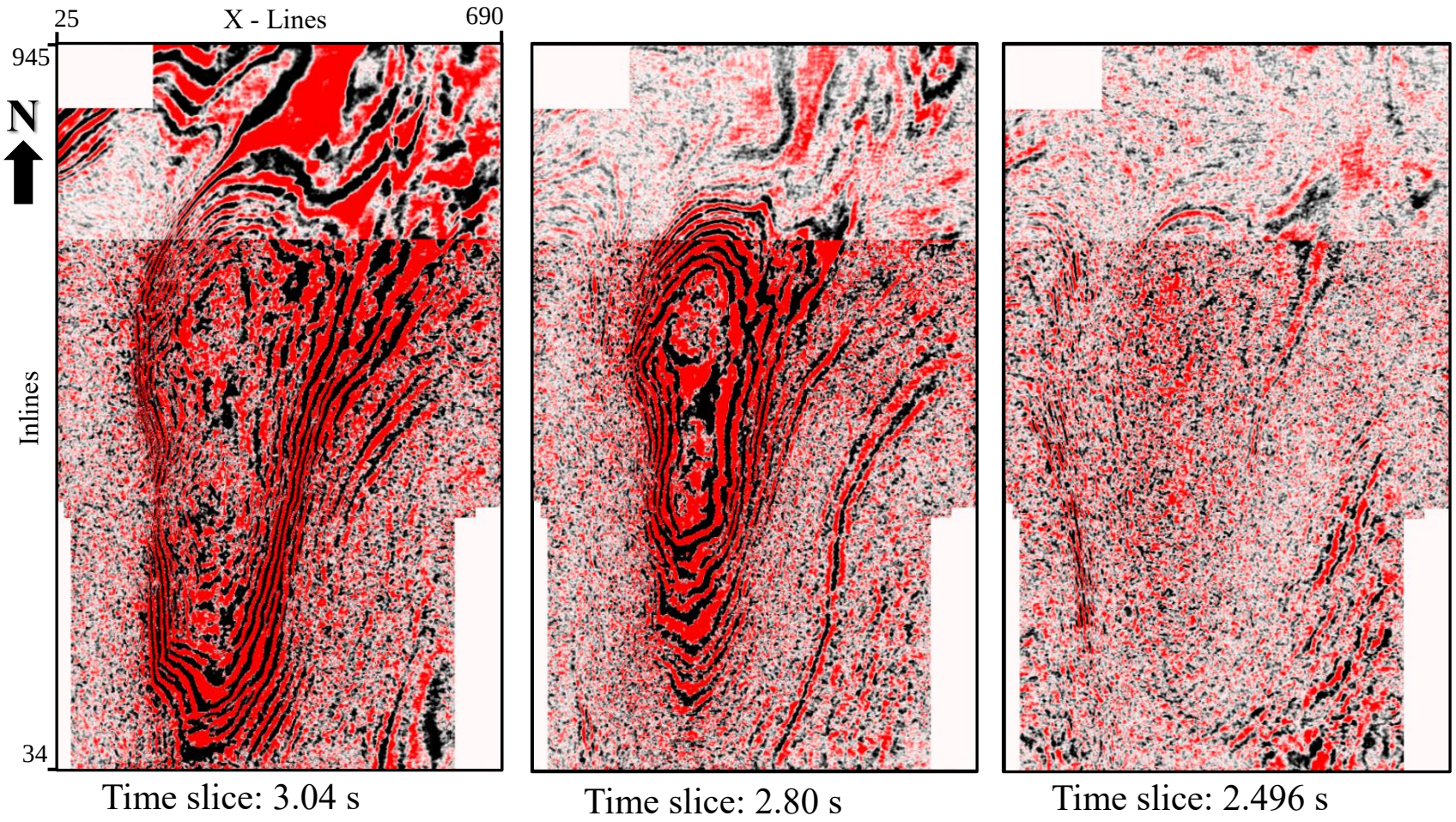

Figure 3.2. Time slices. Slice 3.04 s cuts through the middle of the Kapuni Group sediments and displays a wider section of the Kapuni anticline. Moving up in section to slice 2.80 s, the top of the well defined anticline is visible but quickly begins to disappear as looser sediments above slice 2.496 s begin to display chaotic reflection.

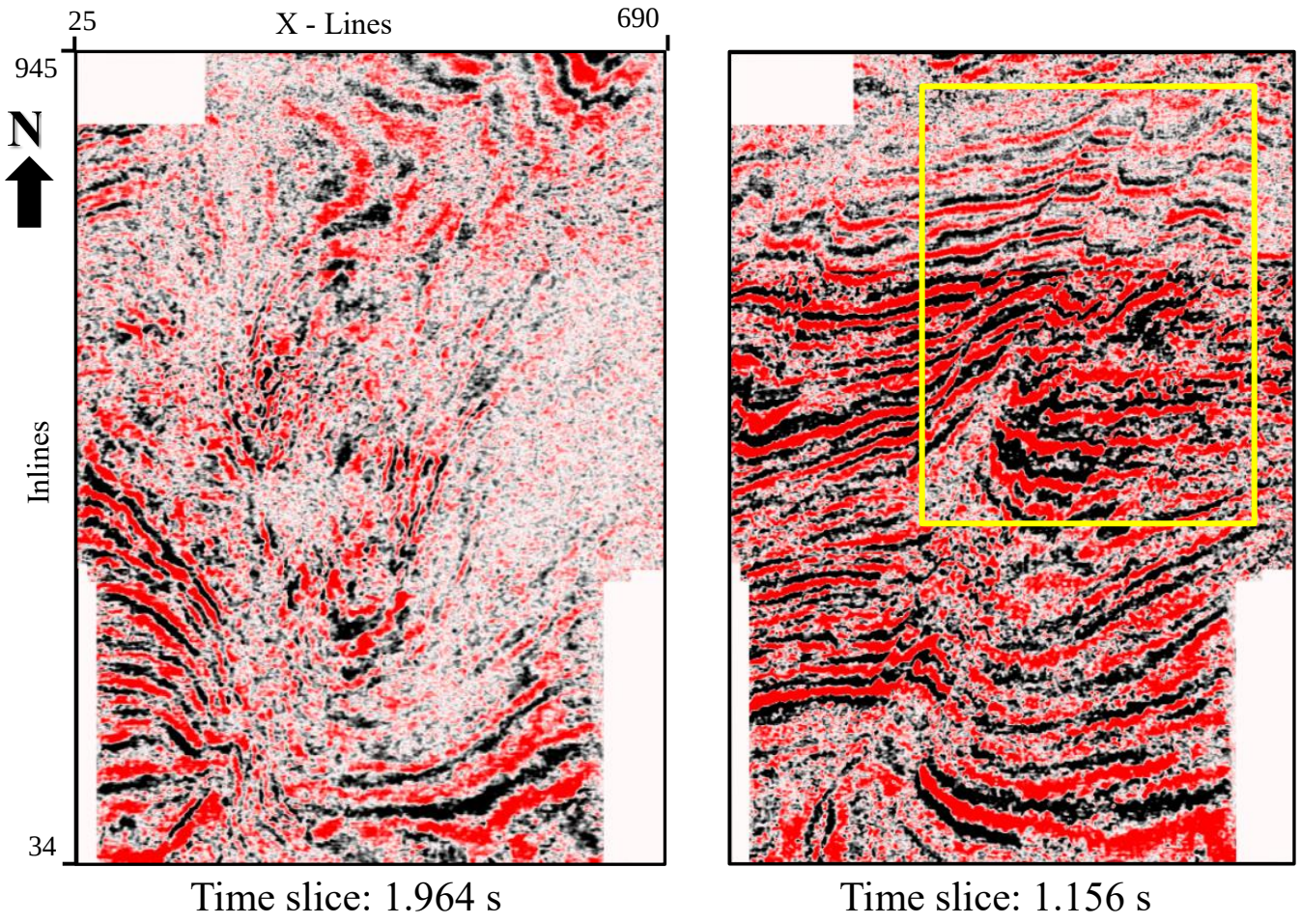

Figure 3.2. Time slices. 1.964s and 1.156 exhibit the extensional regime found in unit A of Figure 2.4. Note the sudden color changing artifact in the northernmost segment of the slices. The yellow box in time slice 1.156 s indicates area containing the Mangatoki Fault zone. Both slice 1.964 s and 1.156 s are within the local extensional fault regime. (cont.)

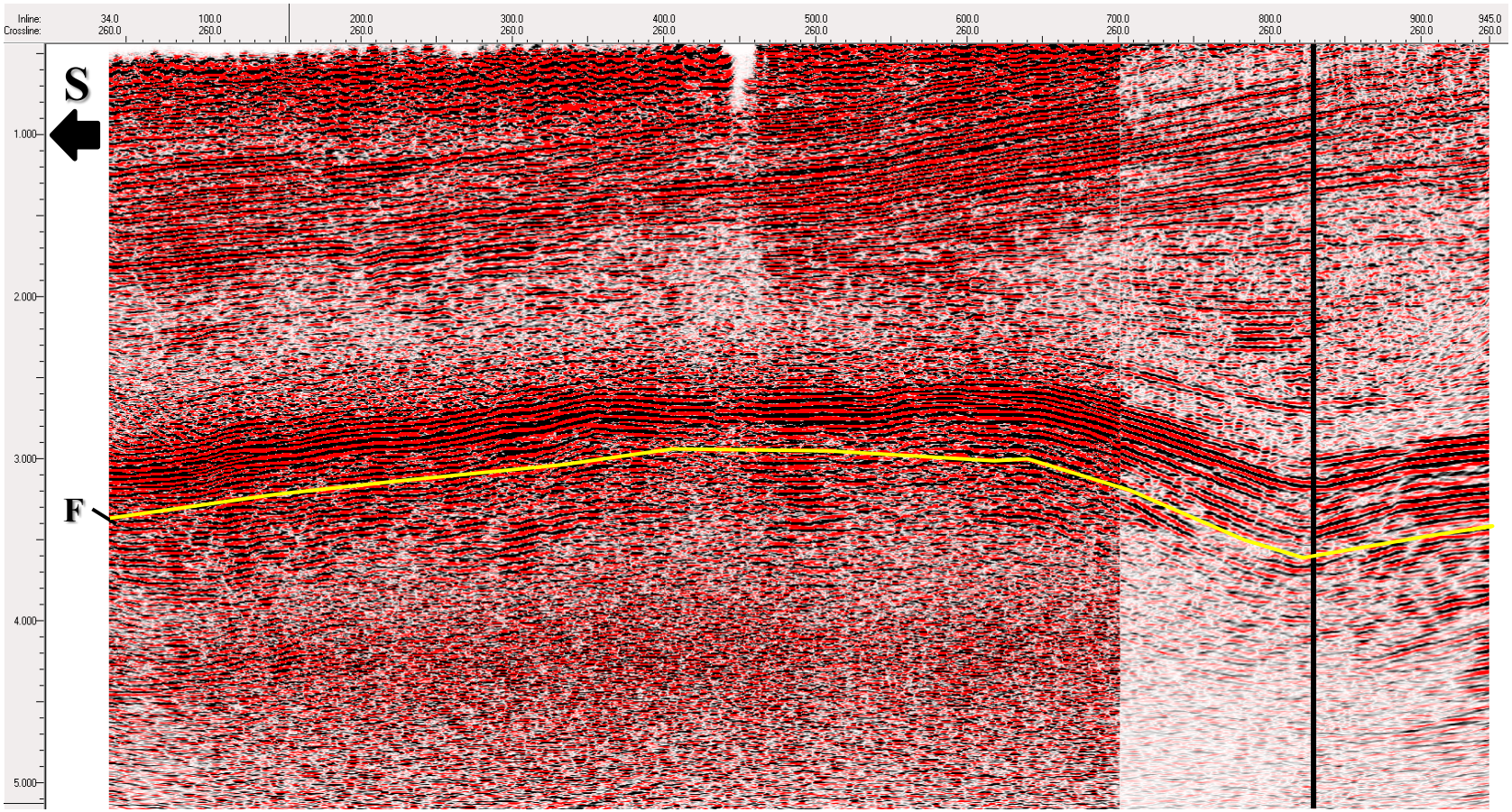

Figure 3.3. Crossline 260 and Inline 830. Although the data set was recorded to a TWTT of 6.59 seconds, all of the data below the top of the Farewell Formation around F (yellow line) is useless due to incredibly poor character and chaotic nature. Note the start of the artifact zone and the clear lack of color compared to the rest of the data in the southern end of the data set. Inline 830 is indicated by the vertical black line.

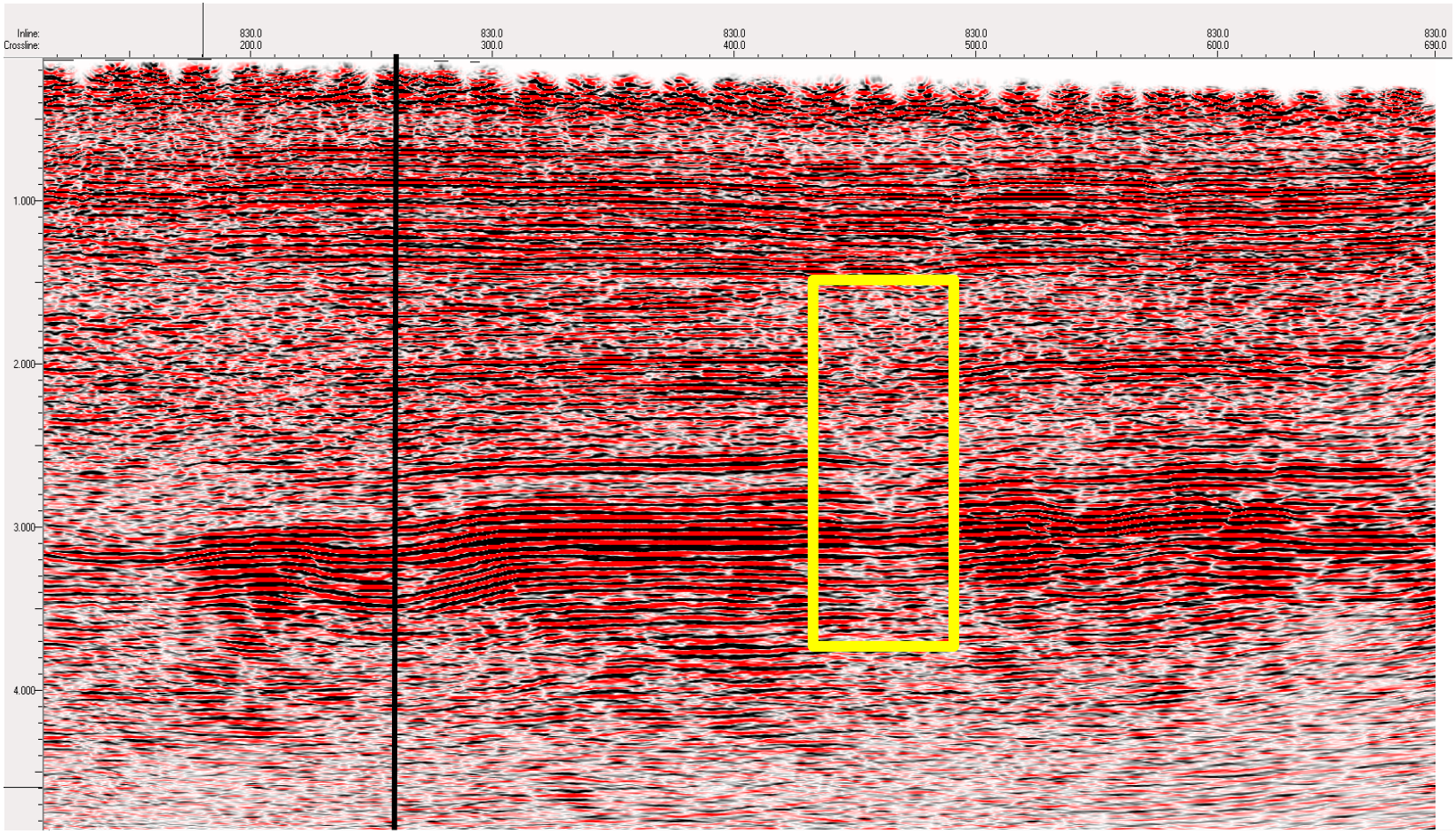

Figure 3.3. Crossline 260 and Inline 830. This inline is within the northern artifact zone. Though the number of color is decreased, the highly reflective Kapuni Group is still visible within this section. Note the highlighted area which shows an example of the proposed gas leak within a time/amplitude vertical display. The Kapuni formations stay relatively flat north of this inline but rise steeply to the anticline peak to the south. The black line indicates crossline 260. (cont.)

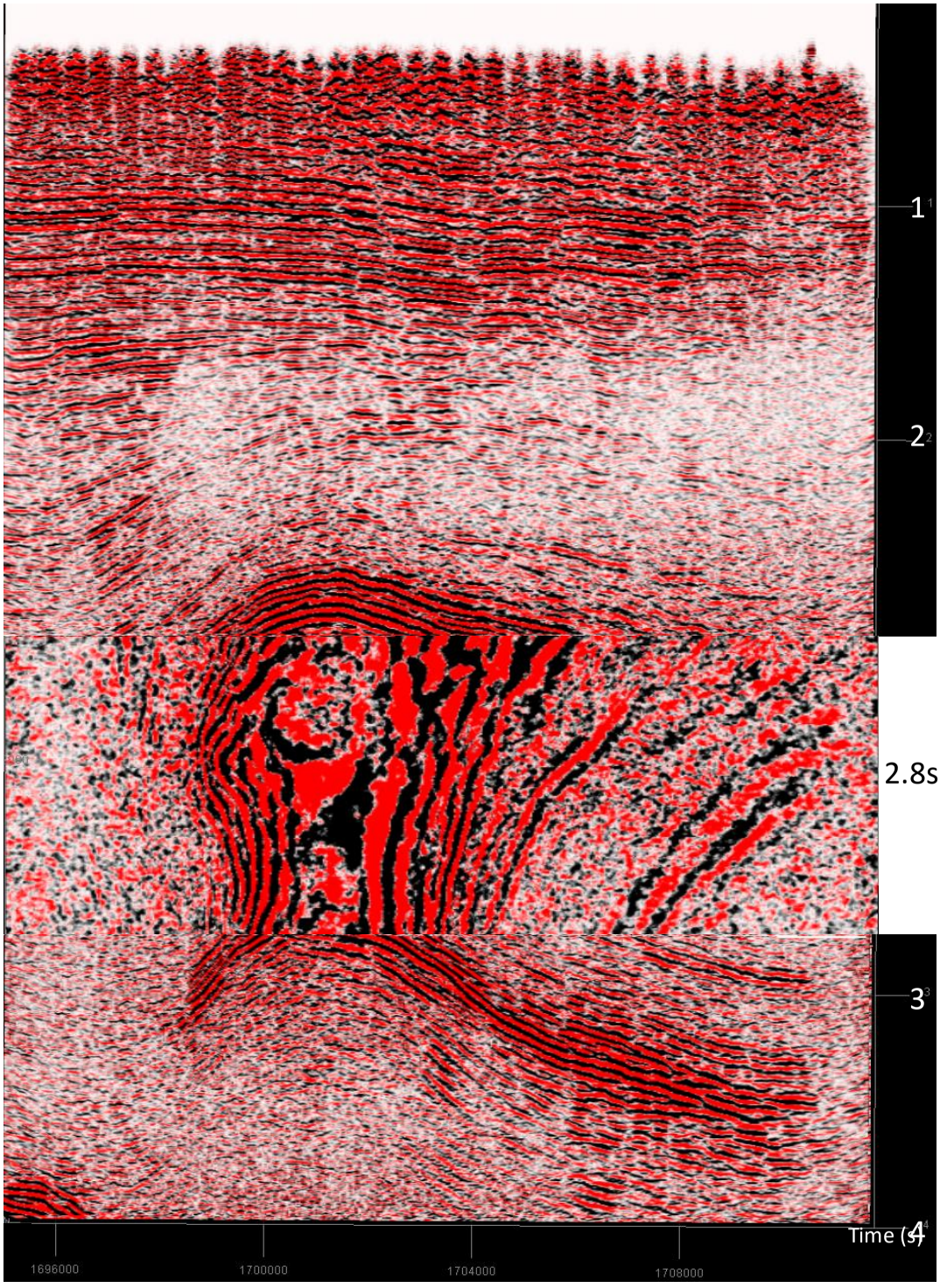

Figure 3.4. Chair display of the Kapuni anticline. (Top) inline 640; (middle) time slice 2.80 s; (bottom) inline 400**.** Note how the anticline narrows toward the south and contains a saddle structure. Discontinuities are pervasive within the time-slice.

as they contained complete TD charts, the most complete sets of logs, and were spatially relevant to the study area. These wells consisted of the following logs; Bit Size, Caliper, Density, DRHO, DTC (Sonic), Gamma Ray, Neutron, PEF, Resistivity (deep, mid, shallow), SP, Temperature, TENS, and Borehole. Though the well logs had previously been processed and formation tops interpreted, they required creation of synthetics to correct the TD charts.

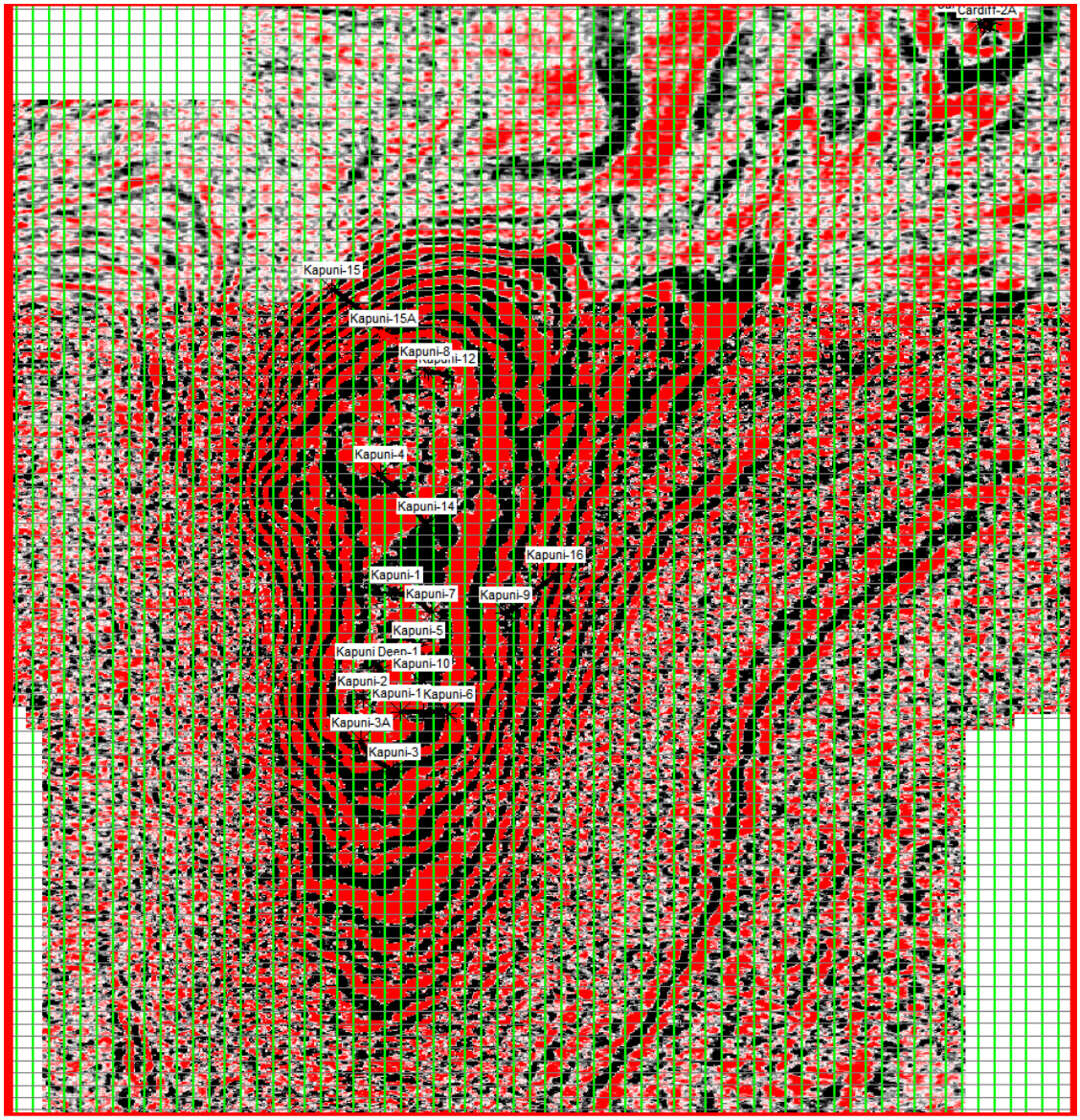

Figure 3.5. Distribution of wells. With a total of 22 wells which were distributed with the dataset, only two contained enough logs for synthetic generation, which are Kapuni-8 located in the northernmost vertical protuberance of the anticline, and Kapuni Deep-1 located within the well cluster of the southern anticlinal lobe. The Cardiff well cluster in the northeast corner were not utilized for this study as they did not provide sufficient data.

Table 3.1. List of all wells provided with the 3D Kapuni Survey.

Well Name	Well Number	Borehole Name	UWI	Bottom Hole Location X	Bottom Hole Location Y	Elevation(m)	End Depth(m)	Formation at TD	Start Depth(m)	Status	Surface Elevation(m)	Total Depth(m)
Cardiff-1	**PR1844**	**Cardiff-1**	**100000131835.00**	**1710452.79**	**5641940.56**	**305.4**	**5050**	**Mangahewa**	**0**	**Abandoned**	**296**	**5050**
Cardiff-2	PR3058	Cardiff-2	100000529019.00	1710420.96	5641815.31	301.2	4898	Kaimiro	0	Abandoned	293	4898
Cardiff-2A	PR3058	Cardiff-2A	100000531767.00	1710372.24	5641656.18	301.2	4072		0	Abandoned		4072
Cardiff-2A ST1	PR3058	Cardiff-2A ST1	100000533377.00	1710249.22	5641788.64	301.2	4934	Kaimiro	0	In Completion	293	4934
Kapuni Deep-1	**PR1024**	**Kapuni Deep-1**	**100000113263.00**	**1700864.85**	**5628545.37**	**172**	**5664**	**Kapuni Group**	**0**	**Suspended**	**162**	**5664**
Kapuni-1	PR427	Kapuni-1	100000021878.00	1701144.43	5630124.74	191.7	3974.6	Mangaotaki	0	Suspended	186.8	3974.6
Kapuni-10	PR876	Kapuni-10	100000022137.00	1701549.39	5628305.58	174	3941.1	Kapuni Group	0	In Completion	169.2	3941.1
Kapuni-11	PR877	Kapuni-11	100000022136.00	1701222.6	5627706.09	157.9	3910.6	Kapuni Group	0	In Completion	151.8	3910.6
Kapuni-12	PR879	Kapuni-12	100000164570.00	1701949.06	5634542.82	275.8	3672	Kapuni Group	0	Active	264.9	3672
Kapuni-14	PR1367	Kapuni-14	100000022135.00	1701617.65	5631520.38	240.8	4201	Kapuni Group	0	In Completion	233.9	4201
Kapuni-15	PR1832	Kapuni-15	100000127960.00	1700152.22	5636344.59	274.4	4770	Kapuni Group	0	Plugged	265	4770
Kapuni-15A	PR1832	Kapuni-15A	100000528875.00	1700945.82	5635356.85	274.4	4154	Kapuni Group	0	Gas Well	265	4154
Kapuni-16	PR2879	Kapuni-16	100000474884.00	1703637.19	5630520.14	187.36	4064	Mangahewa	0	Suspended	177.7	4064
Kapuni-2	PR464	Kapuni-2	100000021910.00	1700630.57	5627956.13	157.3	4194.66	Mangaotaki	0	In Completion	152.1	4194.66
Kapuni-3	PR465	Kapuni-3	100000502146.00	1701108.48	5626499.14	136.86	3796.9	Kapuni Group	0	In Completion	131.1	3796.9
Kapuni-3A	PR870	Kapuni-3A	100000022141.00	1700600	5627107.49	136.86	3901.44	Kapuni Group	0	In Completion	131.7	3901.44
Kapuni-4	PR466	Kapuni-4	100000021909.00	1700900.92	5632576.28	232.56	3901.44	Kapuni Group	0	In Completion	226.5	3901.44
Kapuni-5	PR871	Kapuni-5	100000022142.00	1701499.43	5628991.64	173	3825.2		0	Active		3825.2
Kapuni-6	PR872	Kapuni-6	100000022143.00	1701965.07	5627670.62	157	3792.6	Kapuni Group	0	In Completion	151.8	3792.6
Kapuni-7	PR873	Kapuni-7	100000022140.00	1701699.43	5629737.79	192.3	3919.7	Kapuni Group	0	In Completion	187.5	3919.7
Kapuni-8	**PR873**	**Kapuni-8**	**100000022139.00**	**1701597.99**	**5634694.76**	**270.1**	**4079.7**	**Kapuni Group**	**0**	**In Completion**	**265.2**	**4079.7**
Kapuni-9	PR875	Kapuni-9	100000022138.00	1702847.11	5629713.89	182.5	3932		0	In Completion		3932

Many wells have been suspended since their completion but still contain valuable information. The Majority of the wells were drilled to absorb multiple layers of the Kapuni Group, mainly the Mangahewa and upper Kaimiro formations. The deepest well drilled in the field is Kapuni Deep-1 which was completed in 1984, to a depth of 5665 meters.

4. STRUCTURAL INTERPRETATION

The structural interpretation aspect of this study was conducted using data from several high quality well logs and generated seismic attributes. The efforts of DEM production resulted in interpretation of four acute surfaces, three prominent faults, and one potential gas chimney. Surfaces and tops were correlated with previous studies along with specified faults. Two surfaces (Kapuni cycle A &B) and all three faults (Tuikonga 2 and Mangatoki faults 1&2) were used in the creation and interpretation of the fluid flow model in section 5.

The overall structure of the survey reflects a transpressional regime generated from the reverse nature of the Taranaki and Manaia faults. The result of this force is seen as the large anticlinal structure within the 3D survey. As described in Voggenreiter (1993) and Higgs et al. (2013), the Kapuni anticline contains a minor saddle structure which separates two lobes. Both of which have been coveted for their use in conventional hydrocarbon extraction. Though the bulk of attention has been focus upon these areas, the source coals and shales are not truly discontinuous within the survey. They appear to continue trending toward the north of the survey area, outside the bounds of the Manaia fault's direct influence. Although empirical enhancement of the northernmost segment of the data cube was necessary due to artifact effects, solid and probable conclusions were discerned through horizon and fault tracking alongside seismic attribute manipulation and interpretation.

4.1. SYNTHETIC SEISMOGRAMS

Synthetic seismograms are generally used as a form of forward modeling which gives a one dimensional representation of acoustic energy propagation. Using the well logs and the SynPak modules in the Kingdom software, synthetics of the Kapuni Deep-1, Kapuni-8, and Cardiff-1 (Table 3.1) were generated to correct the TD charts and better visualize specific formations and lithological transitions within the wells. The accuracy of the produced synthetics in this study was diminished due to poor quality data from the extracted traces as well as the Density and DTC logs. As shown in Figure 4.1, the best matched synthetic was Kapuni-8 with a cross correlation (r) value of 0.631.

To generate the synthetics, the TD charts were first imported into the synthetic generator. For the cases of Kapuni-8 and Cardiff-1, the TD charts required correction before importation, as they were generated using the sonic "DTC" log which was measured in English units as opposed to the Metric units shared by all other well logs. A simple unit correction to the DTC log fixed all issues and allowed for Density log entry, the extraction of wavelets, and extraction of the real seismic trace from a 100 meter average around the borehole. Once all reference logs were imported, manual stretching and squeezing of the synthetic was conducted until the r value reached its peak.

4.2. ATTRIBUTE GENERATION

The use of seismic attributes in structural interpretation of 3D data is both vital and ubiquitous. As described by Chopra and Marfurt (2007), seismic attributes are seismic data which aid in empirically justifying specific features or visually enhance them for interpretation purposes.

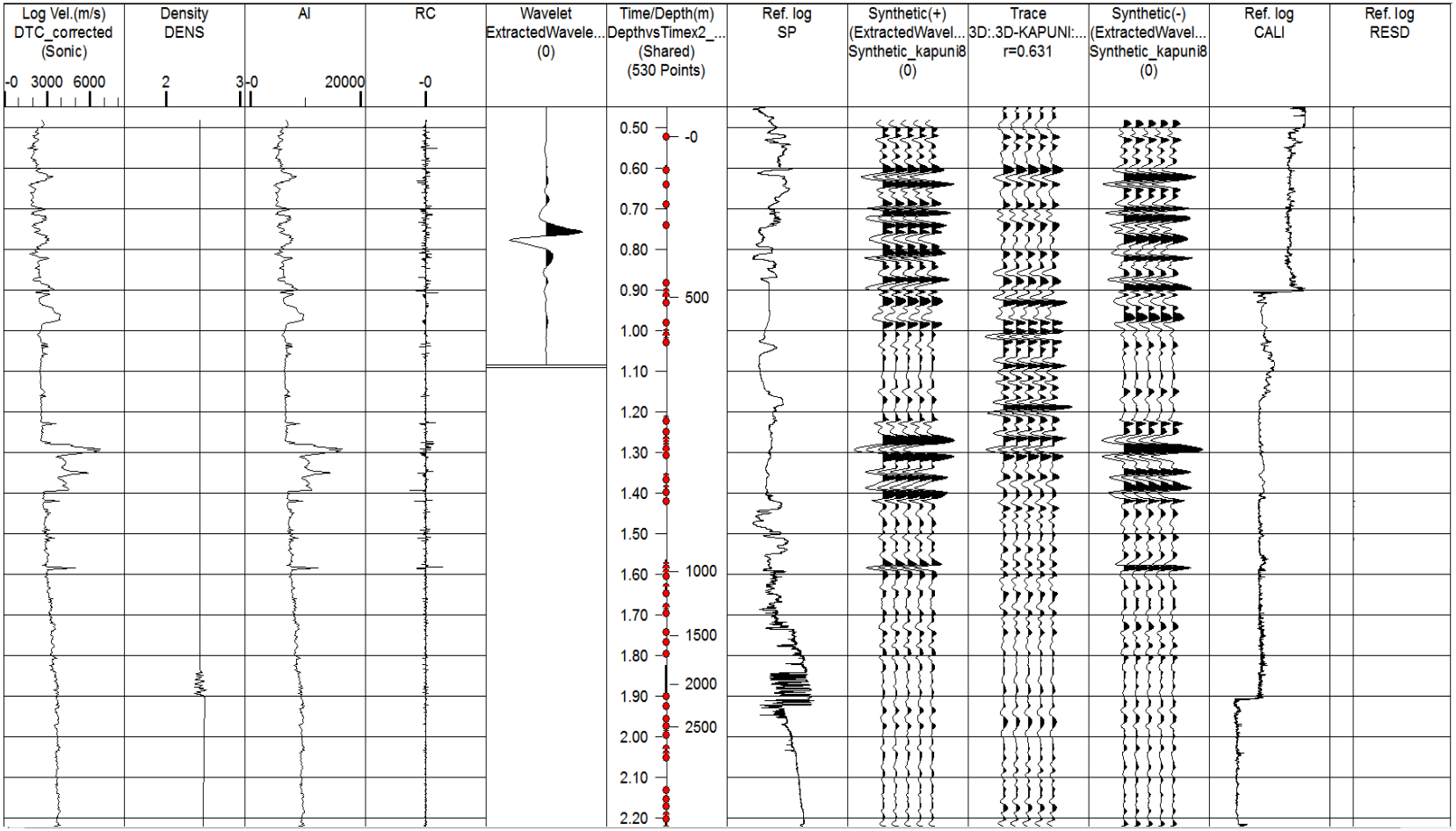

Figure 4.1. Synthetic trace of Well Kapuni-8. Extracted wavelet was converted from zero to 90° phase for synthetic to seismic trace matching. The Caliper and SP logs were the main reference as they were the most reliable logs of the well. Kapuni-8 contained the highest r value of .631 and placed the top of the Kapuni Group at 3400 m. Several logs including the RESD, DENS, and DTC required correction due to unit conversion.

In this study (for structural interpretation purposes), the Petrel software was used to generate multiple seismic volume and surface attributes. Seismic volume attributes are used to identify specific zones within a data set which could potentially act as source, reservoir, or cap. The total volume of these zones can then be calculated and correlated with the aid of well logs and other volumetric attributes. This study generated three volume attributes within Petrel for the purpose of identifying source and cap rock, which are instantaneous phase, instantaneous frequency, and envelope. Seismic surface attributes are used to identify specific structures, such as faults, within a given data set. For the identification of faults and seeps, chaos, dip variance, and dip symmetry attributes were generated over the entire 3D data cube.

4.2.1. Instantaneous Phase. Instantaneous phase is considered a volume attribute by Petrel. The purpose of this seismic attribute is to show continuity and discontinuity of events/reflection surfaces. In this study, it was used to aid in bed and superficial surface tracking. The equation used to calculate instantaneous phase is

$$\phi(t) = \arctan\ [\![|H(t)/T(t)\,|]\!], \qquad (1)$$

where T(t) is the seismic trace and H(t) is its Hilbert transform. To generate this attribute, a Hilbert filter window of 33 was utilized as greater detail was not plausible or necessary for the purpose of this study due to the resolution and size of the data set. Figures 4.2 and 4.3 display an inline and a crossline of the 3D data after it is transformed into the Instantaneous Phase attribute.

4.2.2. Instantaneous Frequency. Instantaneous frequency is typically defined as the time derivative of the phase. This rate of change calculation allows interpreters to

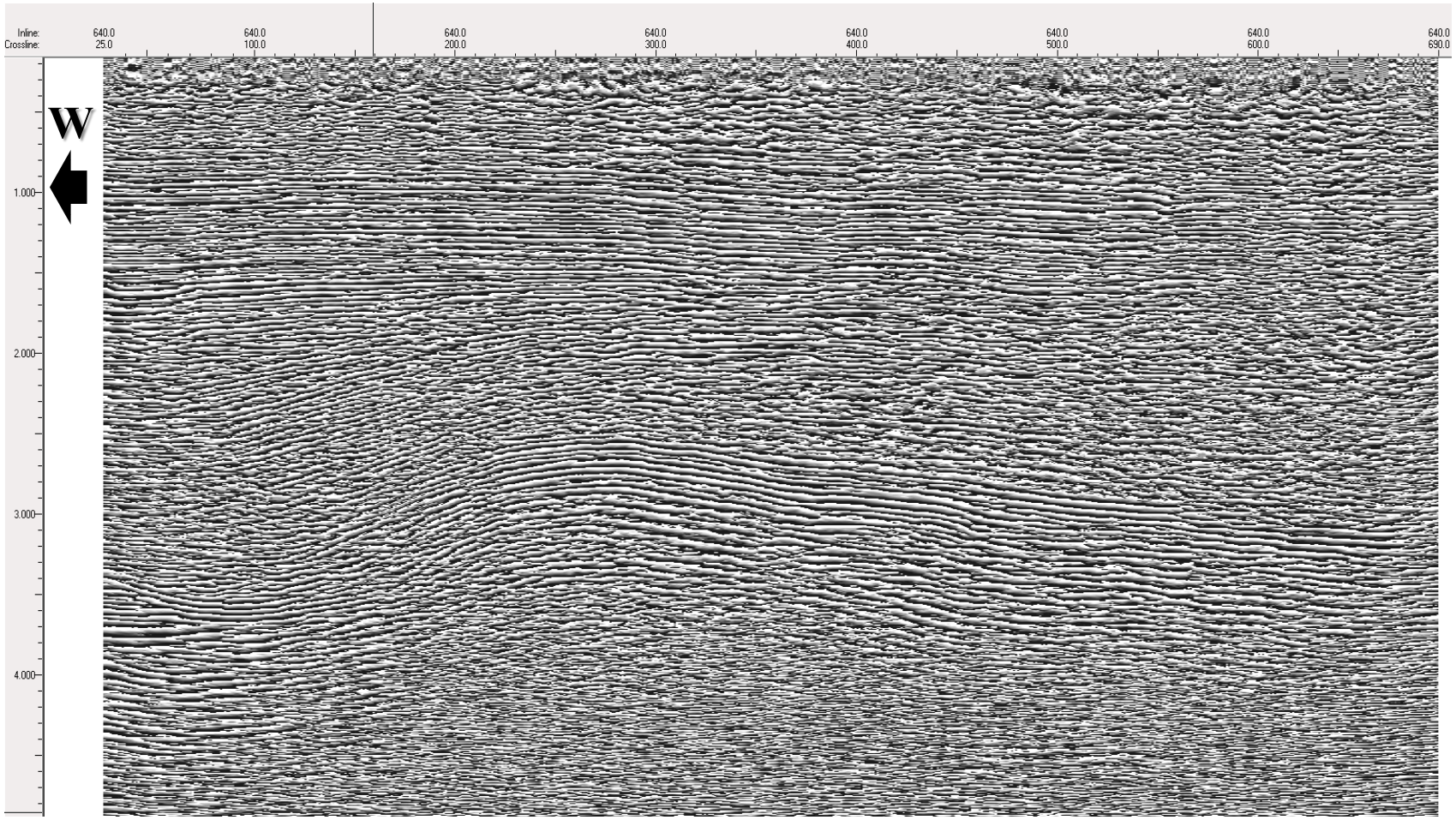

Figure 4.2. Instantaneous phase attribute. Inline 640. Black color indicates a positive phase while white reflects negative phase. The top of the anticline is visible as well as onlaped sediments (between 1.5 s and 2.3 s) in the hanging wall of the Manaia fault. This attribute aided in identification of the top and bottom source rock horizons.

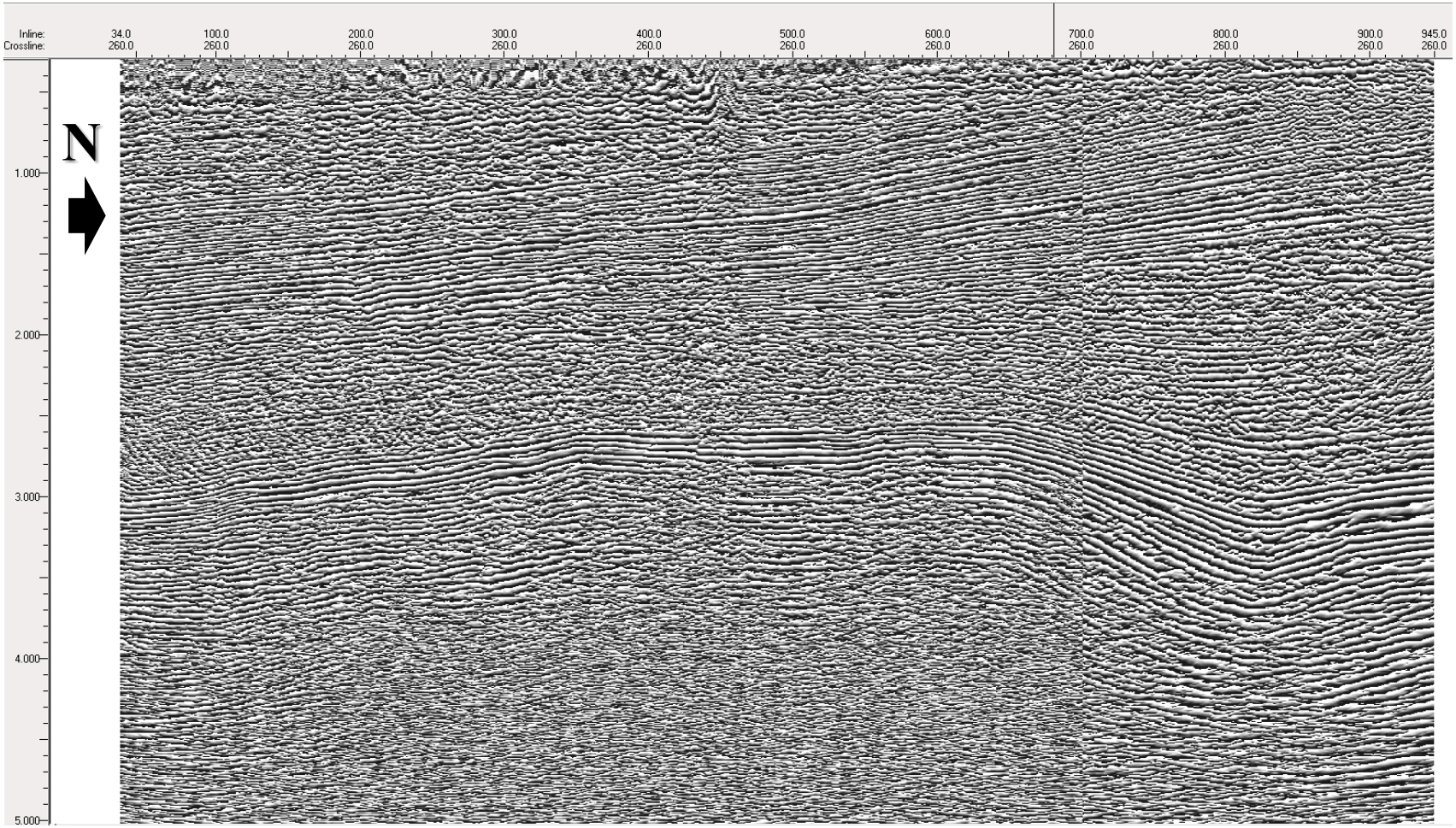

Figure 4.3. Instantaneous phase attribute. Crossline 260. Black color indicates a positive phase while white reflects negative phase. The top of the anticline is visible as well as onlaped sediments (between 1.5 s and 2.3 s). This attribute aided in identification of the top and bottom source rock horizons.

identify zones of low frequency hydrocarbons such as gas or gas condensate (depending on knowledge of stratigraphy), identify fracture zones, and thickness of particular beds. Since this attribute can be used to indicate dimensions of layers, it is considered to be a volumetric attribute.

In this study, the instantaneous frequency was processed in the Petrel software with a Hilbert window between 33 and 85 respectively. Upon inspection of multiple runs, it was decided that, due to the presence of coal beds and extensive fracturing, the use of highly defined instantaneous frequency was not advantageous as the difference between the two windows was minimal. Figures 4.4 and 4.5 display the instantaneous frequency (window 33) as it was imported into the Kingdom software before interpretation. Several thin coal layers within the Kapuni Group sediments are vaguely defined, however they become nonviable once tracked into the northern artifact zone.

4.2.3. Dip Variance. Dip and azimuthal guided variance (or coherence) are the most common seismic attributes used in the detection of edges, discontinuities, faults, and reflective local geologic and depositional events such as reef structures and gas migrations. The calculations for variance are conducted using specified dip and/or azimuthal guides which give higher definition to the identifiable characteristics mentioned above. When calculated in Petrel, the dip variance attribute required multiple parameters which included, an inline and crossline range of 4 respectively, a vertical smoothing filter of 20 samples per filter, a dip correction filter which used an inline/crossline/vertical scaled window of 2.0 for each, and a plane confidence threshold of 70% (meaning only filter iterations with 70% or greater confidence are then re-filtered with dip-guided correction).

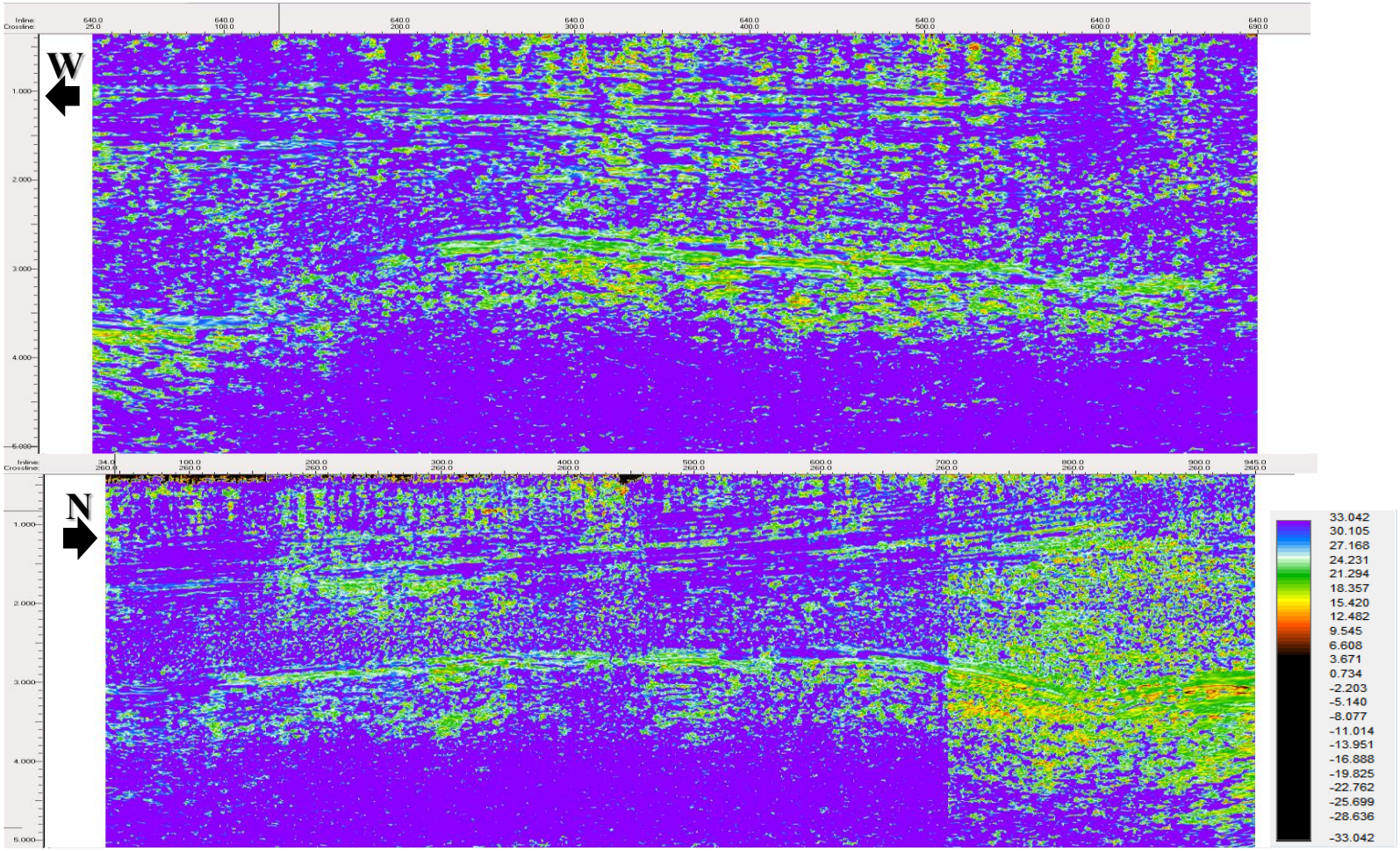

Figure 4.4. Instantaneous frequency attribute. (Above) Inline 640, note the low frequencies within several layers of the Kapuni anticline as well as sections of seismic unit B. (Below) Crossline 260, several low frequency layers are discernible within the anticline, but note the abrupt increase in low frequency prevalence within the artifact zone.

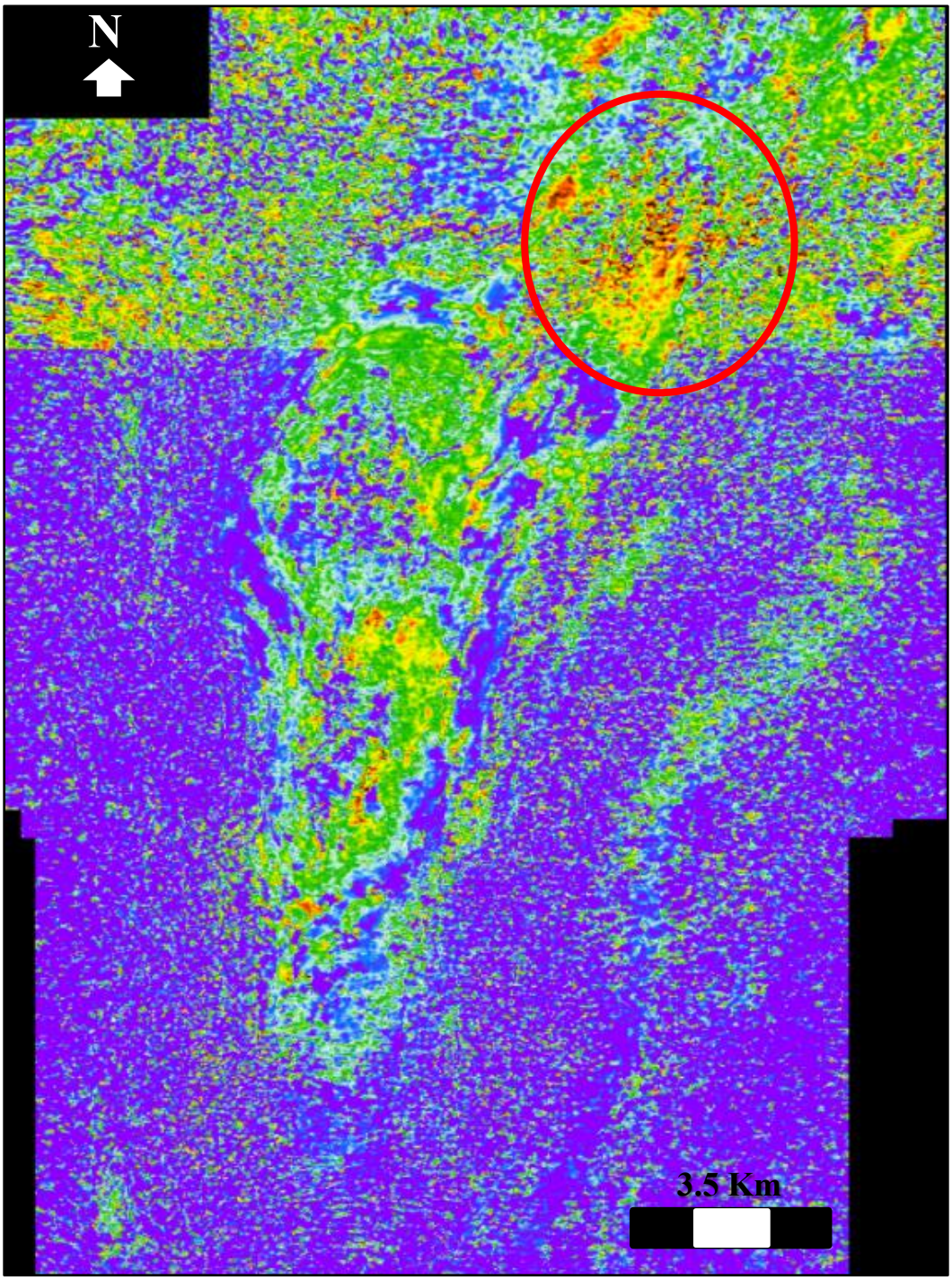

Figure 4.5. Instantaneous frequency time slice. 2.8 s. Same color bar as Figure 4.4. Note the excessive low frequencies in the north east of the anticline.

The finished attribute processed only faults of high angle (Figures 4.6 and 4.7). Due to an excess of chaotic reflectors in the survey's vertical sections the total clarity and resolution of the inlines and crosslines was reduced. However the horizontal time slices provided much higher resolution and detection of smaller faults and structures within the survey.

4.2.4 Chaos. The chaos attribute is a form of the variance attribute which specifically measures the lack of organization in dip/azimuth estimations. It is generally used as an input for other processes such as "ant tracking" which automatically identifies faults based on a system of discontinuity and dip guided algorithms which are distinguishable from variance calculations. This attribute is often used to delineate edges and discontinuities within a system, just as the variance attribute.

In this study, the chaos attribute was calculated in Petrel using three dimension window of 1.5 (measured in a ratio scaling) for Sigma X, Y, and Z respectively. The final output is visualized in Figures 4.8 and 4.9. The overall resolution of this attribute is quite poor compared to the dip variance attribute which exhibits virtually the same concept. Though the vertical sections (Figure 4.8) display poor resolution, the time slice(Figure 4.9) exhibits greater resolution, which is due to the innate higher contrast of discontinuity. This reduction in resolution is due to the algorithms used for calculation. Where dip variance requires more specific input variables, the chaos attribute is more generalized and uses larger windows and filters.

4.2.5. Dip Symmetry. The dip symmetry attribute is specifically a fault detection attribute which is generated in the Kingdom interpretation software. This attribute is specifically used for identifying linear fault features.

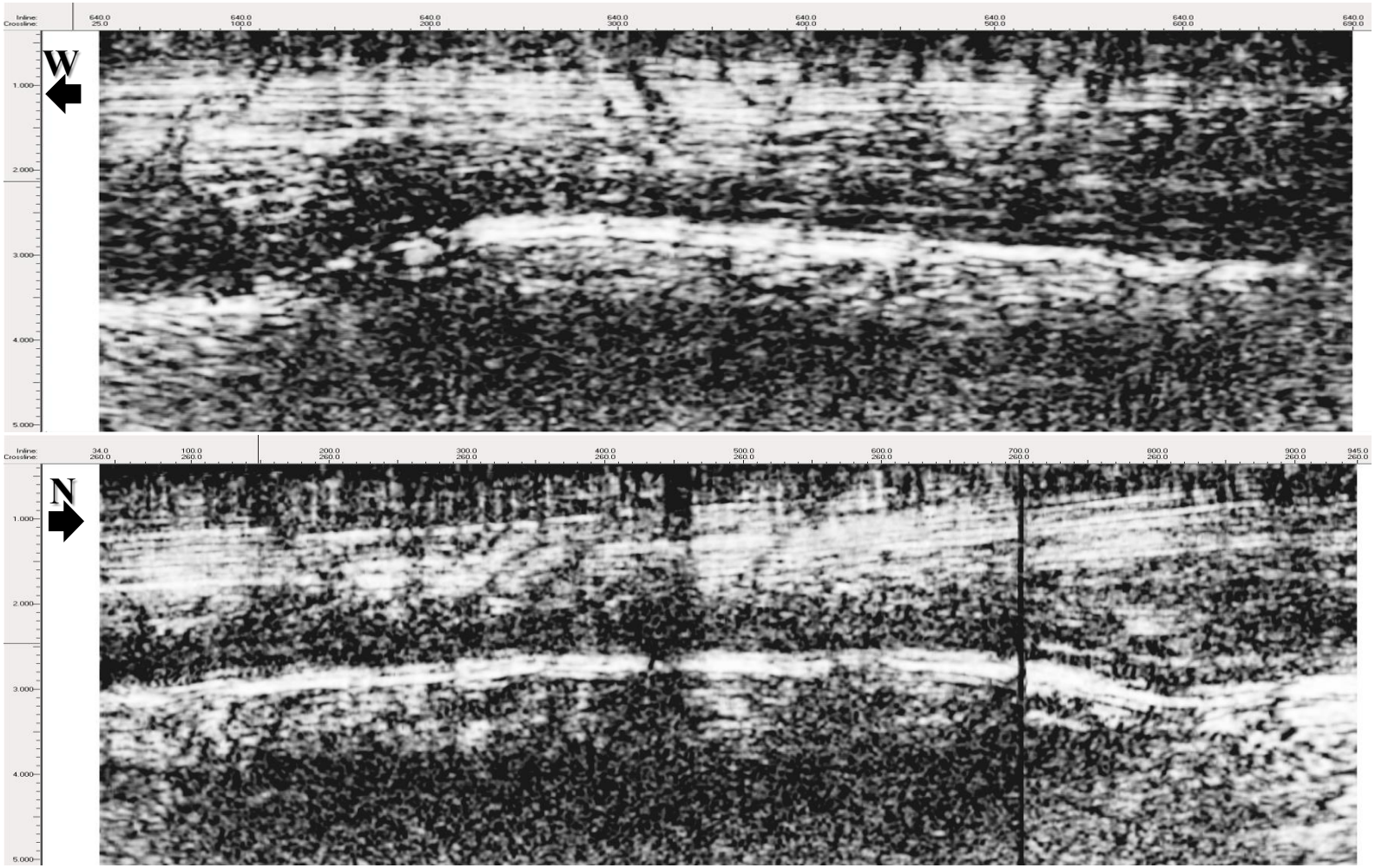

Figure 4.6. Dip variance attribute. (Above) Inline 640. Multiple large faults are visible in the upper layers whereas relatively few are visible within the anticline. This is due to the relative chaotic nature of the vertical sections as a whole. (Below) Crossline 260.

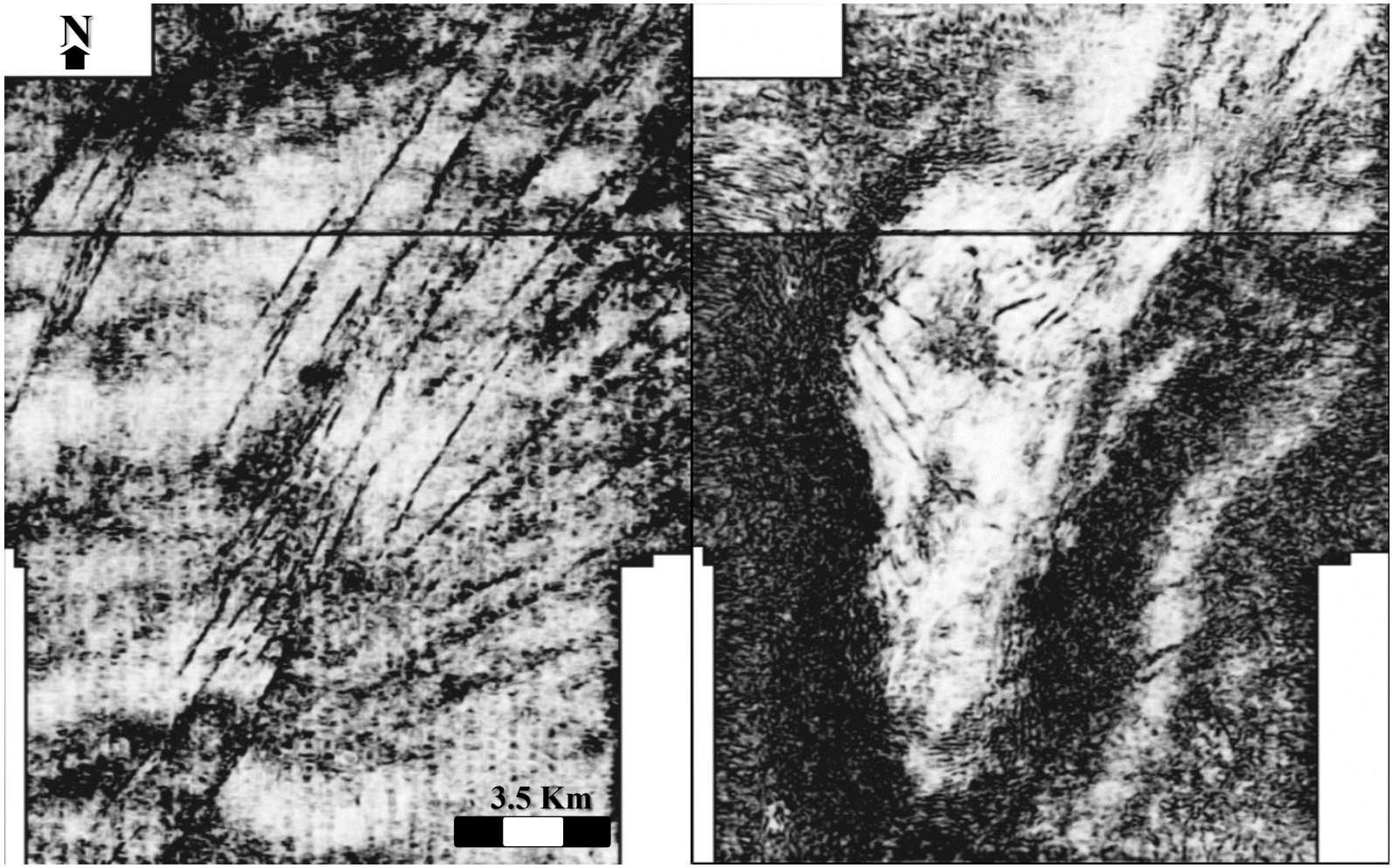

Figure 4.7. Dip variance attribute time slices. 1.156 s (left) and 2.8 s (right). Note the clarity of faults compared to the vertical slices in Figure 4.6. This is due to a lack of chaos in each respective laterally distributed trace.

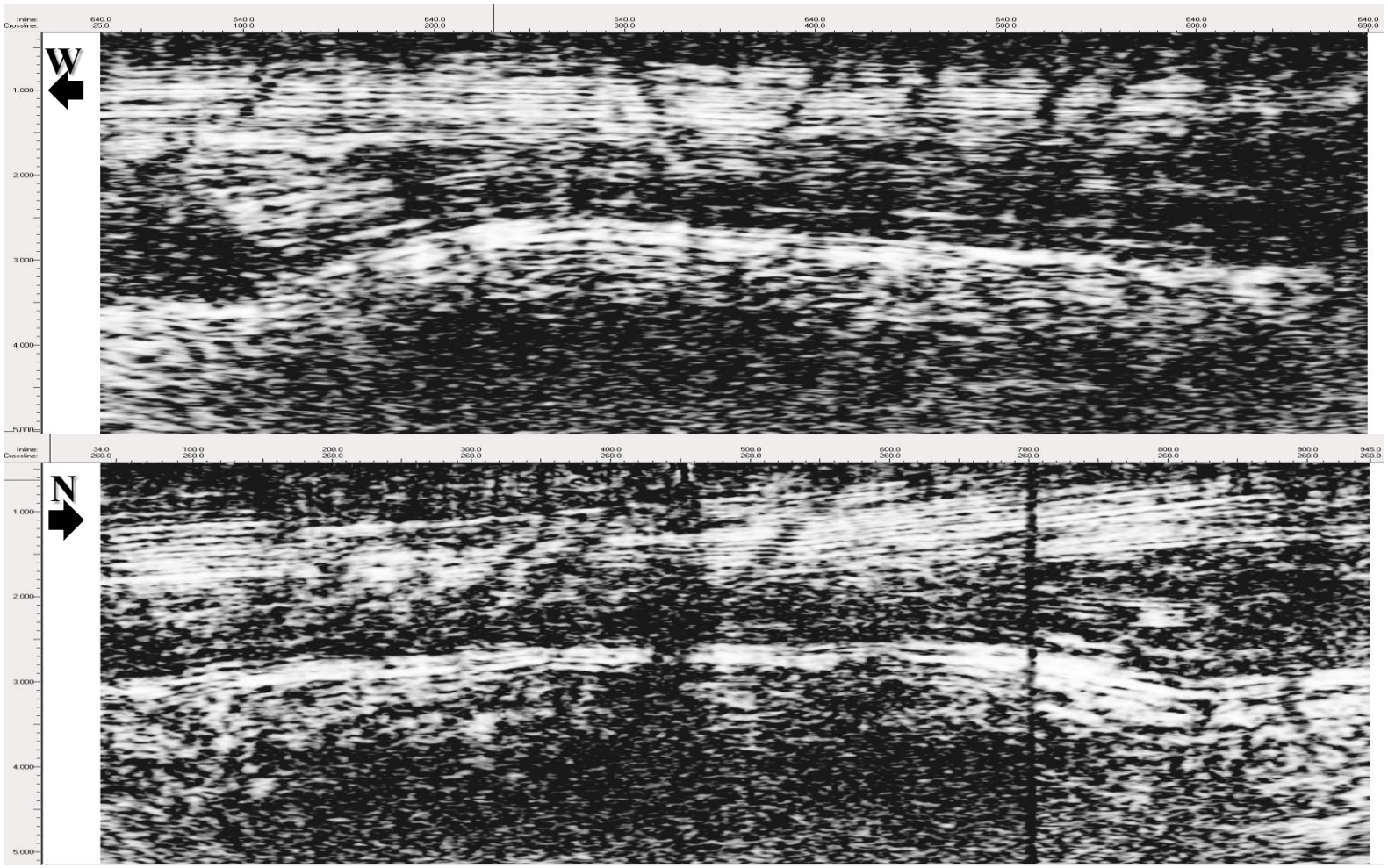

Figure 4.8. Chaos attribute. Inline 640 (above) and crossline 260 (below). Despite the ability to observe and identify the largest of faults within the sections, when compared to the dip variance attribute in Figure 4.6 these vertical slices show inadequate resolution.

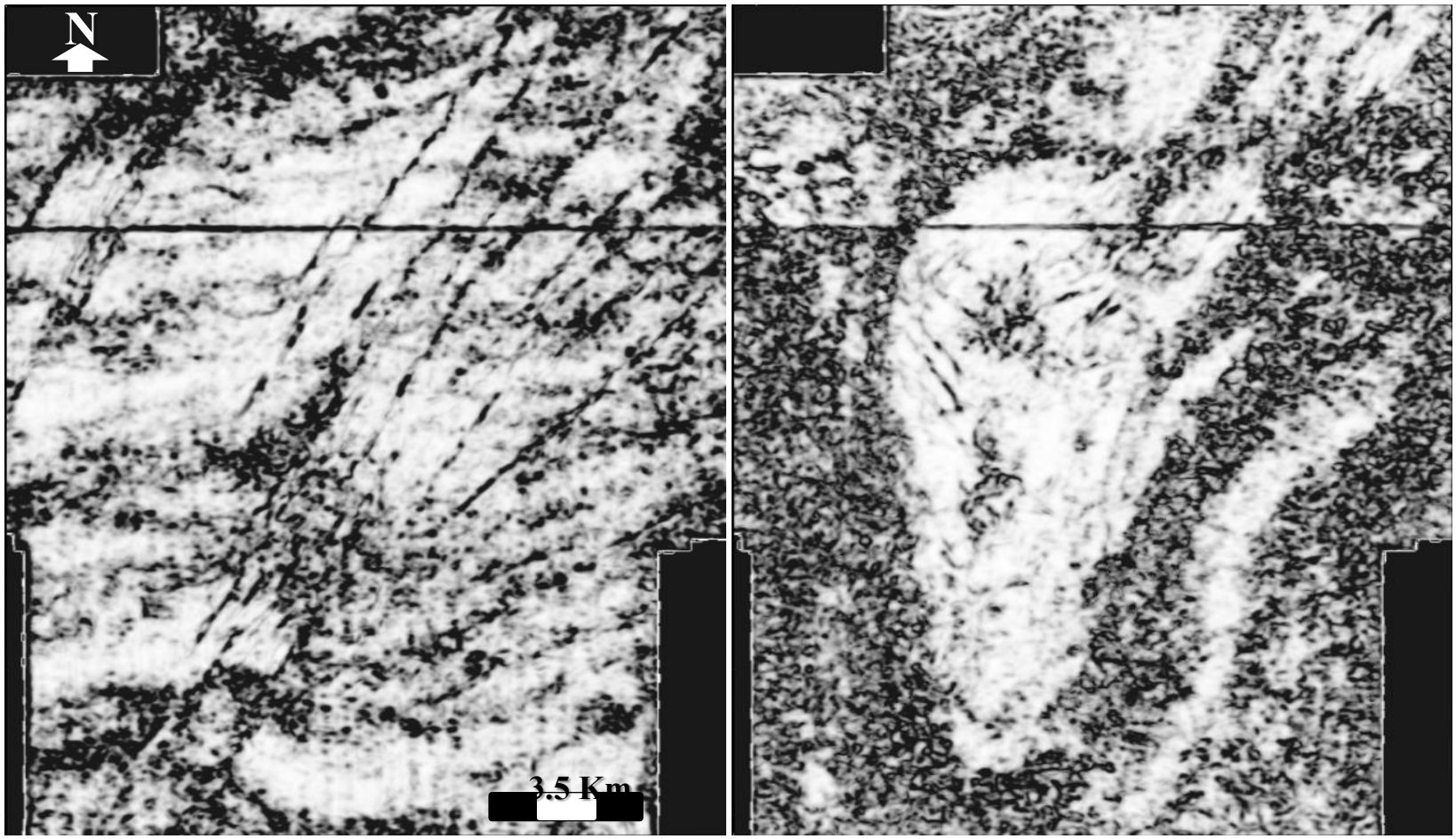

Figure 4.9. Chaos attribute time slices. 1.156 s (left) and 2.8 s (right). Note that similar to the variance attribute, the horizontal slices show greater resolution than the vertical sections. The overall resolution compared to the variance however is lacking.

To generate the symmetry attribute, a window size of 5x5 (inline x crossline) was used in conjunction with an overlapping time window (Z) of 0.04 seconds. Dip guiding was also utilized for the calculations, which allowed for only high angle faults (i.e. > 30°) which passed through more than one window to be considered. Just as the previous variance attributes, the dip symmetry calculations over the vertical components exhibited low resolution compared to the horizontal slices, as was expected. However, using the same color scheme which is displayed in Figures 4.10 and 4.11, alongside different variations in amplitude range, helped to identify smaller faults and potential gas chimney structures. This attribute's ability to do this was likely a benefit of "in house" processing which used different algorithms and formatting compared to the Petrel software. The resulting data files which were then set for Kingdom standards allowed for better visualization and manipulation compared to the Petrel processed attributes.

4.2.6. Envelope. The signal envelope (or simply the Envelope) is an attribute which demonstrates the reflection strength of a seismic trace. It is calculated using the simplified formula:

$$E(t) = \sqrt{(T^2(t) + H^2(t)}\,, \qquad (2)$$

where T(t) is the seismic trace and H(t) is the corresponding Hilbert transform of T(t). This attribute is mainly used by interpreters to identify bright spots, gas accumulation, major changes in boundaries/depositional environments, and porosity spatial correlations. Generation of the envelope for the Kapuni survey was conducted in the Petrel software. The final results are displayed in Figures 4.12 and 4.13. For the sake of visualization, a Hilbert filter window of 40 was used to create this attribute.

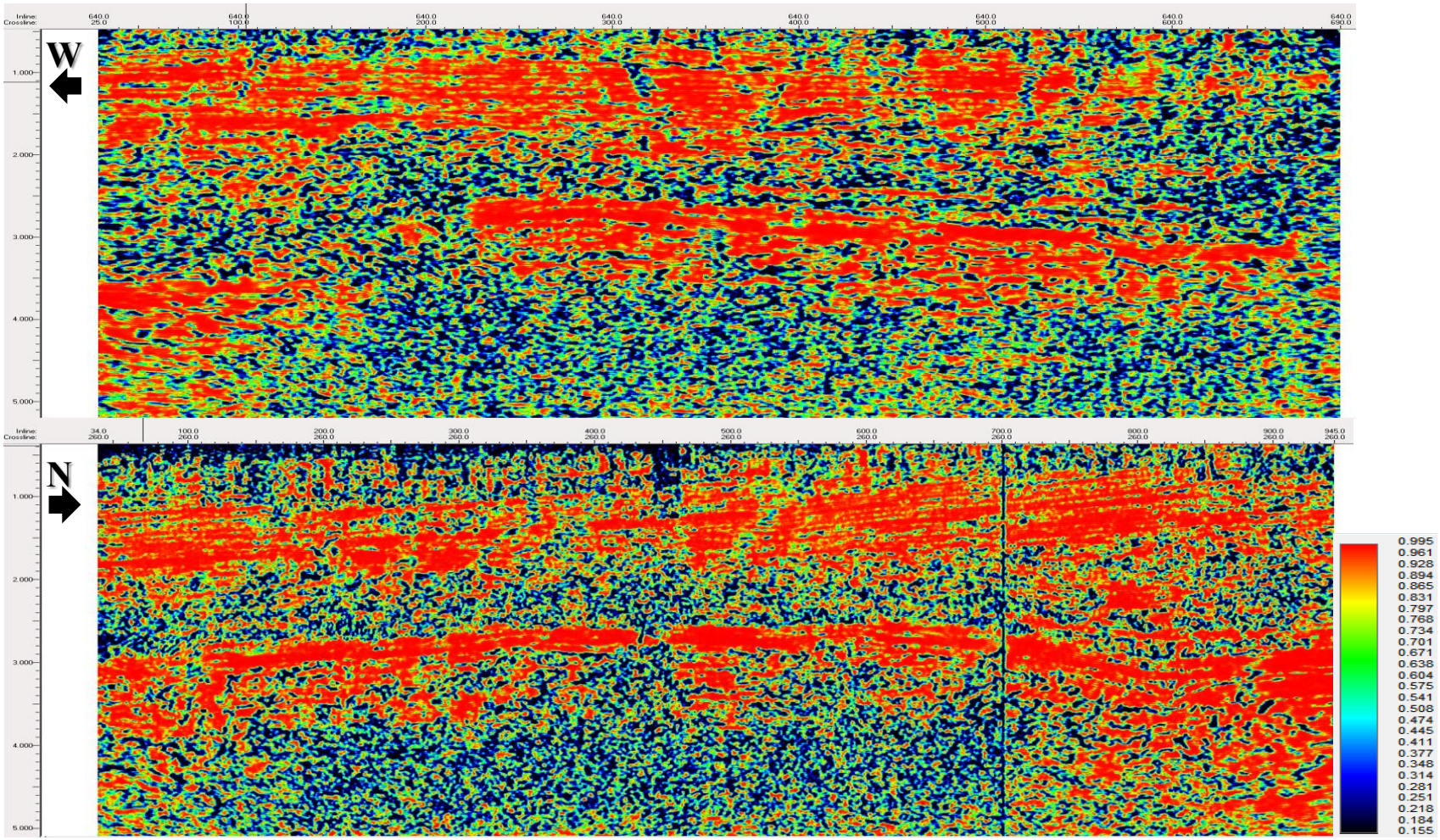

Figure 4.10**.** Dip symmetry attribute. Inline 640 (above) and Crossline 260 (below). Note the lack of coherency, just as in the variance and chaos attributes. The Kingdom software preset the corresponding color bar to highlight all possible amplitudes. Blue highlights are representative of areas which have the greatest chaotic natured reflections, or distinct seismic reflection

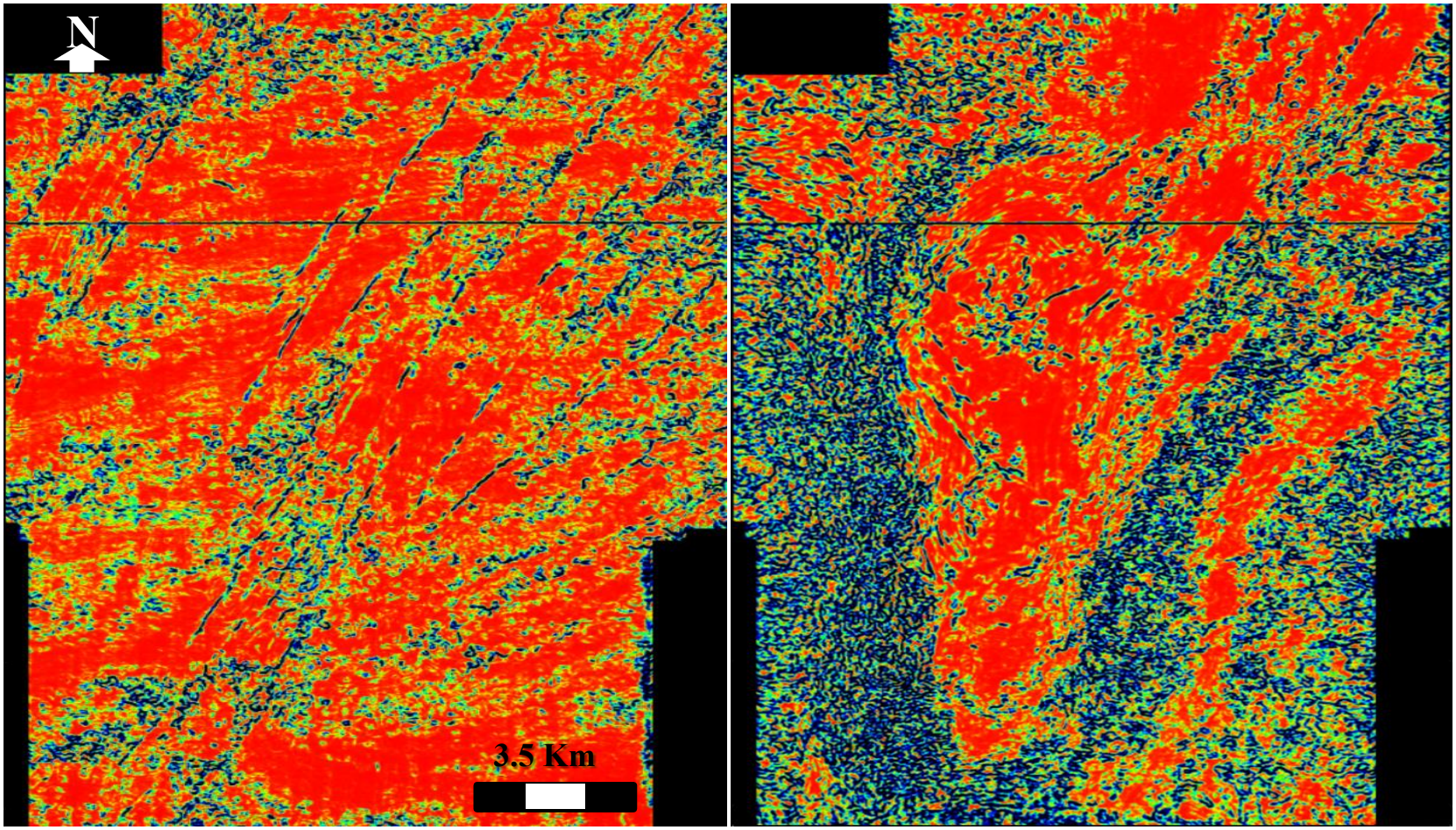

Figure 4.11. Dip symmetry attribute time slices. 1.156 s (left) and 2.8 s (right). Just as previous variance style attributes the horizontal slices provide better resolution compared to the vertical sections. This attribute however, along with the color scale, allows for a semblance of intensity, with chaotic and distinct surface reflections being displayed as blue and solid structure in red.

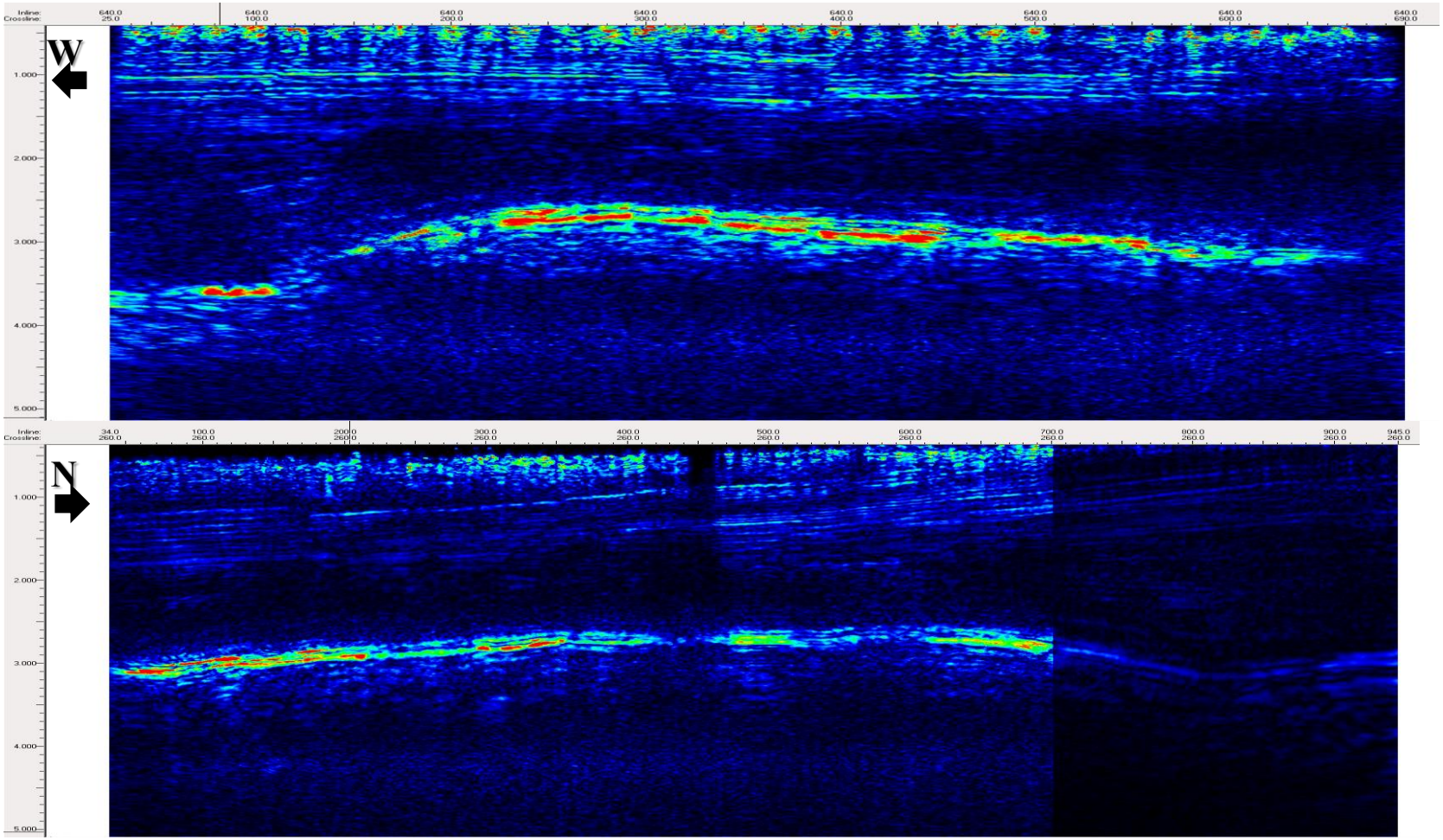

Figure 4.12**.** Signal envelope attribute. Inline 640 (above) and crossline 260 (below). Areas in red indicate bright spots within the system. Note that in crossline 260, the envelope intensity is drastically reduced in the artifact zone, making the use of such an attribute impractical for that area under high amplitude gains (as displayed here).

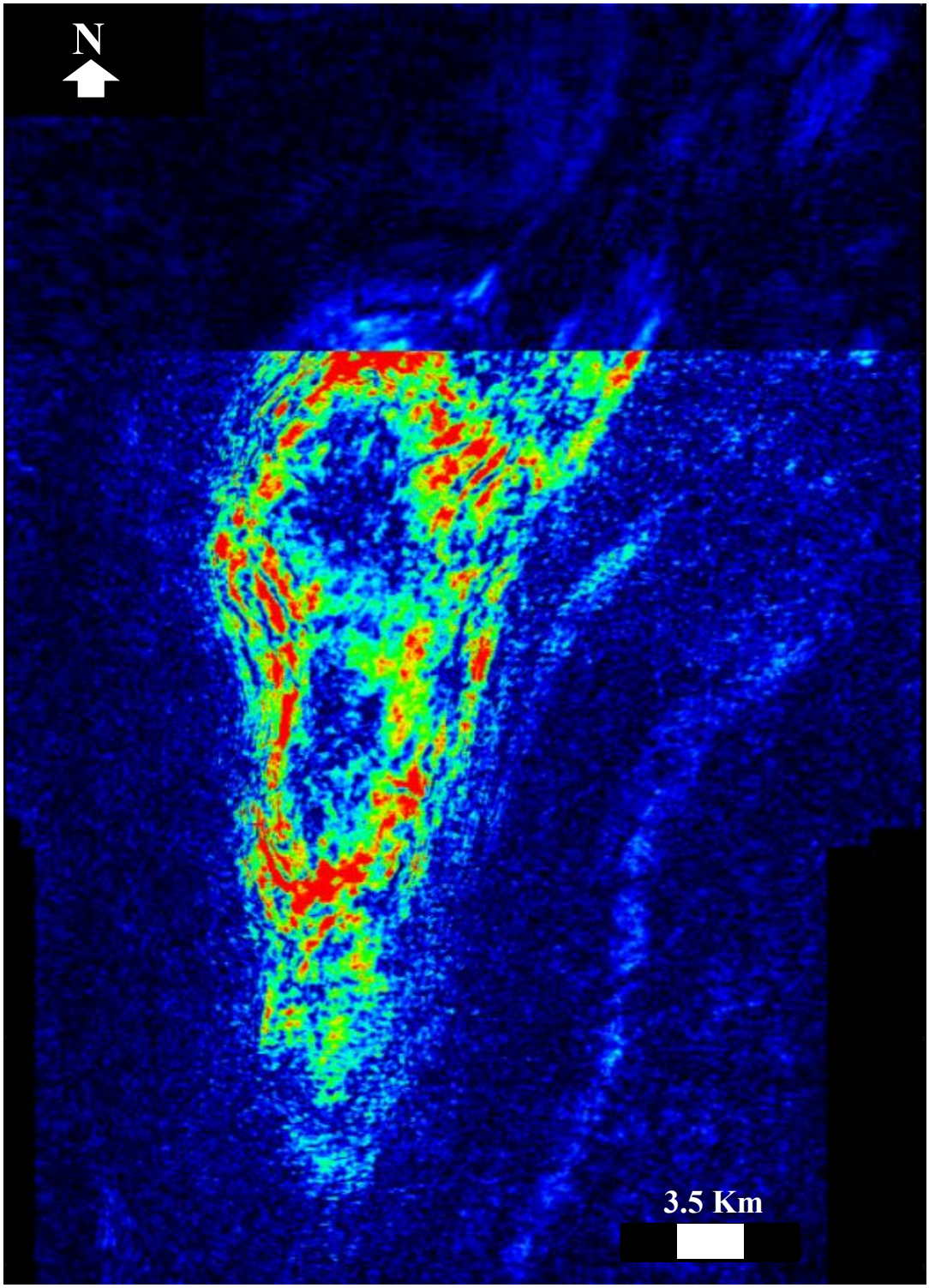

Figure 4.13. Signal envelope attribute time slice. 2.8 s. Note at the bright spots of the anticline encircle the structure as opposed to be centered within it.

This larger window allowed for cleaner resolution within the middle and lower Kapuni Group sediments, which contained excessively high reflection strength.

4.3. DIGITAL ELEVATION MODEL

For the identification of formation top and fault continuity as well as calculation of fluid flow within the system, several horizons and faults were generated and tracked through the 3D Kapuni survey. All horizons and faults were generated to the farthest extent which was both identifiable within the data cube and effective for further processing. All generated faults and horizons were used for final formulation and conclusion of the structural interpretation and fluid flow model.

4.3.1. Horizons. Four distinct horizons were identified and tracked in an effort to track tops of formations and structures which prove crucial to the construction and constraint of the proposed fluid flow model as well as the characterization of the play. All horizons were generated within Kingdom via combination of manual selection and the sub-automatic 2D seek function. The horizons were tracked to the southernmost extent, to which any confluence of fluids would have accumulated away from the northern lobe of the anticline. Any picks south of Inline 375 were truncated during processing and gridding of the horizons.

Each horizon was picked at an inline interval of five (meaning the horizon was picked once every fifth inline), and a crossline interval of five. This interval resulted in a final resolution of approximately 250 m^2. In order to increase the resolution and generate properly formatted digital elevation models (DEMs), the horizon files were gridded within Kingdom. The gridding process imported the horizons in depth measurements of time, as depth conversion was not possible due to lack of reliable T-D charts and

program licenses, and constrained by a polygon which truncated any data south of inline 375. The process utilized the Natural Neighbor gridding algorithm over a pixel resolution of 40 m^2. In using this gridding algorithm, accurate resolution is possible as the natural neighbor method allows for the underlying "true" transition of depth to be visualized. Upon completion of the calculations, the final grids were exported as an "irregular XYZ" data format. Though this method of exportation did not allow geographic metadata accompaniment, it allowed transcription of the projection's x and y components for each pixel. As a consequence, the files retained the ability to be imported into GIS based software and be transposed into correct geodetic position with manual datum and projection input. These final exported DEMs were later used in the construction of the proposed fluid flow model.

4.3.2. Interpreted Faults. For the use of both structural interpretation and fluid flow model construction, multiple faults were picked, delineated, smoothed, and gridded. All fault surface were picked in the same 5x5 resolution as the horizons, however many faults required use of arbitrary lines for accurate tracking (Figure 4.15). Each fault was picked manually and consequently tracked to the furthest possible extent through correlation with dip variance, chaos, dip symmetry, and instantaneous phase attributes. Due to the low seismic character within section B most faults could not be tracked within the upper Kapuni segments or through the Farewell Formation, located in the lowest Kapuni strata.

Once all faults were picked, they were smoothed in order to remove outliers and interpreted. Fault throws along the interval of specified faults were calculated to assess fault direction and displacement. Faults which provided potential impact upon the

proposed gas chimney were considered with a higher degree of scrutiny. The Tuikonga fault system displayed (Figure 4.15) was used for the fluid flow model due to its relation to the gas chimney structure. Due to the fault systems significance filtering of individual faults was necessary in order to identify weak zones which would act as a pathway for hydrocarbon migration. After correlation with attributes and selection of significant segments, the same gridding process employed in horizon exportation was utilized for the faults.

4.4. HORIZONS AND SURFACES

Although the well logs provided multiple formation tops, only four surfaces of interest were selected for further study and interpretation; the detachment surface proposed by Voggenreiter (1993), the true top of the anticline, and the capping tops of Kapuni cycles B and A respectively. These surfaces were chosen due to the significant roles they play in both the analysis of fluid migration as well as their importance to the overall structure and hydrocarbon system. Horizons of Kapuni cycles B and A are treated as near perfect impermeable capping surfaces when used for the fluid flow model in Section 5.

4.4.1. Detachment Surface. The detachment surface proposed by Voggenreiter (1993) was observed and tracked to a limited extent in this study (Figure 4.14). This horizon was not picked and tracked to the same limits as the others due to its discontinuous nature within the seismic sections. Voggenreiter (1993) stated that the faults which lie above the anticline cannot be seen within the area that this study entitles seismic unit B, suggesting that there must be a detachment surface which directly inhibits any fault from propagating into the anticline. That hypothesis is supported by

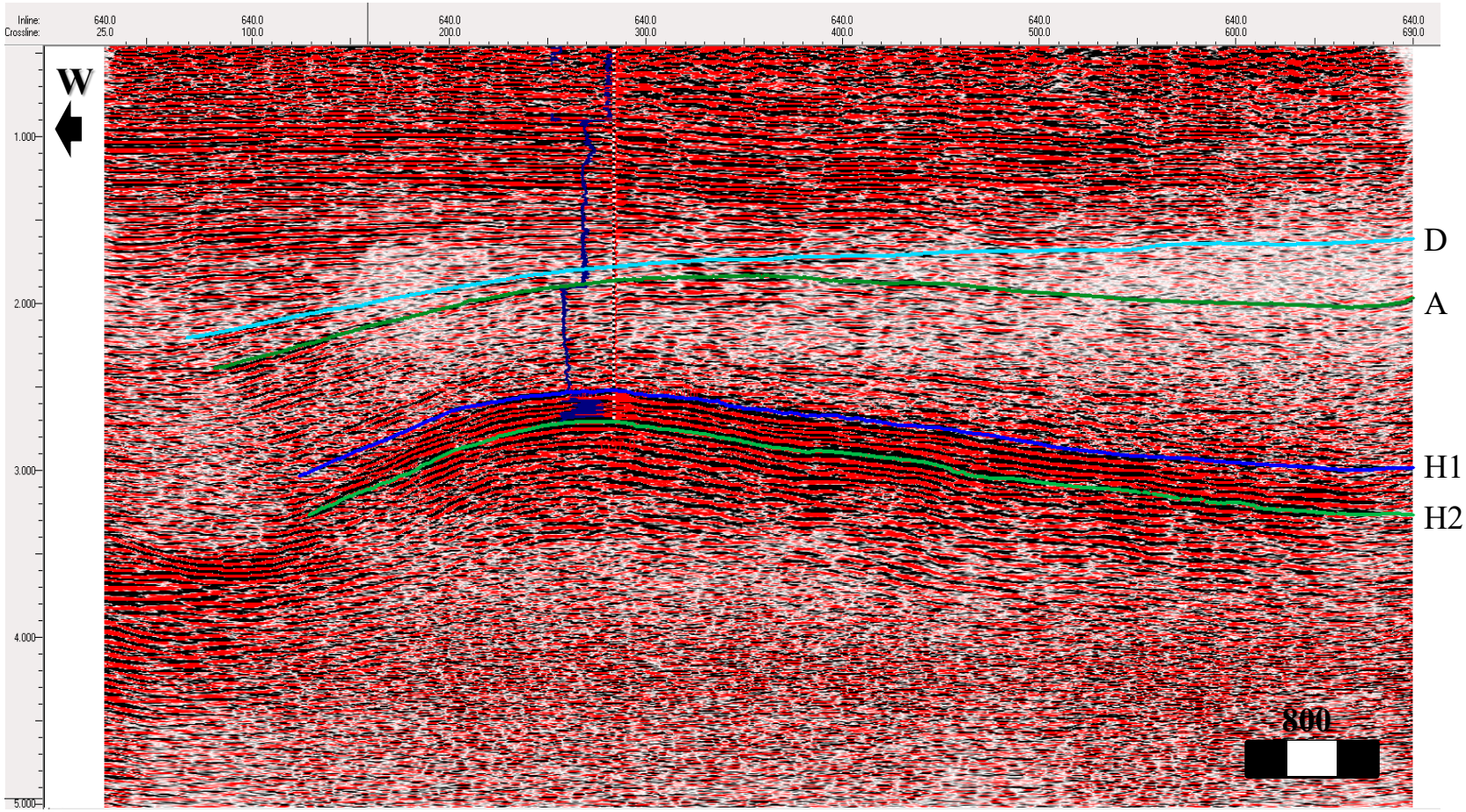

Figure 4.14. Interpreted horizons within inline 640. The light blue line designated D is the proposed disconnect surface described by Voggenreiter (1993). Green line (A) represents the proposed true top of the anticline structure. Horizons H1(blue) and H2 (green) represent the top of Kapuni cycle B and A respectively, and are consequently used for the fluid flow model interpretation and processing. The Caliper (dark blue) well log is displayed and was extracted from Kapuni-8.

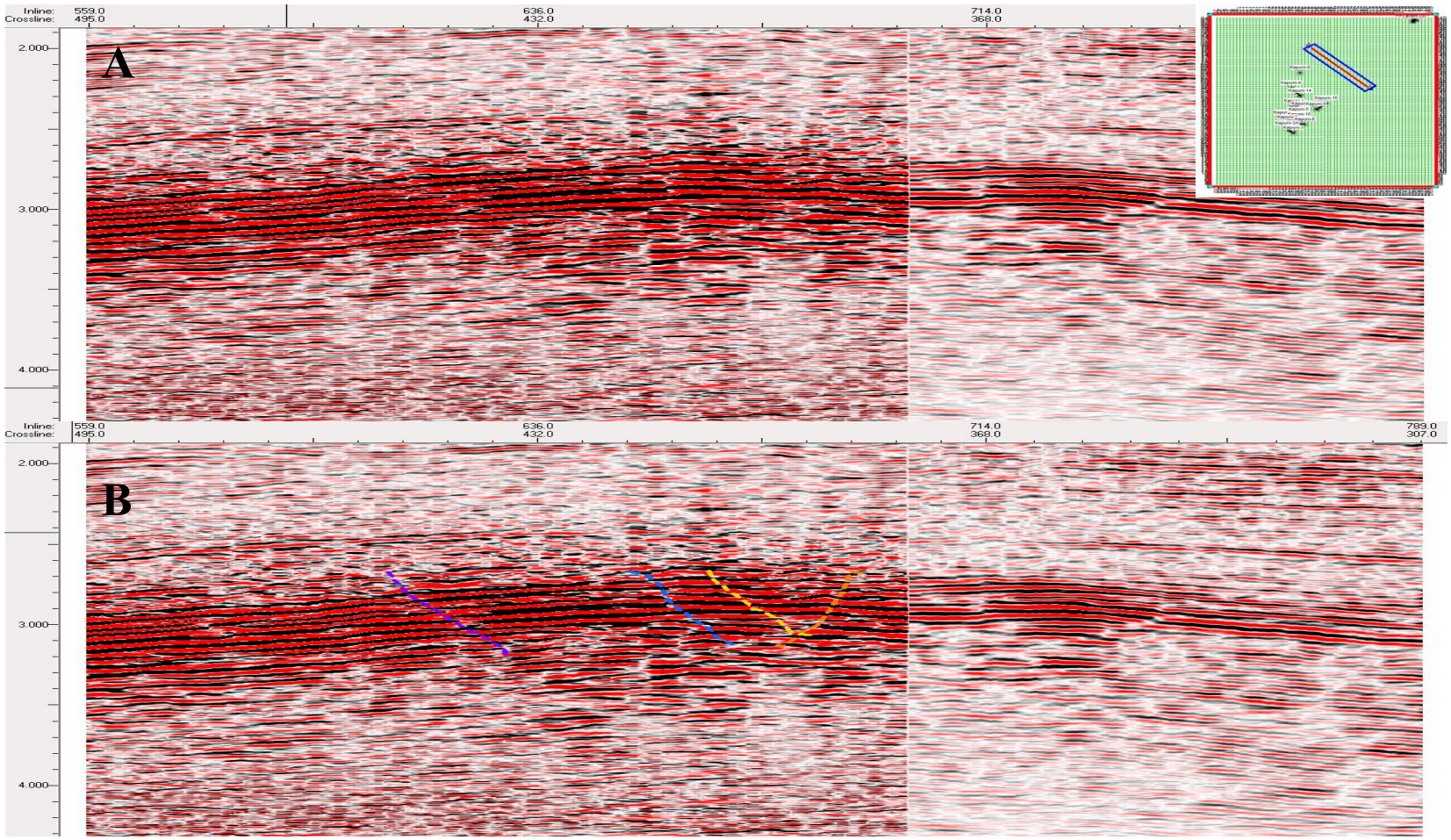

Figure 4.15. Fault picking along an arbitrary line. Image A exhibits a portion of the line before faults were pick, image B shows the picked fault surfaces as they trend through the vertical section. Both image A and B are of a single arbitrary line which was digitized through the survey. Such a display was necessary for picking the faults displayed as their trend did not align with either inlines or crosslines.

interpretation of faults within the upper seismic section A which appear to terminate at specified, progressive depths. This concept is not supported however by any well log data, as stating in Voggenreiter (1993).

Upon inspection of the reports from wells surrounding Kapuni-8, the lithology of formations around and below the proposed detachment consist of a variety of sandy mud and siltstones with interbedded, fine grained, and sub angular sandstones. This lithology both falls in line with the chaotic reflections seen within seismic section B and holds potential for a pseudo detachment surface. Due to the impure nature of the lithology, the interaction of transtentional forces within the northern portion of the survey, and overpressure of migrating fluids from deeper sources, the concept of a pseudo detachment is probable. The extensive interbedding and consequential variation in density and poor space which exists within the surrounding lithology provides difficulties in processing of the seismic section, resulting in the observed chaotic reflections with dispersed minor seismic clarity. As a consequence, it becomes difficult to discern the extent of above section faults without correlation with seismic attributes, as conducted by this study. As indicated in Figure 4.16, some of the faults show extended propagation into the formations below the supposed detachment, however tracking of some faults proved that the depth of penetration along trend varies greatly. In some cases the truncation of the fault was observed to be above the pseudo detachment by tens of meters, but be hundreds of meters below the surface following the north eastern trend. This could indicate other variables such as overpressure or differential far-field force vectors acting as a determinate of oblique fault extent. All these facts and

variables corroborated apt to infer not a solid detachment, but a pseudo detachment which acts more as a buffer zone for the extensional regime above the Kapuni anticline.

4.4.2. Anticline Top. This horizon was tracked using a correlation of Time-Amplitude vertical sections alongside seismic attributes such as instantaneous phase and instantaneous frequency. The final DEM (Figure 4.17) represents the interpreted top of the anticline and consequently the tectonic shift toward regional compression during the Late Eocene and Early Oligocene.

In vertical cross section, the on-lap of newer sediments from the Moki Formation (post uplift) above this surface are visible along the westernmost segment of the hanging wall, which aided in the interpretation of the surface. These on-lapped sediments are also visible when observing the full transition from local compression to extensional regime (Figures 2.4 and 3.2.), The top of the anticline is not highly debated within publications regarding the Kapuni Field as the distinction is quite clear in both seismic section and core logs.

4.4.3. Kapuni Cycle B. This horizon (Figure 4.18) is interpreted to be the uppermost capping shale/coal layer within the Kaimiro Formation, not the true top of the Kaimiro. According to the well report of Kapuni Deep-1, this coastal-marginal marine cycle which lies between 3843 – 4553 m deep was the original target of early drilling. However, upon penetration of the lowermost interval the formation was found to be highly water saturated with significant hydrocarbon indications in sidewall cores. This horizon contains multiple faults which vary in nature from normal to reverse and include the significant Tuikonga faults (Figure 4.19). The introduction of these faults to this surface allow for water and hydrocarbons beneath the capping

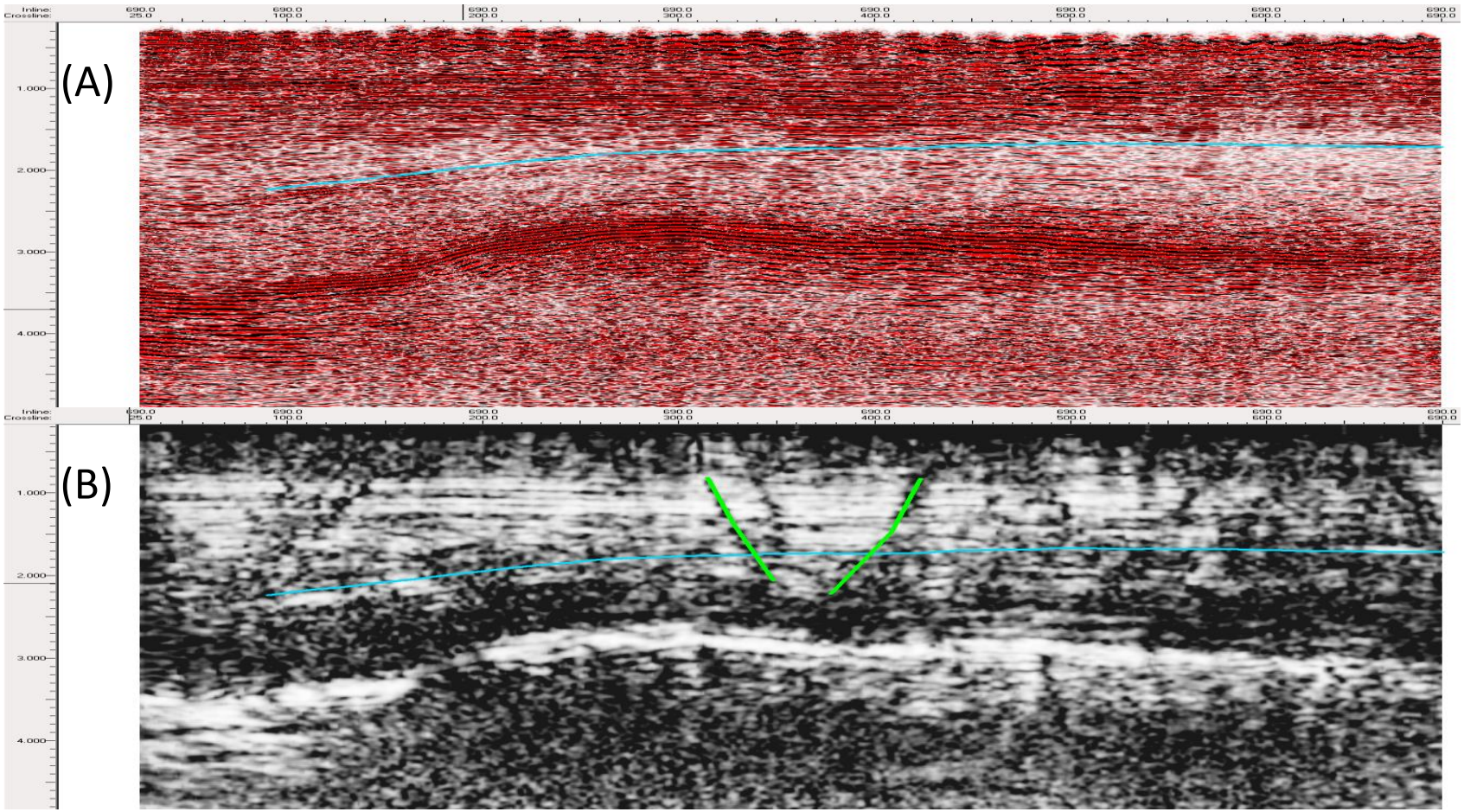

Figure 4.16. Fault and detachment surface tracking. Inline 690. The dip variance attribute of the inline below in (B) displaces the traces of the detachment surface and two faults that continue to propagate below said surface. The blue horizontal line represents the traced result of the proposed detachment surface, as tracked by the baseline Time-Amplitude seismic sections. The green vertical lines are two of the traced Mangatoki faults. Note how the faults cannot be traced in the Time-Amplitude section in (A).

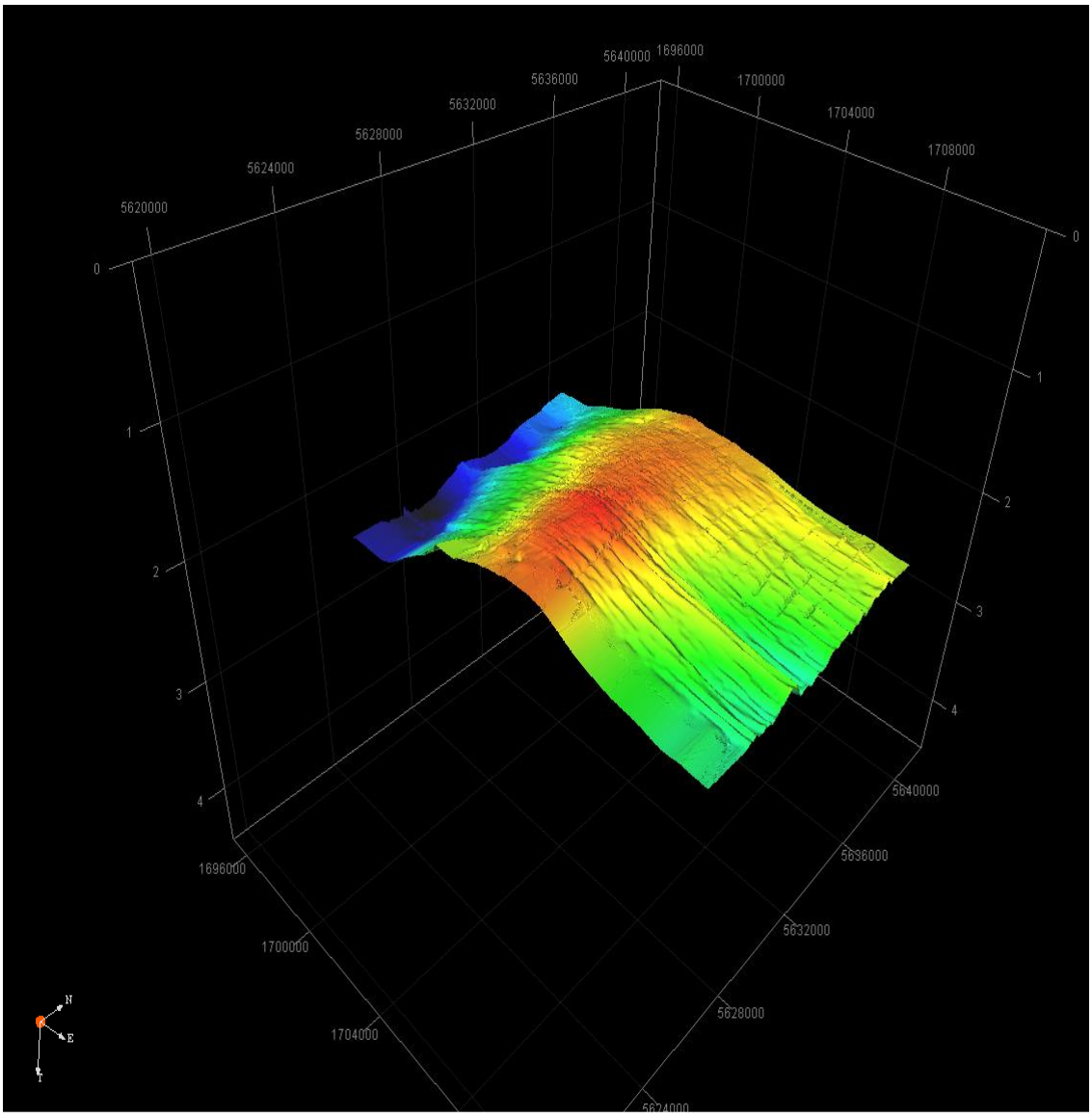

Figure 4.17. 3D DEM of the Anticline Top horizon. Note the larger lobe to the south. This was the first area of interest to be drilled during the anticlines discovery post 1959. The steep slope toward the western edge is indication of the prevailing major fault, the Manaia. This westernmost section of the hanging wall contains numerous faults but due to the relative minor displacement of these faults and resolution of this surface in vertical section, they are not easily discernible, even through use of Iso maps.

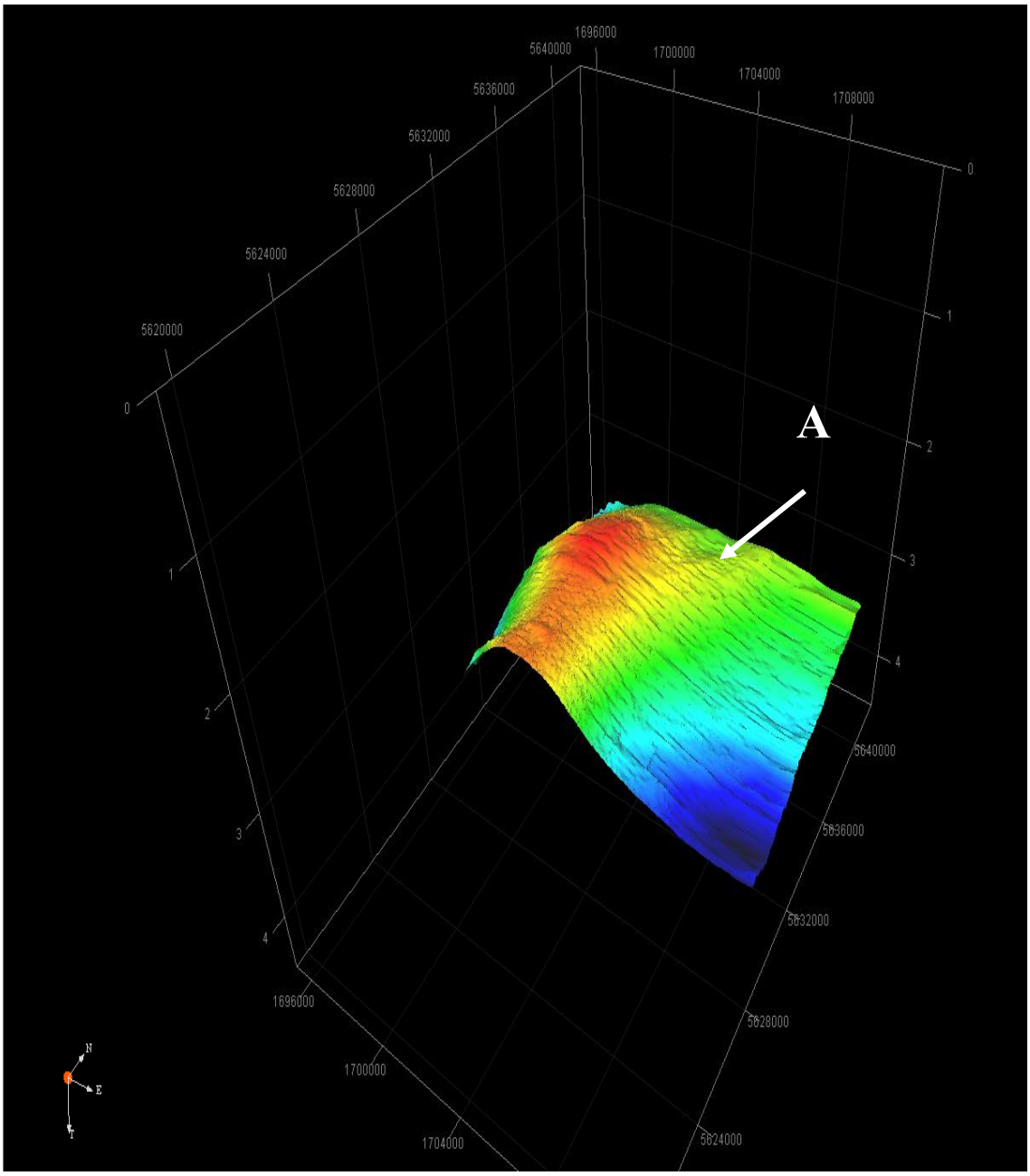

Figure 4.18. 3D DEM of the Kapuni Cycle B horizon. Note that the peak of the horizon is within the northern segment as opposed to the anticlines peak being in the south. The relatively high area around A indicates the area which is uplifted by the Tuikonga fault system.

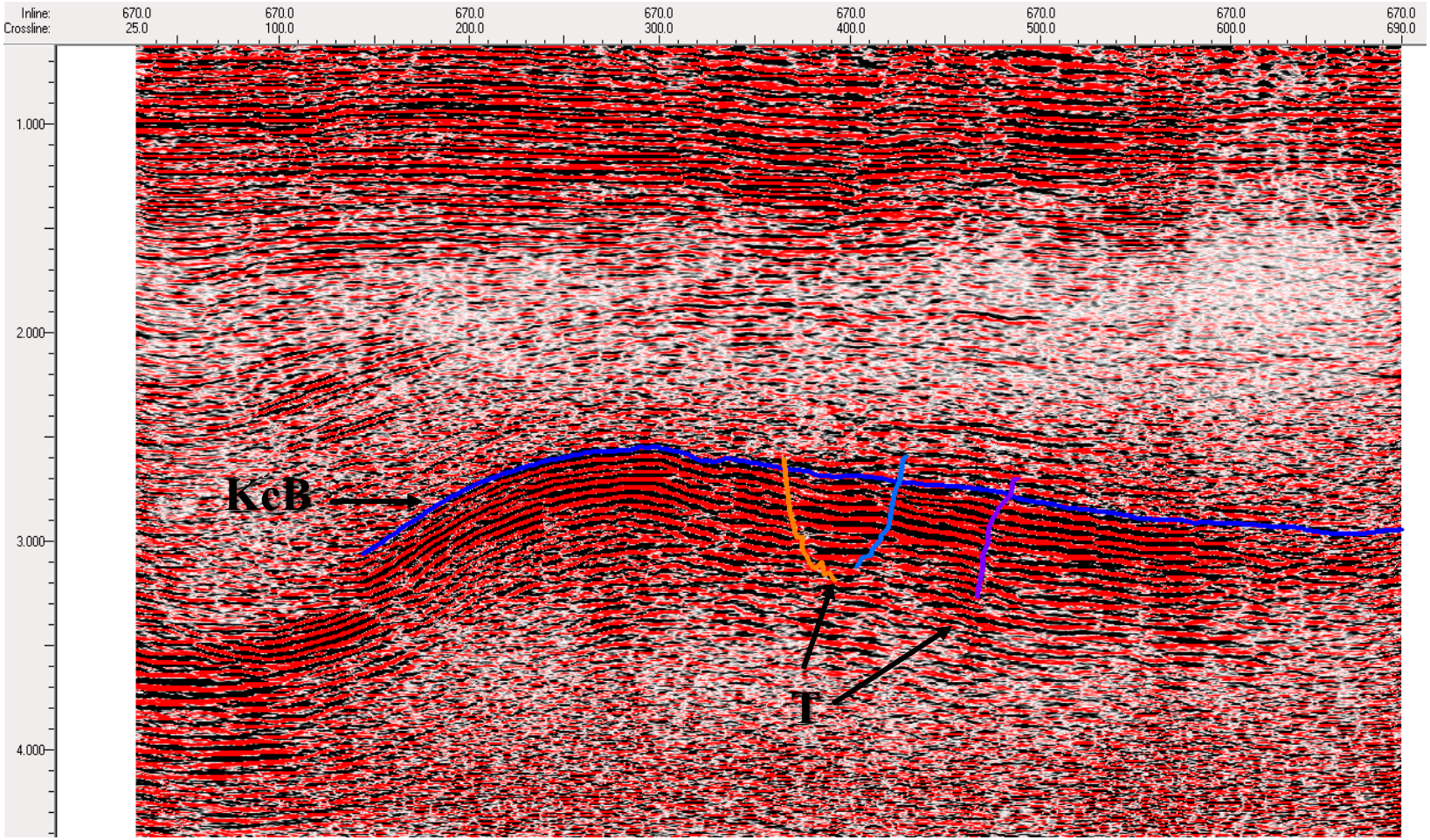

Figure 4.19**.** Horizon and fault interpretation of inline 670. The blue horizon KcB is the extent of Kapuni Cycle B. The three faults indicated as T are three of the four interpreted Tuikonga faults. Note how they cut through the KcB horizon.

surface to migrate further up sequence into multiple reservoirs. Though the interpretation of this surface could have been continued into the foot wall of the Manaia Fault, any and all fluids migrating from that segment of the formation would be lost in the large area encompassed by the fault or trapped underneath it. This negates the need to add such an extent to the final horizon interpretation.

4.4.4. Kapuni Cycle A. This horizon is interpreted as the relative top of the Farewell Formation and the lowermost idententifiable capping layer of shales and coals within the seismic data. As seen in Figures 4.20 and 4.21, this horizon contains a definitive peak at its northernmost extent and is cut by several Tuikonga system faults. The coastal cyclothem lies at a depth interval of 4553 – 5664 m whilst the interpreted horizon peaks at 4890 m below the Kapuni Deep-1 well.

According to well reports, this cycle showed great promise for hydrocarbons with a saturation of >40%. The potential of this cycle was diminished by the existence of a heavy kaolinite cement which reduced the porosity by up to 97% in some cores. However, secondary porosity is extensive and in conjunction with multiple carbonaceous and shale lenses infers great potential as a source cycle. The lowest interval of the cycle which was drilled indicated good oil staining along multiple fractures, enhancing the source potential.

4.5. FAULTS

The structural interpretation and fluid flow model portion of this study both necessitate the delineation of major faults within the 3D Kapuni survey. Due to the immense number of faults throughout the survey, only faults which contribute to the

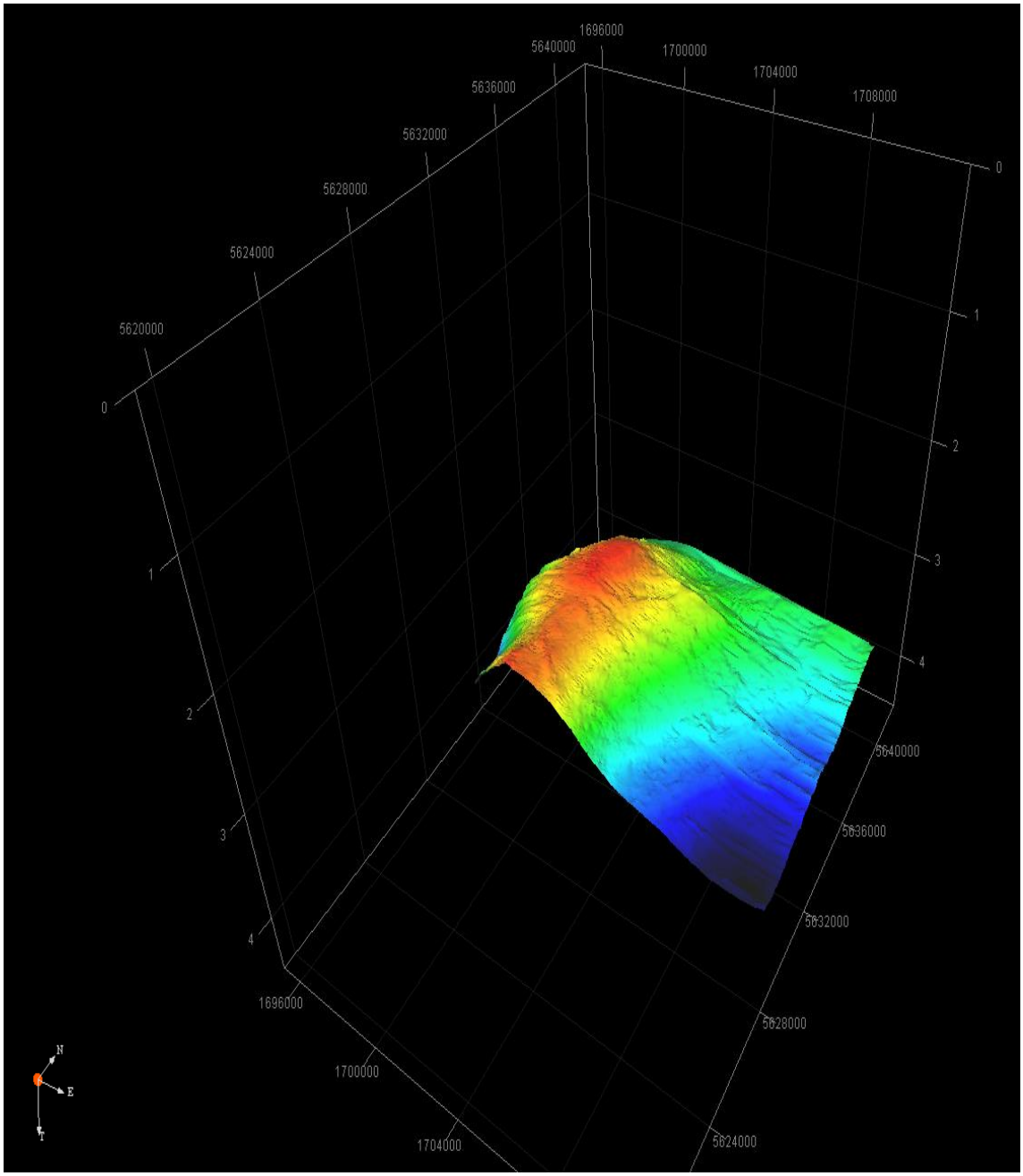

Figure 4.20. 3D DEM of Kapuni Cycle A horizon. Note the sudden topography change at A, this is likely due to the excessive number of faults in the area as well as in vertical section.

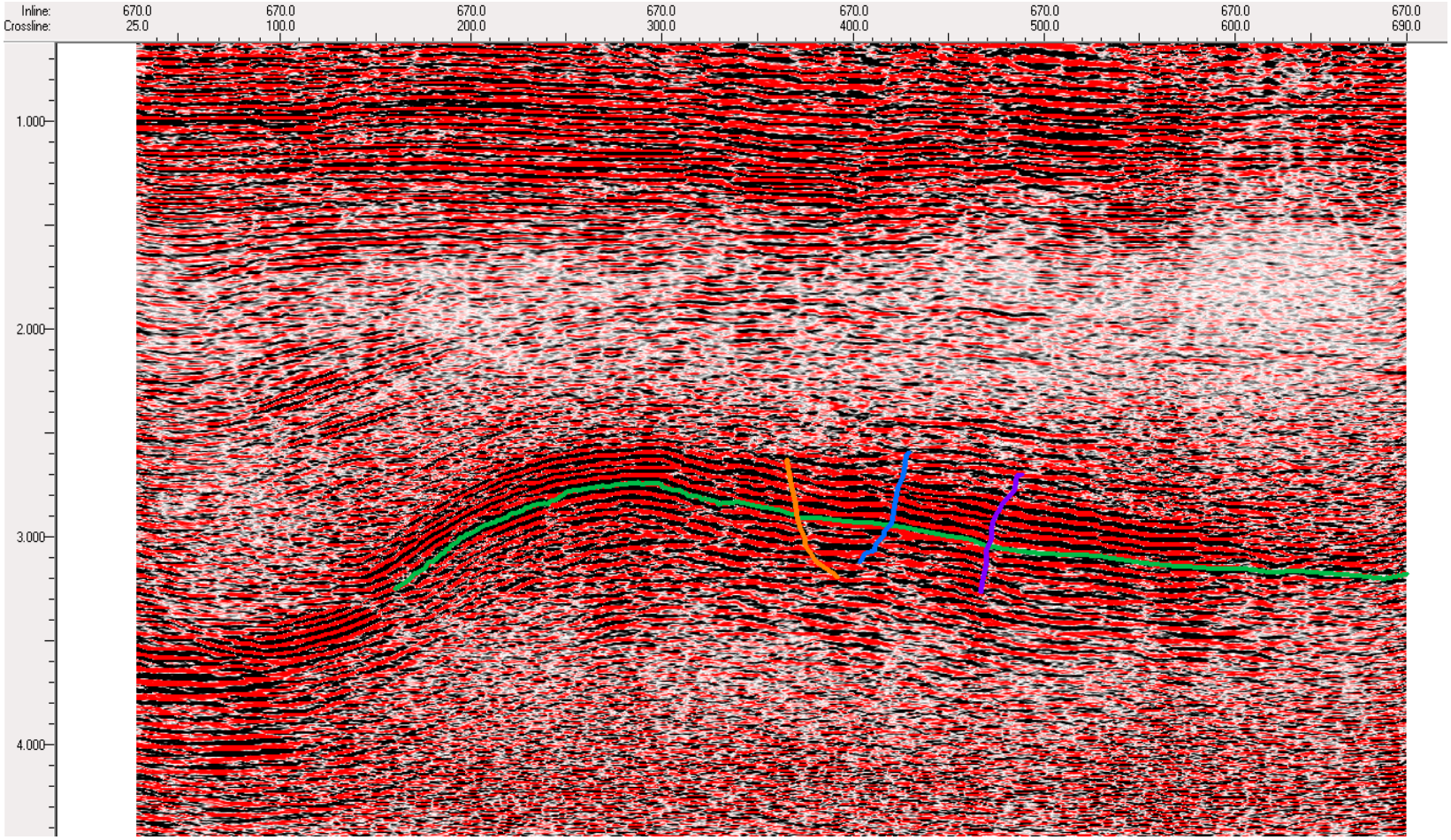

Figure 4.21. Horizon and fault interpretation of inline 670. The green horizon indicates the extent of the Kapuni Cycle A horizon. Fluids from multiple layers below this point channel through this horizon by the use of the Tuikonga fault system.

northern half of the data cube and model where considered and tracked (with exception of the Manaia). The main fault in the system is the Manaia Fault whose compressional force drives the propagation of all compressional and transpressional faults found within the study area, including the Tuikonga transpressional system (Figure 4.22). The existence of the many faults has produced structural traps within the anticline. Voggenreiter (1993) described how several faults and fault systems within the anticline provide substantial barriers for hydrocarbon flow. These faults however contain a much stronger compressional component than the Tuikonga fault system due to their location within the hanging wall (Figures 4.23 & 4.24). Many of the younger faults found in the upper strata of the survey (seismic unit A) could not be identified past the top of the anticline structure due to the nature of the overlaying mudstone-rich layers.

4.5.1. Manaia. The Manaia Fault is the main driving force of all local tectonics within the study area and is considered to be an active reverse fault which originated during the Late Eocene – Early Oligocene uplift of the Taranaki Fault. An average throw of approximately 3 km is regularly observed in this study area along with an eastward dipping, high angle strike. A debate of this fault's activity persists and stems around the observation that the majority of seismicity is recorded to the east of the fault at low frequency and great depth (15-40 km). Due to the depth extent of the Manaia Fault however (~20 km), it continues to be considered an active fault. The Manaia Fault is often cited as being a distinct terrane boundary due to its size, paleo-tectonics, and resultant anticline (King & Thrasher, 1996; Higgs et al., 2013; Reilly et al., 2015). However some subsurface studies have suggested that this major fault and terrain

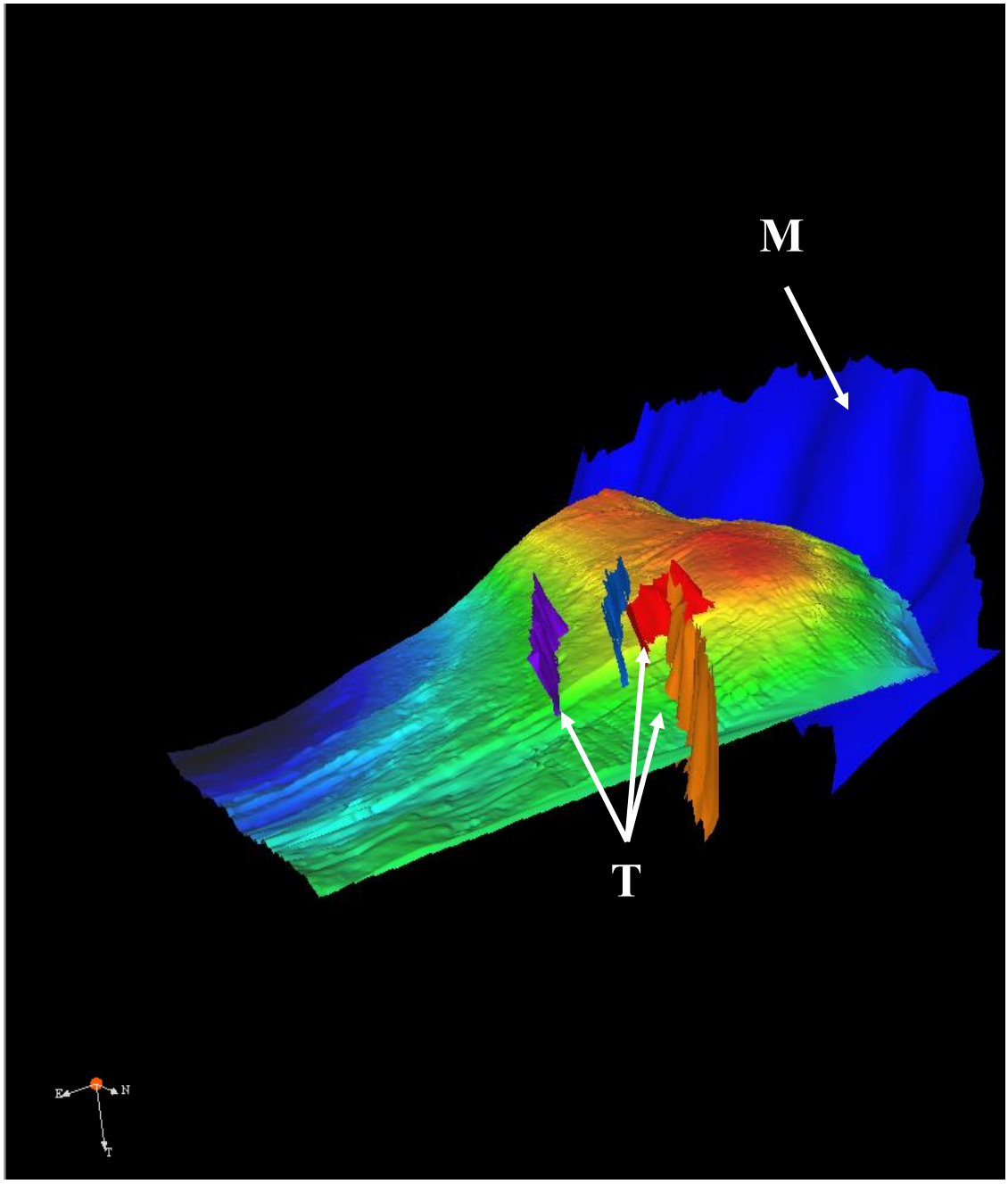

Figure 4.22. 3D display of significant faults intersecting Kapuni Cycle A horizon. M indicates the traced Manaia Fault and T denote the major Tuikonga faults. Note the angle that the Tuikonga faults trend against the Manaia Fault.

boundary is actually the northernmost extension of another major fault, the Waimea Fault (Figure 4.23) (Beck 1964, Johnstone 1996).

For this study, the Manaia Fault was traced to the farthest reasonable extent within the survey. As seen in Figure 4.24 the fault extends across the entire westerner border of the survey and maintains a north-south trend until it reaches the zone around the Kapuni northwest fault system (approx. inline 620) , where the trend transfers to a northeastward trend before observable termination. Upon inspection of the trends of the hanging wall faults (Tuikonga, Kapuni NW, and Mangatoki), it was observed that each fault system's trend and displacement was based on two distinct force vectors which result from the Manaia's sudden trend redirection. It's observed that the Tuikonga system parallels the northeast trending segment of the Manaia while the Kapuni NW system (due to it confluence location) is prone to both vectors and as such generates a more complex, mixed bundle of trends and displacements. The westward force vector (Figure 4.24) is likely the more dominant force however, as it falls in line with the general movement from the large Taranaki fault to the east and the Waimea Fault to the south (Figure 4.23).

4.5.2. Tuikonga. The Tuikonga Fault Zone is one of two fault systems of interest for this study. It is located in the north eastern sector of the survey and is identifiable in vertical seismic section to a max time/depth of roughly 3.26 seconds (or ~ 5670 m). This fault system visibly displaces the majority of the Kaimiro Formation and likely extends upward through the Mangahewa, and downward into the Farewell Formation. The true extent of these faults are however unconformable due to the poor imagery in the Mangahewa and Farwell formations.

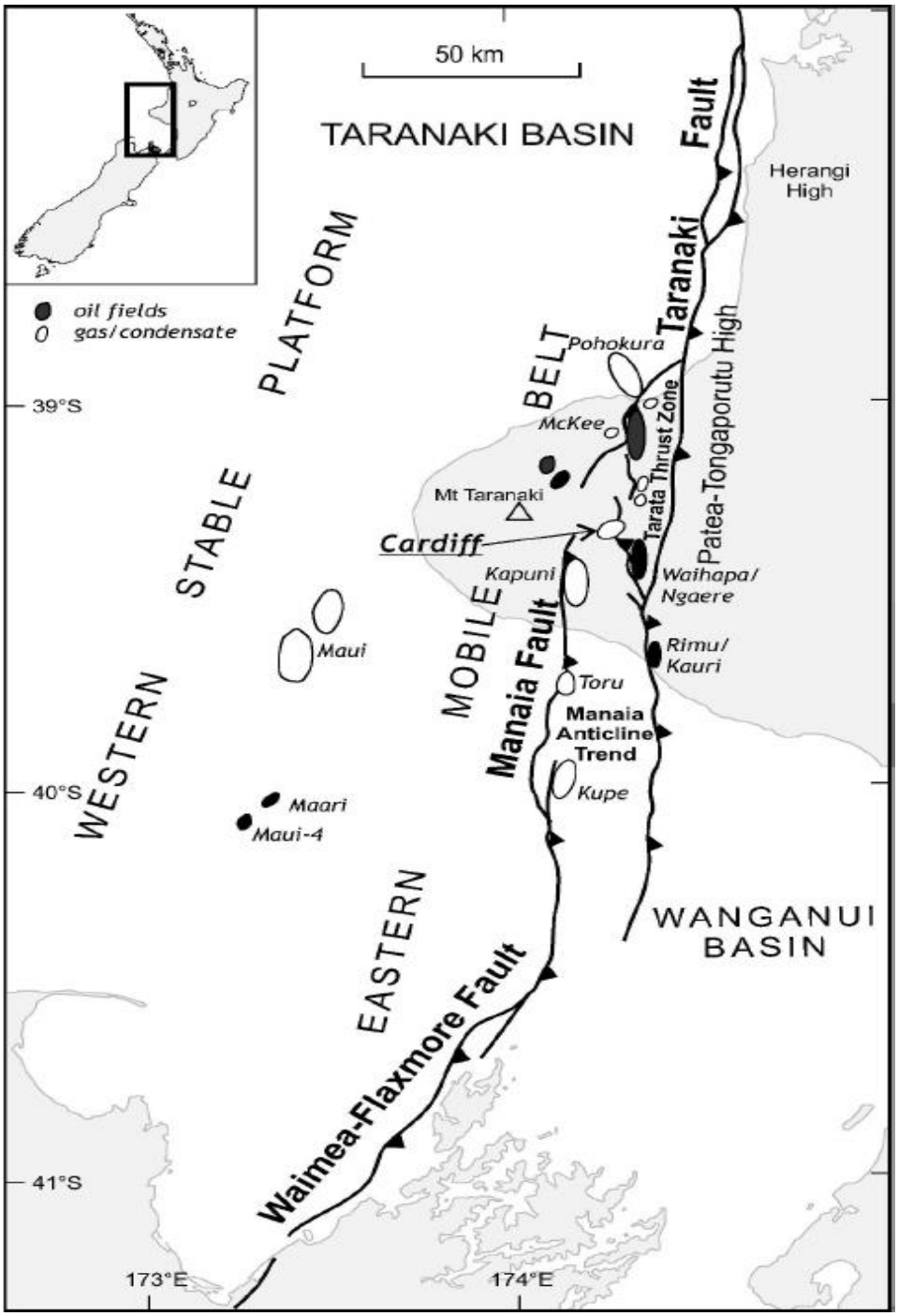

Figure 4.23. Major faults within the Eastern Mobile Belt. Note the connection between the Waimea-Flaxmore and Manaia Faults and how the Manaia truncates toward the north east. (Modified from Higgs et al., 2013).

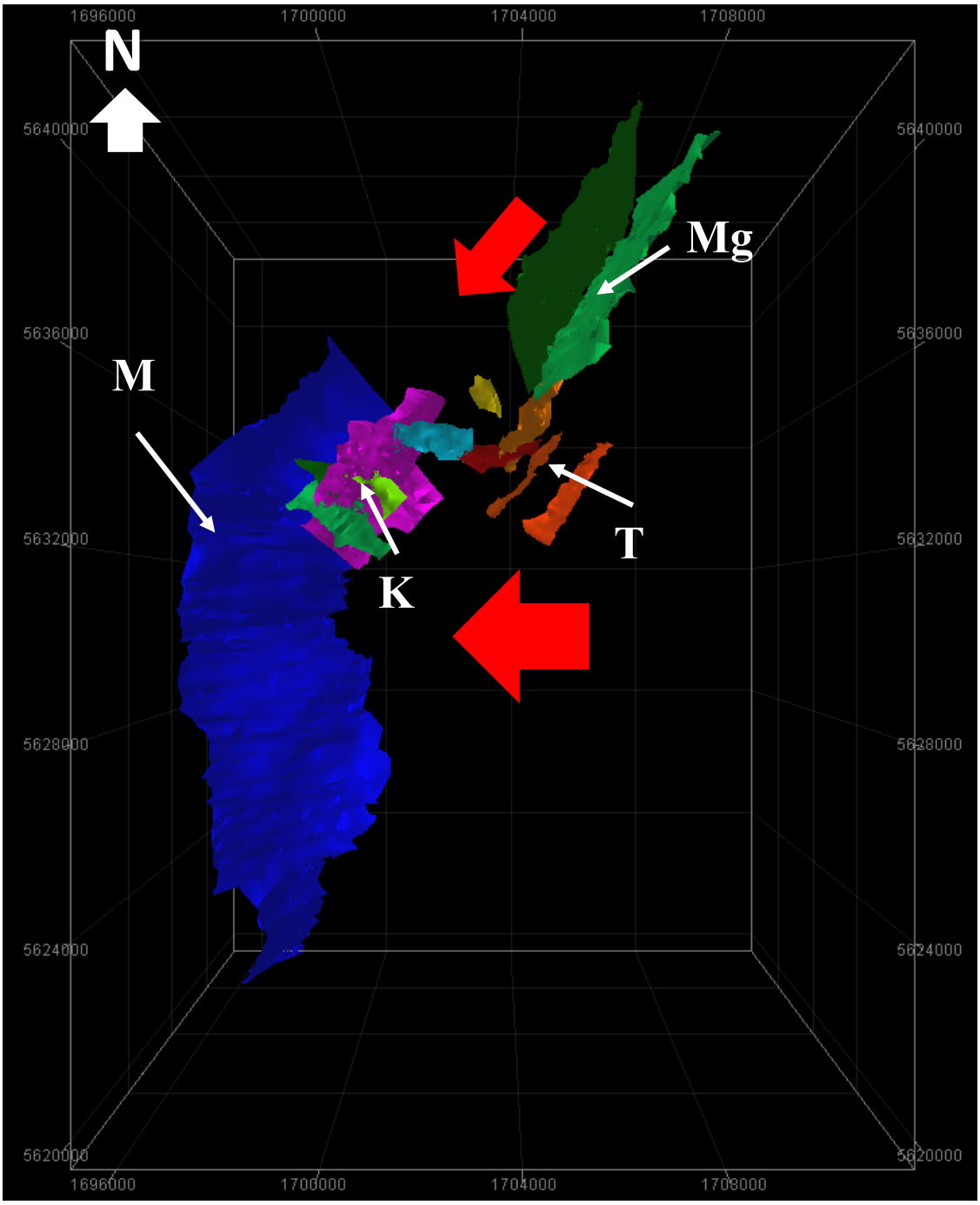

Figure 4.24. Birds eye view of all interpreted faults. M and Mg indicate the blue Manaia and dark green Mangahewa Faults respectively. K labels the pink/light green/blue Kapuni northwest system and T designates the brown/orange Tuikonga fault system. Red arrows indicate the dominate force vectors of the Manaia Fault.

Voggenreiter (1993) first identified this fault system and described it as having similar dimensions to what was observed in this study. The Tuikonga Fault system is spread over a 5-6 km wide area with all larger faults conforming to a northeastward trend, which parallels the Manaia Fault at similar latitude. The high angle strikes (≥ 65°) of the Tuikonga Faults' vary conversely and appear in cross section to be a re-activated graben. The maximum throw observed by Voggenreiter (1993) was 110 m, while in this study the peak fault throw was found to be between 80-110 m for each respective fault. This displacement however was found to not be equal along trend as the northeastern extent of the faults showed significantly less compressional movement (and in many cases normal movement), with displacements of -25 to 50 m. This variation in throw leads to an interpretation that the Tuikonga system is not a simple re-activated normal fault system, but a rotating block which is driven by the southwestern force imposed by the Manaia Fault (Figure 4.25).

4.5.3. Mangatoki. The Mangatoki Fault Zone is located within seismic section A (Figures 2.3, 3.2, and 4.24) and consists of a series of normal faults with conversing strikes. This fault zone is one of two significant fault interpretations conducted by this study. This was due to the two largest of the faults, which after interpretation provided information which aided in the debate of the detachment surface and additionally appeared to be part of the proposed gas chimney in conjunction with the Tuikonga Fault System. Like most faults in this survey, the Mangatoki Faults have a high angle 60 -70°, and contain a strike-slip component. This strike-slip displacement ranges from 170 -200 m for both of the interpreted faults (Figures 4.24 and 4.26). No wells were drilled through the traced faults of this study, and therefore no conclusions of their

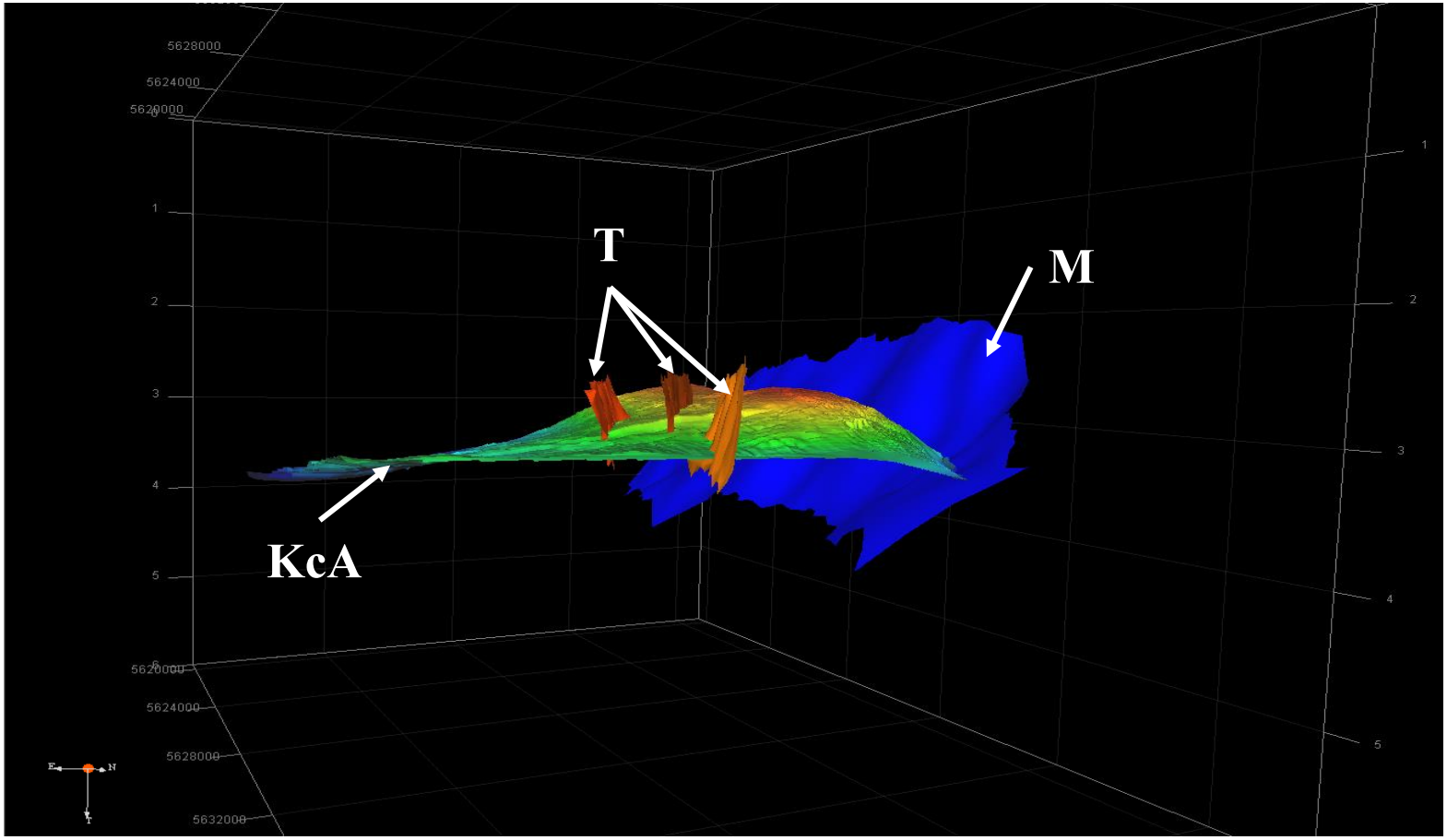

Figure 4.25. 3D visualization of the Tuikonga graben system. The horizon (KcA) base layer is the generated DEM of Kapuni Cycle A. The three brown/orange faults (T) are the interpreted Tuikonga faults which form a high angle graben structure. The large blue fault (M) is the Manaia Fault. Note how the Tuikonga faults extend below the capping horizon (KcA) and seem to tilt up toward the south of their respective trends.

significance as a trap or migration pathway are possible. However when observing the gas chimney structure, its chaotic seismic effects terminate at the base confluence of the faults just above (in some places within) the anticline.

4.5.4. Kapuni Northwest. Within the westernmost edge of the Manaia hanging wall, multiple fault systems exist as secondary fractures to the Manaia Fault. Voggenreiter (1993) identified three such systems, but the largest and densest was the Kapuni Northwest Fault Zone (Figures 4.24 and 4.26). This fault zone lies at the confluence of two major force vectors imposed by the western momentum of the Manaia Fault (Figure 4.24) and as a result has produced a series of east and northeastward dipping reverse faults which offset the immense transpressional deformation.

The majority of these faults appears to no longer be active, but do provide a distinct boundary and occasional trap for hydrocarbons that dwell below (Voggenreiter, 1993). The largest faults are identifiable to the same extent as the Tuikonga Fault Zone due to the same issues described in Section 4.5.2, but thanks to well data from studies such as Voggenreiter (1993) and Higgs et al. (2013), it has been determined that these faults extend farther than what was interpreted in this study and additionally contain numerous smaller faults which are not realized in seismic section.

4.6. GAS CHIMNEY

Studies conducted within the terrestrial bounds of the Taranaki Basin such as King & Thrasher (1996), Johnston et al. (2001), Bradley et al. (2012), and Higgs et al. (2013) have concluded that east of the Manaia Fault lies a plethora of gas and gas condensate fields which inherently contain abundant gas chimney structures due to the

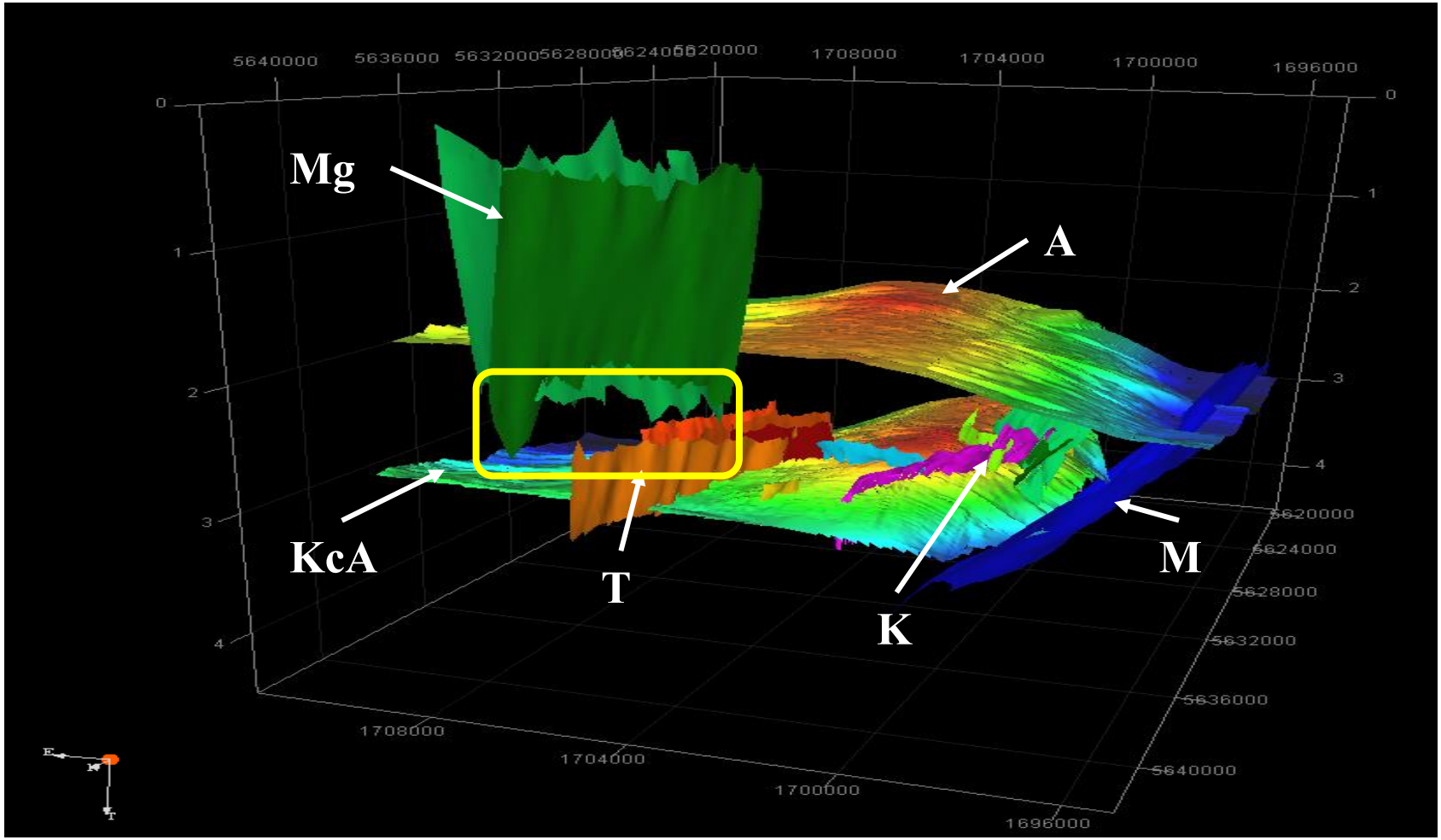

Figure 4.26. 3D visualization of all interpreted faults against anticline horizons. The upper horizon (A) is the extent of the anticline top, whereas the lower horizon (KcA) is Kapuni Cycle A. Note how none of the fault zones penetrate the top of the anticline. This is due to the inability to interpret structure in seismic section B. The yellow box indicates the relative area where the gas chimney is observed. Mg:Mangatoki Faults; T:Tuikonga faults; K:Kapuni NW faults; M:Manaia Fault.

abundance of normal faults. Within the 3D Kapuni survey gas chimney structures are present, although one in particular is the subject of this study and fluid flow model. As seen in Figure 4.27, it is located in the north eastern section of the survey directly under the Mangatoki Fault Zone.

Through use of fault identification, gain control, well logs, well reports, and seismic attributes, this chaotic and faulted structure is a fluid migration chimney which likely exhumes various amounts of gas and gas condensate which is solute to over-pressured water. As seen in Figure 4.27, the chimney starts at the uppermost extent of the Tuikonga fault, which is known to cut through both Kapuni Cycle A and B (Figure 4.28). As noted in Section 4.4.3, Kapuni Cycle B contained excessive amounts of water compared to the layers/formations both above and below this interval. High hydrocarbon saturation was observed in the lower Farewell Formation and above in the upper Kaimiro and Mangahewa formations (which already contain active gas/gas condensate saturated reservoirs). The Tuikonga faults (particularly the largest one displayed in Figures 4.27 and 4.28) act as a prime migration pathway for fluids both hydrocarbon and benign which are greatly over-pressured due to nearly 5 km of overburden and a high potentiometric surface. Once the gas and water has transferred into the upper strata of the Kapuni Group which contains significant sandy reservoirs, it is observed to be trapped below the bottom of the Mangatoki fault system. It is likely that any fluids which reach this point do continue migration upward into porous rock which lines these normal faults; however due to the nature of the mudstone and coal effects on the seismic section and lack of well data within the local area, it is not possible to conclude that these normal faults act as either trap or open pathway.

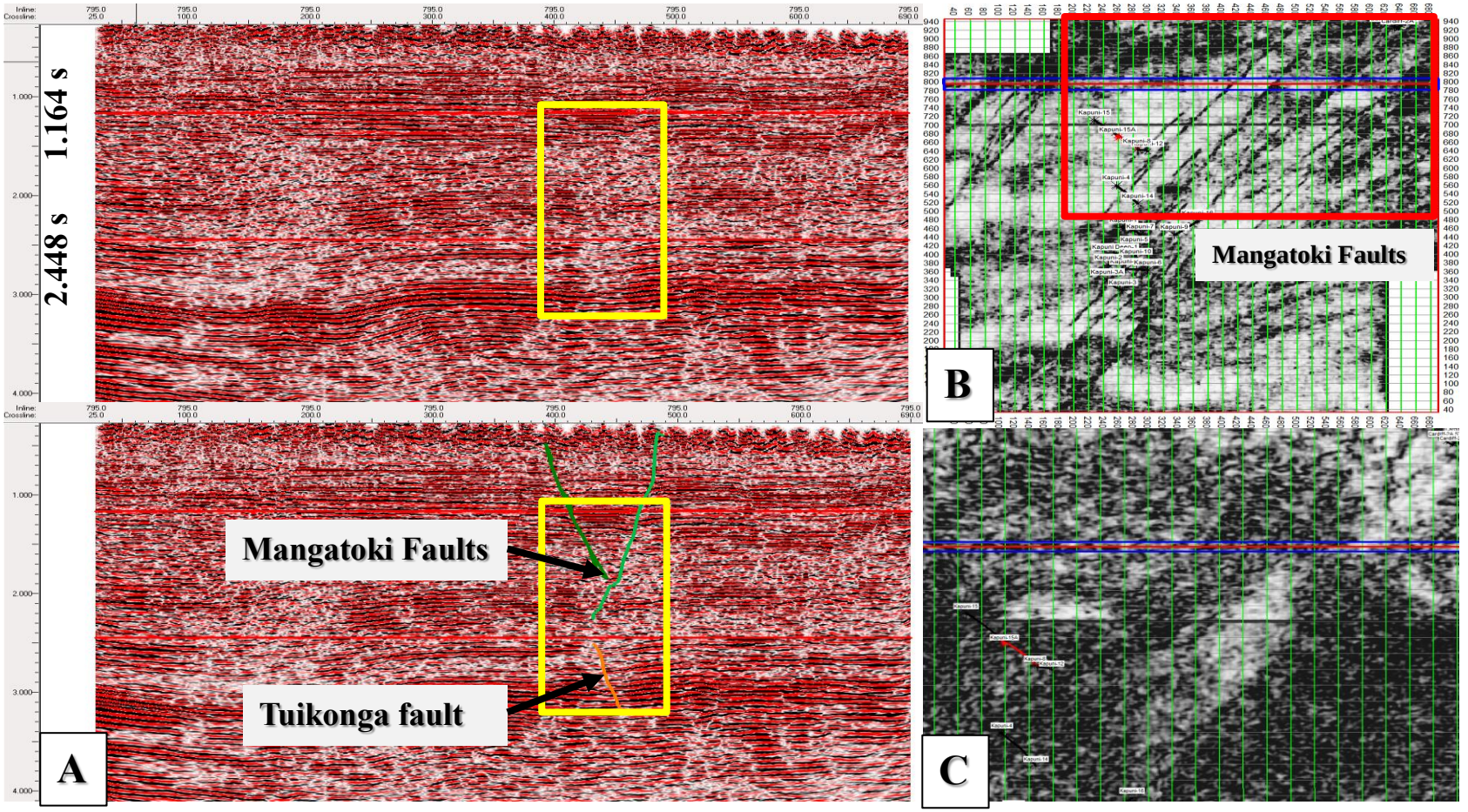

Figure 4.27. Gas chimney interpretation. Image A displays inline 795 with a before (above) and after (below) interpretation. The highlighted yellow box indicates the area containing the gas chimney structure. Note how the seismic reflections are depressed and chaotic. Image B displays the dip variance time slice 1.164s. The highlighted red box indicates the area displayed in image C below, which is the dip variance time slice 2.448 s. This time slice lies just below the realized Mangatoki faults.

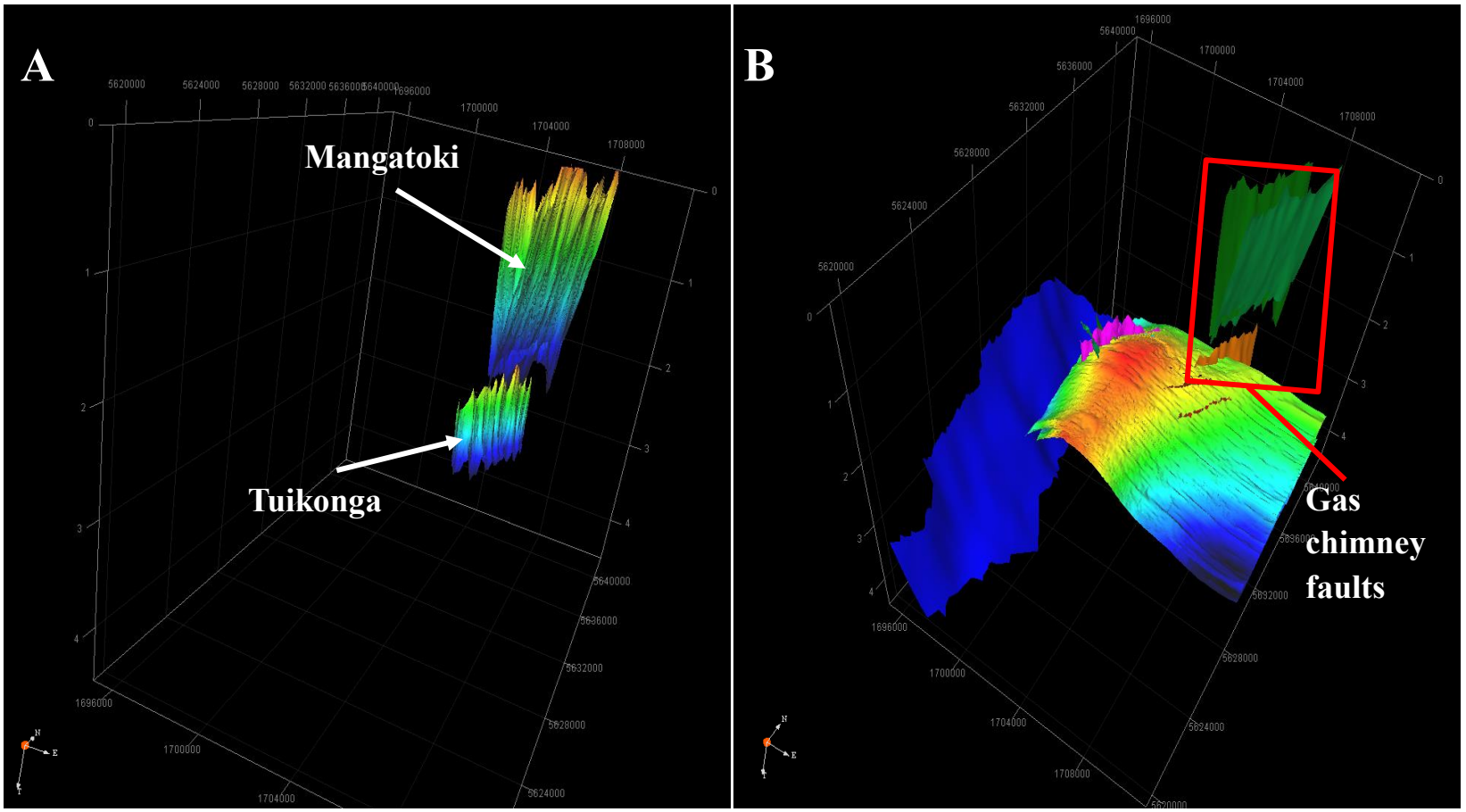

Figure 4.28. 3D DEM of gas chimney faults. Tuikonga 2 and Mangatoki 1 & 2. Image A displays the largest Tuikonga Fault and two Mangatoki faults which together allow for fluid migration and gas chimney structure in seismic section. Image B displays all digitized faults and their extent through both Kapuni Cycle A & B. Note how the Tuikonga Fault extends farther than the others within its respective fault zone.

5. FLUID FLOW MODEL

5.1. MODEL CONCEPT

The premise of this fluid flow model was to generate a base raster and vector layer within a GIS environment which can then be manipulated via importation of additional layers or empirical modifications which act as corrections to the 2D/3D fluid pathways and reservoirs, leading to a more accurate and geospatially realized model. Any data which is generated through this process can then be exported into any geospatial based visualization software for use by analyst of various professions.

A prime example of use would be as such; an oil or water extraction company does not use the expensive all-in-one platform software used by larger companies. They already have GIS software which is relatively inexpensive and used for keeping track of well placements, customers, land acquisition, etc. They can now use the standard and inexpensive software provided by subsurface exploration companies in conjunction with their previously owned software, giving the company an inexpensive alternative to data acquisition. Potentially, the company could also purchase a copy of a completed model which is readily compatible with their own software. With the ability to overlap the model onto various maps, it becomes easier to identify surface locations of interest for anyone interested in extraction of hydrocarbons or water from the subsurface system. For this study the model was generated to display the migration of fluids which make up the gas chimney structure discussed in Section 4.6.

5.2. FLUID FLOW MODEL GENERATION

The fluid flow model proposed in this study was generated using the RiverTools software, which is a GIS based hydrogeologic computation and analysis system. The software is used in the industry and USGS to identify, track, and calculate variables related to surface and subsurface hydrology. Like all GIS software, it relies on creation of multiple raster and vector layers to produce a fully functioning model which can be manipulated with addition or stacking of new data. This method of modeling fluid dynamics is of great benefit to researchers who seek the ability to add variables into any empirical and geospatially referenced 3D model as it allows for accessible and precise corrections. In addition, this method allows for results to be exported to other software and systems for use by others with access to GIS software such as ArcMap. The final output of this method is a 3D model which is projected as a series of 2D surfaces which contain multiple values corresponding to individual raster pixels or vector traces.

For this study only one variable, elevation/topography, was considered for the model as temporal demands did not allow for generation of additional masks and layers. This variable was chosen due to its use as a solid base-line raster layer which is solely controlled by geophysical and/or universal constants, namely potentiometric pressure, and impermeability of constraining surfaces. The model proposed by this study assumes ideal conditions for both these constants. Corrections for these conditions are possible using this method, however they were not generated because of the amount of time required for calculation and processing.

The main input for creation of the model was the gridded DEM XYZ files that were exported from Kingdom. All horizons and faults were imported as irregular XYZ ".dat" files and treated as individual surfaces. The RiverTools import process

determined that the data points were float values, which was not altered. The resolution of each final input raster was 40 m and all extreme outlier values (including border values seen in Figure 5.1) or negative values were converted to a threshold of zero. The depth values of the rasters was kept in measurements of time (ms). This was done in an effort to not require manipulation of the depth data, as the depth values would be considered negative by the software and require inversion to properly calculate how fluids would naturally migrate upward. After the data was imported, a shaded relief image was generated to act as a visualization. Figure 5.1 displays the relief raster of Kapuni cycle A, and is being used as a base layer. Note that there appears to be strait lined artifacts at the northern edge of the raster. This artifact was the result of the gridding algorithm used in Kingdom.

5.2.1. Extraction and Masking. Once each raster file was imported, extraction of values and generation of various mask polygons commenced. The first step in the process was extraction of the D8 flow grid, which generates additional variables and files which are later used in delineation of watersheds and creation of the Horton-Strahler river network. The main task of the D8 flow grid is to produce a gridded contour that contains a “flow code” which indicates the down slope direction that fluids will follow from a corresponding pixel. The process additionally results in the creation of RiverTools Mask (RTM) files which includes indicated zones of depression where fluids would conceivably stagnate, and “basin” masks which indicate low points and the corresponding area which drains toward them.

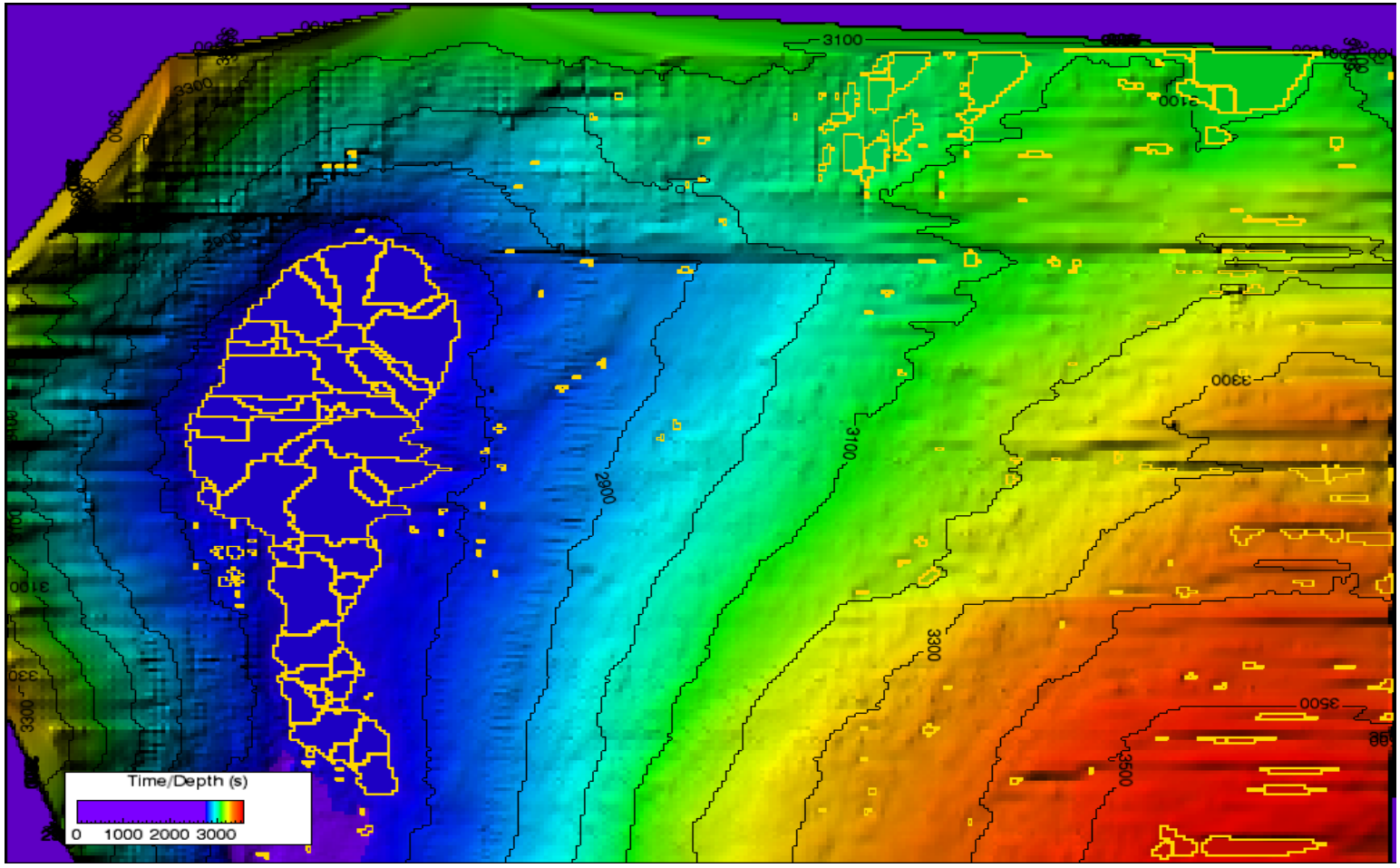

Figure 5.1. Layered display of RiverTools imported DEM. The base layer raster is 40 m resolution of the Kapuni cycle A horizon and is color coded to depth in measurements of two way travel time in milliseconds. The gold polygons indicate the pits mask, which indicates areas that the algorithms consider flat or plateaued, where fluids will attempt to migrate toward. Note the edge effects in the northern portion of the raster.

For all horizons and faults processed, two parameters were used to constrain the flow grid; pit resolution method and flat resolution method. Pit resolution indicates whether or not the fluids drain toward points within the given raster file or drain toward multiple points, including those outside the raster. For this option, closed basins were chosen, as the anticline lobes would be the true or ideal drain point for any migrating hydrocarbons within the system. Interactive linking was chosen for the flat resolution method as it provided more accurate results for floating point data.

After generation of the D8 flow grid comes the extraction of the Treefile, which is a vector-formatted file which contains the extracted flow vectors from the flow grid. These vectors are then used to calculate and consolidate the Horton-Strahler order stream network.

5.2.2. Horton-Strahler Order Network. The Horton-Strahler order is a method of delineating and measuring water networks through definition of stream size by use of an increasingly complex mathematical tree which is based in the hierarchy of tributaries. This method of organization uses the previously generated Treefile vectors and assigns Strahler numbers based on confluence of surrounding vectors.

For example, if the vector or node does not have any others coming together to form said vector (i.e. “children”), it is considered a “leaf” and given an order number of 1. If the node has one child with order *i* and all other children have numbers less than *i*, then the order number stays *i*. If the node contains two or more children with *ith* order and no children with orders higher than *i*, then the node’s order is $i + 1$. Figure 5.2 provides a visual for this concept.

In this study, the networks for each raster were set to prune all Strahler orders less than 1. In order to prevent visual misconceptions, the pits mask was used to cover up large area which would have generated numerous parallel, strait line vectors generated during flow grid processing. These areas suggest extremely flat surfaces where fluids such as water and oil would pool into a proverbial lake. Therefore the peak area of the anticline was masked out, indicating that any network connecting into the mask would “deposit” any in-transit fluids at that point, halting the migration.

5.2.3. Horizons. Each horizon which was considered a capping strata was chosen to be used in the fluid flow model. As the outputs were in 2D, multiple iterations of the process was conducted to obtain the optimal result which could be used in conjunction with the fault models. Figure 5.1 displays the base raster file of Kapuni cycle A (top of the Farewell or horizon H2 in Figure 4.14).

5.2.4. Faults. The exported fault DEMs were projected in the same 40 m resolution as the horizons, however due to the total area of coverage the visual quality is poor. This did not however effect the overall results obtained through modeling. Due to the 2D nature of the horizon and faults it was essential to connect the two by using GIS traced polygons. The fault intersection with the horizon would be noted and traced with a line polygon, then overlaid upon the horizon. This provides a precise and accurate indication of where the fault is located in relation to the horizon raster surface, and aids in interpretation of what fluid paths would be interrupted by the fault.

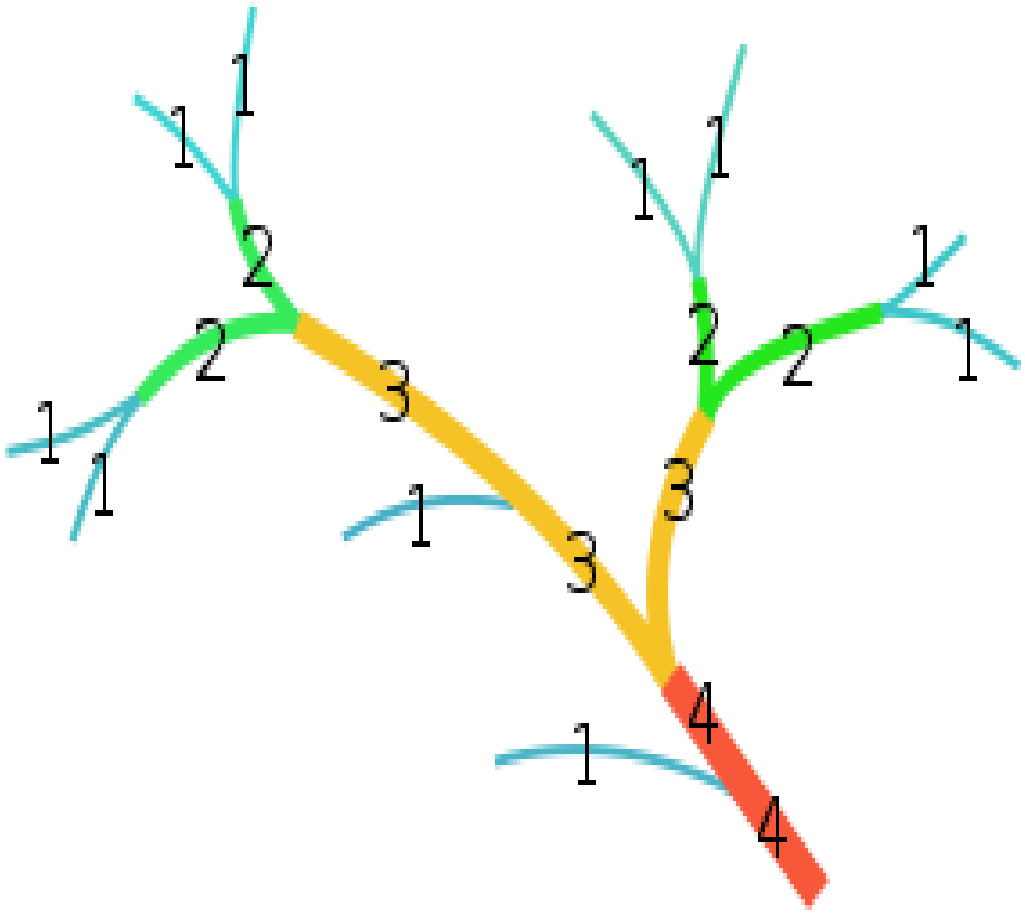

Figure 5.2. Strahler stream order hierarchy. This method is generally used for surface water tracking, however its applicability as a base layer for subsurface hydrology is substantial.

5.3. SOURCES

For any petroleum system to exist, source rocks with viable migration pathways must be present. The basic concept is that a source rock exists at the furthest depths of a system, to which hydrocarbons migrate via porous media or faults that connect the source rock to a reservoir and is then capped by a non-permeable layer. Within the Kapuni anticline this basic system prevails in a cyclic manor. The Kapuni Group consists of multiple transgressive and regressive cycles that ultimately produce a layered cap/reservoir/source rock system. Within each of the three major formations (Mangahewa, Kaimiro, and Farewell) coals are present in spatial variation both vertically and horizontally. These coals are the main source material for the gas and gas condensate which is continually extracted from this petroleum play (Johnston et al., 1991; Bradley et al., 2012; Higgs et al., 2013). Some shales additionally provide source material for hydrocarbon generation, but are greatly overlooked due to the amounts of gas produced by the coals.

For calculation of the fluid flow model, it is assumed that the coal beds are laterally continuous throughout the survey. Since this flow model is considered a base line to a complex empirically layered model, it additionally assumes that the source points where fluids originate are evenly distributed across the whole of the DEM, just as it would be during a rain storm on earth's surface or as gas seeping through pores in a sandstone. This assumption can be altered within the RiverTools software, as "source-points" for the flow grid can be manually changed to generate a more accurate flow pattern.

5.4. FLUID NETWORK

The final results of the fluid flow model processing are displayed in Figures 5.3-5.7. Due to the nature of calculations, requisite processing and graphic power, and 2D importation method the complete model is a series of bi-layered 2D displays.

As seen in Figures 4.27 and 4.28, the base and source of the gas chimney lies at the bottom of the Tuikonga Fault (Figure 5.4). The first collection of fluids which migrate through this fault must first pass through the lowest capping layer of rock which the Tuikonga system offsets, the Kapuni Cycle A horizon. The complete model visualizes the fluid migration in the Horton-Strahler stream order network (Figure 5.3). The color spectrum for the order numbers starts with the dark blue lines or "streams" indicate Strahler order 1, green indicates order 3, and red indicates order 7, the highest order in the study. The complete legend of color to order is displayed in Figure 5.7. The completed stream network appears to indicate a general trend for upwards migrating fluids to flow northwards before they are trapped in the peak of the anticline at P (Figure 5.3). This is only true however for any hydrocarbons or water which are to the east of the anticline crest.

In order to incorporate the faults, an enhanced intersection line of the Tuikonga Fault was transposed onto the Kapuni Cycle A DEM. If assuming a high porosity and low pressure within the fault, any flow paths which intersect this line should theoretically be drawn upwards into the fault where they will migrate upwards through Kapuni Cycle B and into the Mangahewa Formation (within seismic section B where the gas chimney was interpreted). Once the fluids enter the Tuikonga fault, they would likely migrate in a fashion similar to what is observed in Figure 5.4. Any water or gas which was trapped below Kapuni Cycle B would also follow this same pathway through

the Tuikonga Fault, assuming the pressure was greater within the formation than in the fault. After any fluids have reached the upper strata of the anticline, they should disperse into the surrounding rock, creating the gas chimney effects observed in seismic section. Due to the lack of well information in the area surrounding the gas chimney and Mangatoki faults, an accurate conclusion cannot be made about the potential of further migration through the graben structure of the Mangatoki system. However, since the interpreted faults are normal and likely penetrate the Kapuni Group sediments, it is plausible to assume some amount of gas or water does escape through the fault system. Figures 5.5 and 5.6 visualize the pathways any fluids would likely take if they are not under trapped or barrier conditions similar to the Kapuni Northwest Zone.

After completion of the model, a series of minimums, maximums, averages, and other statistical data was automatically generated by RiverTools which allowed for several conclusions about how much material could potentially be moving under the subsurface. Within Kapuni Cycle A two major streams or "sub-basins" where identified to be at Strahler order 7, which collected fluids over a 29 km^2 area (Table 5.1). Using an estimated average depth of 50 m (equaling one porous layer below the cap), it was calculated that a total drainage volume of over 1,450 km^3 per stream is possible. This calculation however includes the matrix of the rock. With an average porosity of 10% (Shell BP, 1984) for the sandstones within the upper strata of the Farewell, there is a maximum fluid volume of 145 km^3 within the interpreted Kapuni Cycle A. The Kapuni Cycle B contains similar statistics but with a higher porosity of around 24% (Higgs et al., 2013), the max fluid volume is 348 km^3.

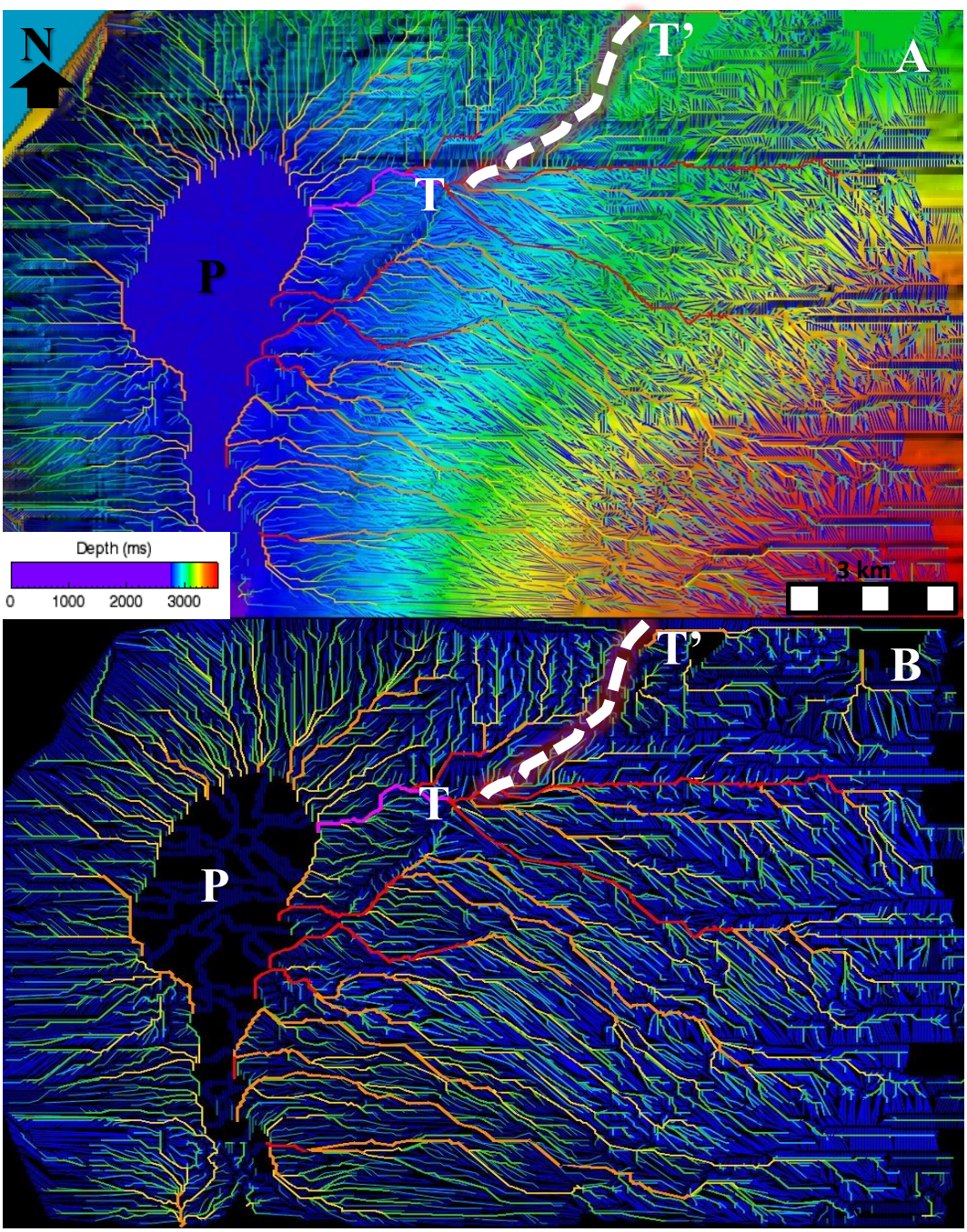

Figure 5.3. Fluid flow model of Kapuni Cycle B. (A) displays the Strahler order streams atop the topographic raster of Kapuni Cycle B whilst image (B) displays only the stream network. The dashed line T is the extent of the main Tuikonga Fault which is the base of the gas chimney. All streams which are cut by this fault theoretically will allow all fluids to the east of the fault to migrate upward through the fault. The large blank area at P indicates the peak of the anticline where all the fluids should collect into a single reservoir area.

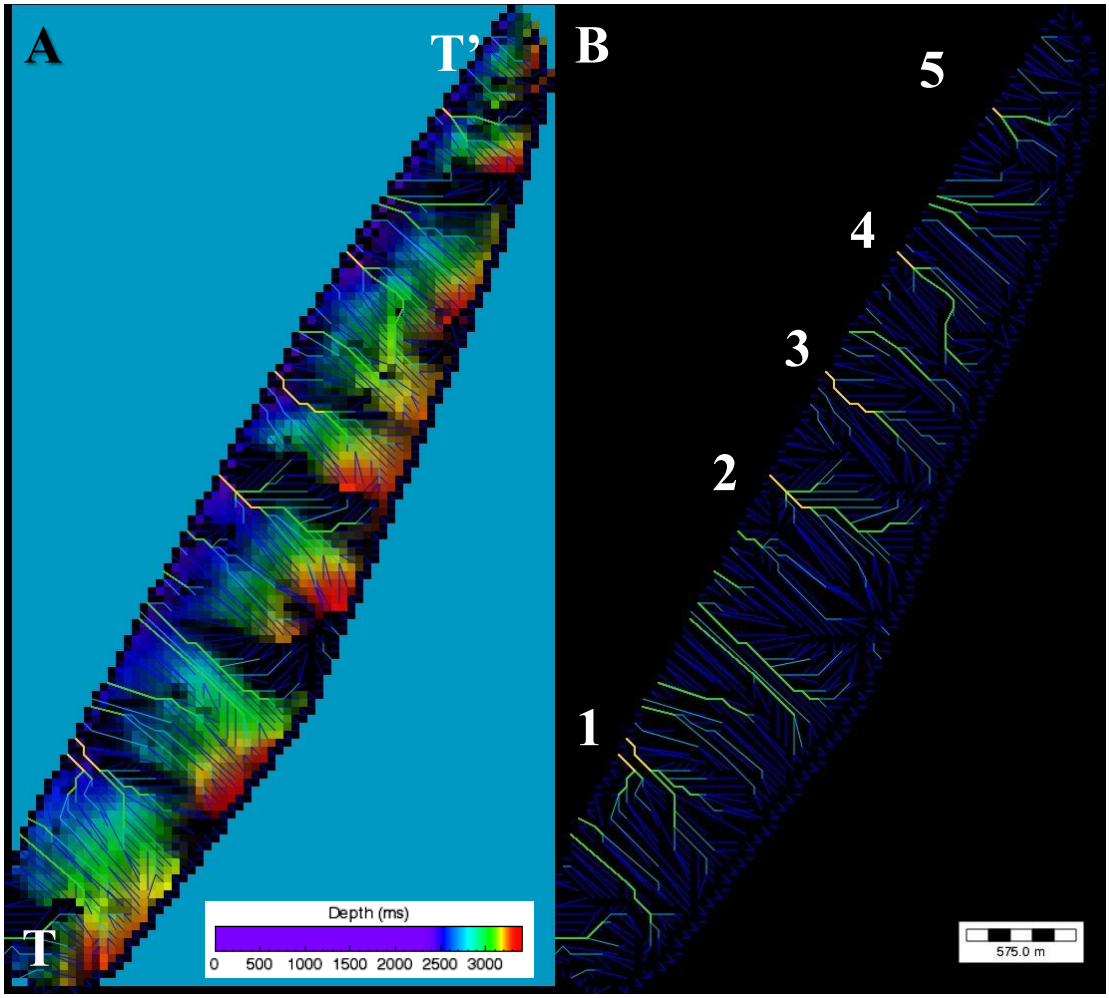

Figure 5.4. Flow model of Tuikonga Fault. Due to the importation methods of RiverTools, the deepest segments of the DEM are red within the color bar. (A) displays the complete two layer model while (B) shows the stream network alone. Note how there appear to be five significant sub-basins which direct the theoretical flow.

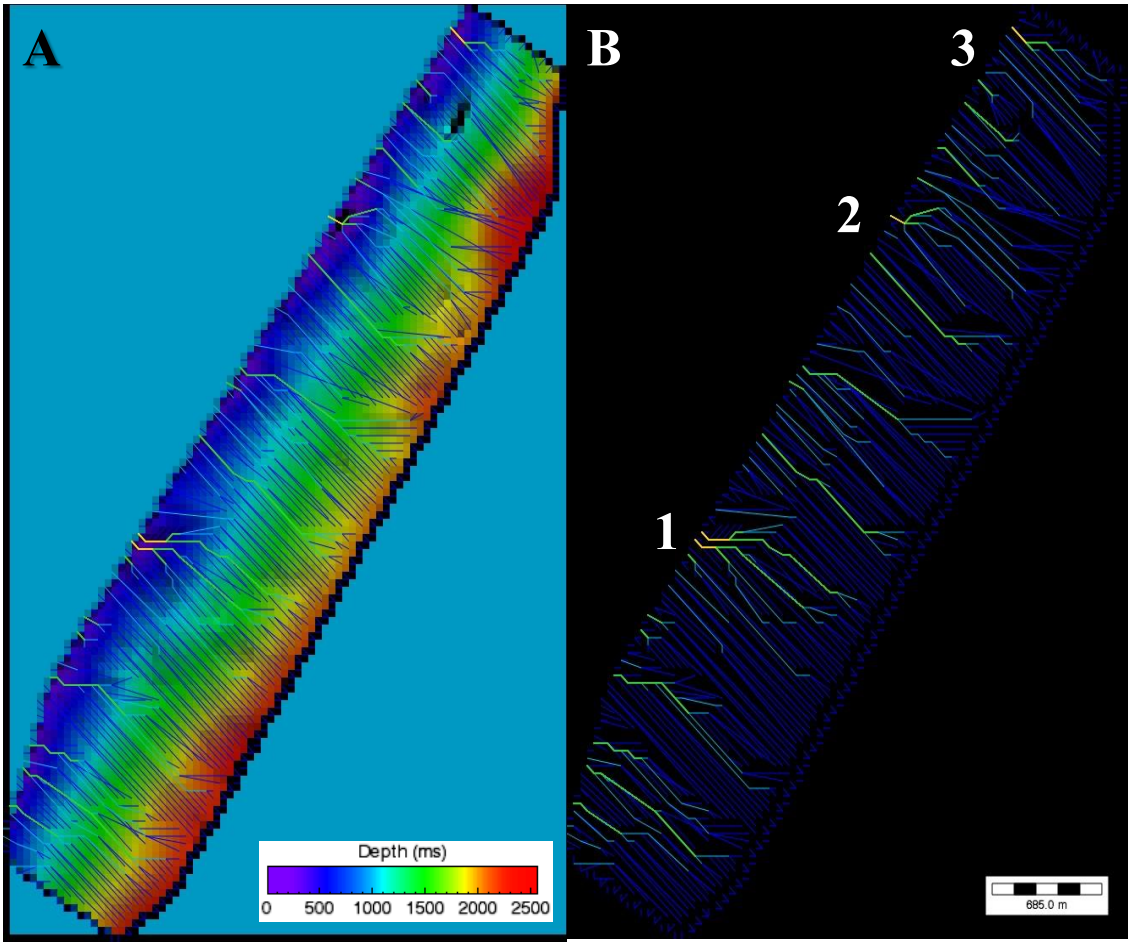

Figure 5.5. Flow model of Mangatoki fault #1. This model displays the southeastward dipping Mangatoki fault. Note in image (B) how there are three significant drainage sub-basins within the topography of this fault.

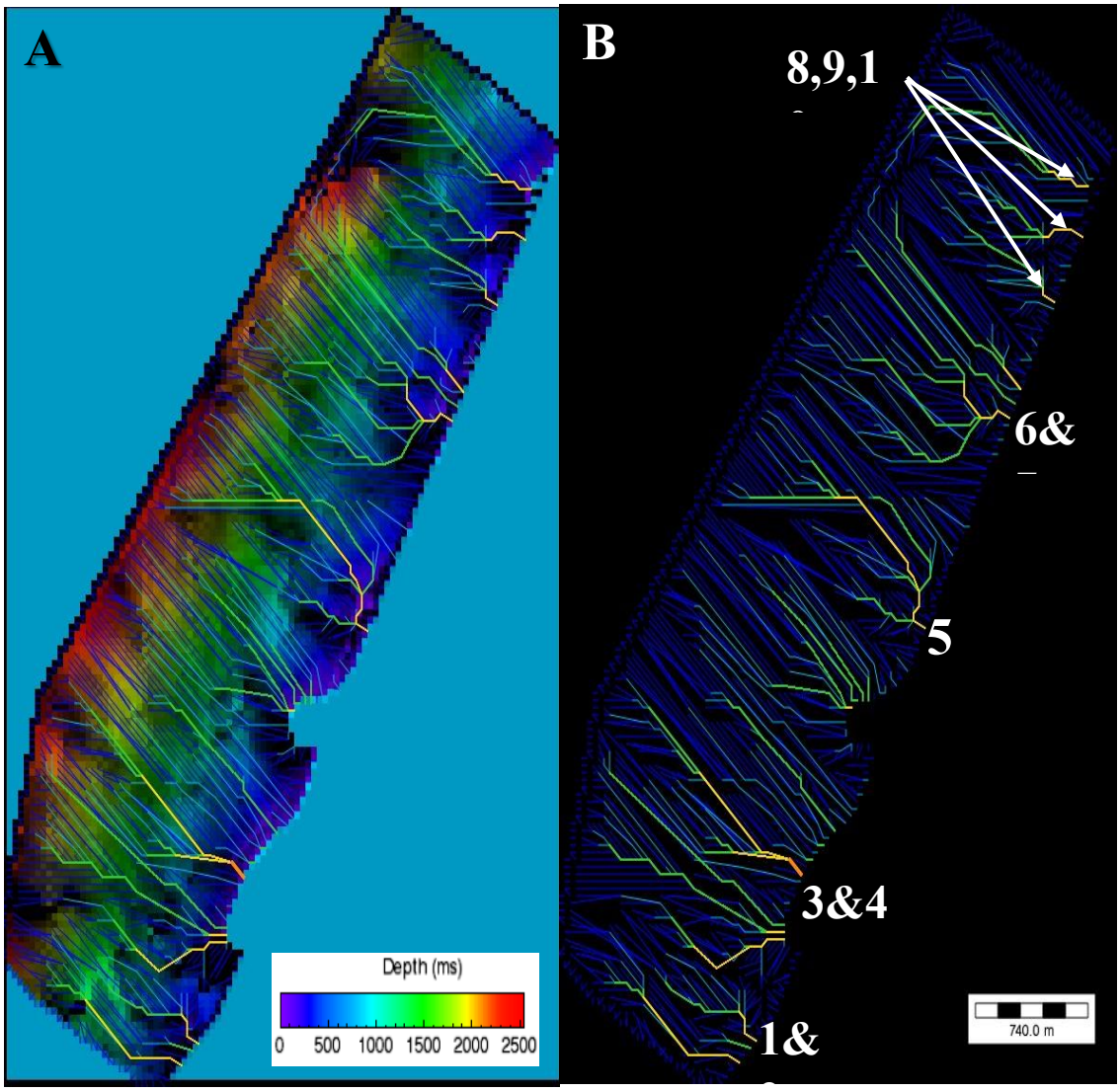

Figure 5.6. Flow model of Mangatoki fault #2. This stream flow network (B) was constructed over the northwest dipping fault in the Mangatoki system. This fault was found to be larger than its southeast dipping counterpart and as such contains more significant sub-basins.

Table 5.1. Summary of basin statistics for Kapuni Cycle A.

DATA SUMMARY FOR Kapuni_sourceCycleA River BASIN

Prune type = HS Order, Threshold = 1.00000
Order 1 prune type = None, Threshold = 0.500000

BASIN AREA (km)^2

Order	Number	Minimum	Maximum	Range	StdDev.	Average
1	42565	1.68317E-003	7.06933E-002	6.90102E-002	4.47317E-003	5.21774E-003
2	7772	5.04952E-003	2.32278E-001	2.27228E-001	2.15845E-002	2.46358E-002
3	1607	1.34654E-002	1.09238E+000	1.07891E+000	1.12828E-001	1.30558E-001
4	375	1.11089E-001	2.98090E+000	2.86981E+000	4.03960E-001	5.94344E-001
5	97	5.04952E-001	7.07944E+000	6.57449E+000	1.45137E+000	2.08752E+000
6	26	1.72694E+000	1.49466E+001	1.32197E+001	3.42909E+000	6.70875E+000
7	2	2.85904E+001	2.97063E+001	1.11592E+000	5.57960E-001	2.91483E+001

TOTAL CHANNEL LENGTH (km)

Order	Number	Minimum	Maximum	Range	StdDev.	Average
1	42565	4.10265E-002	1.81804E+000	1.77701E+000	1.29235E-001	1.50504E-001
2	7772	1.23079E-001	6.19650E+000	6.07342E+000	6.22054E-001	7.14978E-001
3	1607	3.96187E-001	2.78667E+001	2.74706E+001	3.12687E+000	3.75405E+000
4	375	3.16658E+000	8.74085E+001	8.42419E+001	1.16279E+001	1.70859E+001
5	97	1.45681E+001	2.05831E+002	1.91263E+002	4.20402E+001	6.02210E+001
6	26	4.85848E+001	4.37915E+002	3.89330E+002	1.01013E+002	1.94676E+002
7	2	8.27269E+002	8.59551E+002	3.22817E+001	1.61408E+001	8.43410E+002

LONGEST CHANNEL LENGTH (km)

Order	Number	Minimum	Maximum	Range	StdDev.	Average
1	42565	4.10265E-002	1.81804E+000	1.77701E+000	1.29235E-001	1.50504E-001
2	7772	8.20530E-002	2.37541E+000	2.29336E+000	2.76560E-001	4.02913E-001
3	1607	1.98093E-001	3.70817E+000	3.51008E+000	5.32535E-001	9.81097E-001
4	375	6.08358E-001	7.96718E+000	7.35882E+000	9.93331E-001	2.28258E+000
5	97	1.39078E+000	1.13488E+001	9.95807E+000	2.20918E+000	4.28982E+000
6	26	2.69126E+000	1.24032E+001	9.71191E+000	2.64832E+000	7.41427E+000
7	2	1.09245E+001	1.19871E+001	1.06257E+000	5.31283E-001	1.14558E+001

DRAINAGE DENSITY (1/km)

Order	Number	Minimum	Maximum	Range	StdDev.	Average
1	42565	2.43745E+001	3.44707E+001	1.00963E+001	4.28270E+000	2.89767E+001
2	7772	2.43745E+001	3.40669E+001	9.69240E+000	2.34927E+000	2.90636E+001
3	1607	2.44811E+001	3.37663E+001	9.28522E+000	1.88895E+000	2.90489E+001
4	375	2.51093E+001	3.26288E+001	7.51952E+000	1.63550E+000	2.89244E+001
5	97	2.66249E+001	3.21510E+001	5.52610E+000	1.26427E+000	2.88327E+001
6	26	2.73344E+001	3.05953E+001	3.26092E+000	8.48672E-001	2.88762E+001
7	2	2.89350E+001	2.89352E+001	2.59399E-004	1.29700E-004	2.89351E+001

The data were automatically calculated in the RiverTools software upon completion of the processing. It displays the empirical values which are necessary for calculating potential variables of area and volume. Note that within the Kapuni Cycle A horizon, there are only two order 7 streams.

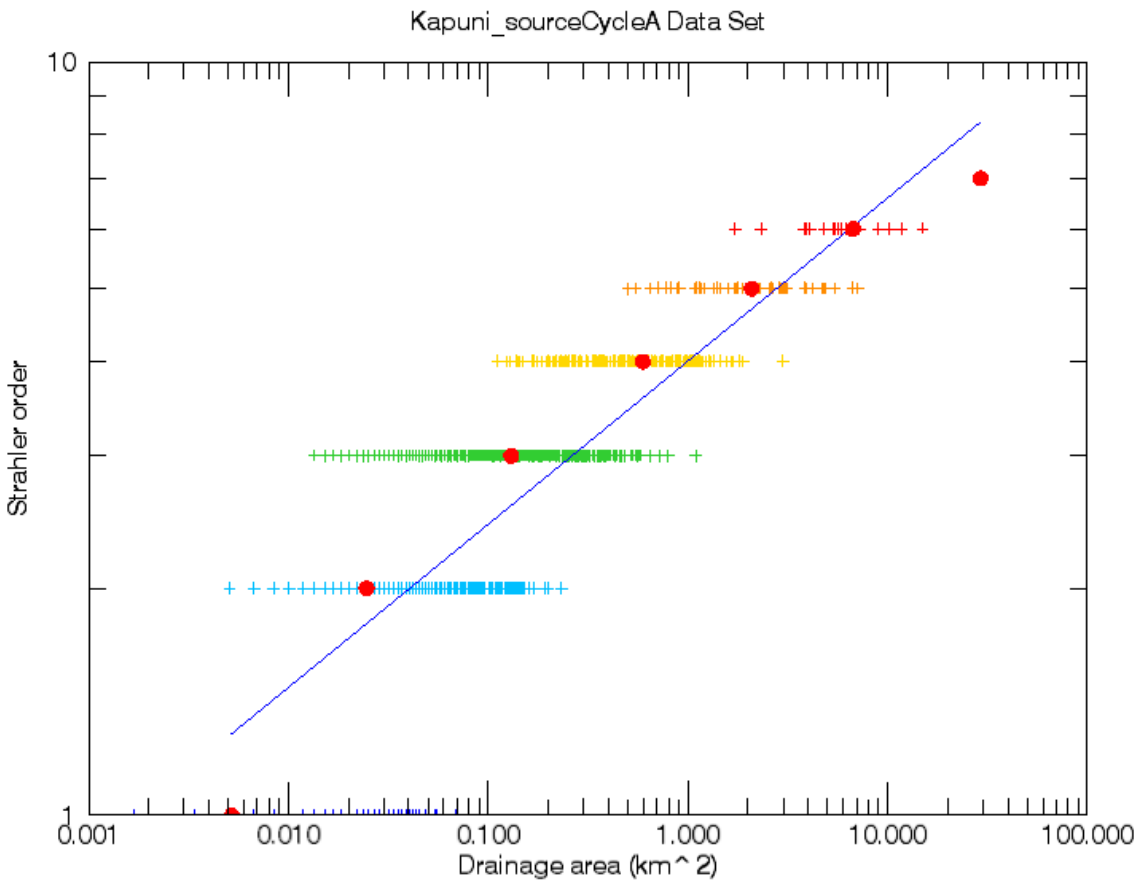

Figure 5.7. Strahler order vs. total drainage area. This graph displays every stream which was calculated over the Kapuni Cycle A horizon in Figure 5.1. Each stream is color coded the same as Figures 5.3-5.6 with one red dot per Strahler order indicating the average of that order. The excessive abundance of order 3 (green) testifies to the large area of coverage and relatively low number of sub-basins within the DEM.

6. CONCLUSION

Through extensive research into regional and basin tectonics, mapping of over twelve faults, four horizons, and construction of a fluid flow model, a better understanding and visualization of the petroleum system in the Kapuni Field, New Zealand has been achieved. Fault systems which were briefly identified and discussed by Voggenreiter (1993) have now been analyzed in greater depth, to which both reconfirmation of previous observations as well as new observations have been made. Evidence for connections between the Mangatoki and Tuikonga fault systems has been recognized due to the observation of fluid migration from the depths of the Kapuni Group sediments. The transport network of both hydrocarbons and water have consequently been modeled in support of these findings.

6.1. FAULT MOVEMENT

During in depth tracing and analysis of the Tuikonga and Mangatoki fault systems, it was found that two force vectors are a play within the northern most extent of the Kapuni anticline. The main force is the result of the reverse nature of the Manaia Fault as well as the greater compressional far field stresses imposed by the Taranaki Fault to the east. The second force lies parallel to the curvature found at the tapered north of the Manaia Fault. This vector additionally applies a compressional westward force but adds a southwestern direction component. The effects of this are observed in the Tuikonga Faults which retain a reverse nature toward their respective southern extent but become normal trending north, signifying a reverse-slip rotation. It is due to this under pressured normal fault extent, that the identified gas chimney structure is possible.

6.2. GAS CHIMNEY

As discussed in many studies of the Taranaki Basin, such as Bradley et al. (2012) and Higgs et al. (2013), it is widely known that east of the Manaia Fault lies a cornucopia of gas fields and gas chimney structures. The existence of these structures and many gas fields is due in part to the extensive coal beds found within the thick Kapuni Group sediments which formed between the Late Cretaceous and Late Eocene.

The gas chimney identified in this study is likely the result of transpressional forces which were imposed on the deep Kapuni Group sediments by residual reactivation of the Tuikonga fault system, and potential low pressure exposition produced by the Mangatoki Faults which lay both above and parallel to the Tuikonga Faults. Though the chimney structure is visible in seismic section and variance attributes, the likelihood of it containing only gas is minimal. This is due to the data collected from well reports which penetrated the same source material, some 10 km away. Due to the Tuikonga system's extent through both the Kaimiro and Farewell formations, large amounts of water are suspected to be mixed with the gas and gas condensate which make up the visible gas chimney.

6.3. FLUID FLOW MODEL

All fluids which migrate through the system to generate the chimney structures must do so in a certain manor, to which the fluid flow model identifies and highlights sufficiently. The feasible combination of gas and water which makes up the gas chimney described in this study likely does not extend past the anticline due series of capping mudstones and fault line barriers. It is highly probable that the bulk of the migrated fluids from Kapuni Cycles A and B are dispersed throughout the upper sandstones of the

Kapuni Anticline. This hypothesis could be either confirmed or disproved with further investigation, by use of new well logs which penetrate the surrounding area.

In addition to the interpretations, processing conclusions are also observed from this study. The resulting fluid flow model accurately represents an empirical baseline to which corrections and additional variables can be introduced, whilst incorporating geospatial awareness and formatting. Any outputs, both raster and vector layers, are exportable in ".dat" or shapefile format, to which any GIS based software should be able to incorporate with ease.

BIBLIOGRAPHY

[1] Adams, R.D., Ware, D.E. 1977, Sub-crustal earthquakes beneath New Zealand: locations determined with a laterally inhomogeneous velocity model. New Zealand journal of geology and geophysics, 20, 59-83.

[2] Allis, R.G., Zhan, X., Evans, C., Kroopnick, P. 1997, Groundwater flow beneath Mt Taranaki, New Zealand, and implications for oil and gas migration. New Zealand J. of Geology and Geophysics, 40, 137-149.

[3] Beck, A.C. (1964), Sheet 14 Marlborough Sounds. Geological map of New Zealand 1:250,000, New Zealand Geological Survey, Department of Scientific and Industrial Research, Wellington.

[4] Beggs, J.M., Cook, R.A. (1993), Prospects for significant undiscovered gas resources in Taranaki Basin, Institute of Geological & Nuclear Sciences, Ltd client report 1993/56.

[5] Cartwright, J., D. James, and A. Bolton (2003), The genesis of polygonal fault systems: A review, in *Subsurface Sediment Mobilization*, vol. 216, edited by P. Van Rensbergen, R. R. Hillis, A. J. Maltman, and C. K. Morley, pp. 223-242, Geol. Soc. London Spec. Pub., London, U.K.

[6] Chopra, S., Marfurt, K.J (2007), Seismic Attributes for Prospect Identification and Reservoir Characterization: Geophysical Developments No.11, Tulsa, Oklahoma, Society of Exploration Geophysicists.

[7] Fohrmann, M., King, P.R., Strogen, D.P., Reid, E., Zhu, H., Roncaglia, L., Hill, M.G., Bland, K.J., Scott, G.P.L. (2012), Seismic reflection character, mapping and tectono-stratigraphic history of the Kupe area (4D Taranaki Project), south-eastern Taranaki Basin, GNS Science, Institute of Geological and Nuclear Sciences.

[8] Higgs, K.E, Funnell, R.H., Reyes, A.G. (2013), Changes in reservoir heterogeneity and quality as a response to high partial pressures of CO_2 in a gas reservoir, New Zealand, Marine and Petroleum Geology, 48, 293-322.

[9] Horton, R.E. (1945), Erosional development of streams and their drainage basins: hydro-physical approach to quantitative morphology, Geological Society of America Bulletin, 56(3): 275–370.

[10] Hulston, J.R., Hilton, D.R., Kaplan, I.R. (2001), Helium and carbon isotope systematics of natural gases from Taranaki Basin, New Zealand, Applied Geochemistry, 16, 419-436.

[11] Johnston, J.H., Collier, R.J., Maidment, A.I. (1991), Coals as source rocks for hydrocarbon generation in the Taranaki Basin, New Zealand: a geochemical biomarker study, J. of Southeast Asian Earth Sciences, Vol 5, 283-289.

[12] Johnstone, M. R. 1996, Geology of the d'Urville area, Institute of Geological and Nuclear Sciences geological map 16, Lower Hutt.

[13] King, P.R., Thraher, G.P (1992), Post-Eocene development of the Taranaki Basin, New Zealand: Convergent overprint of a passive margin, Geology and Geophysics of continental margins, Tulsa, AAPG memoir 53.

[14] King, P. R., and Thrasher, G. P. (1996), Cretaceous-Cenozoic Geology and Petroleum Systems of the Taranaki Basin, New Zealand., Lower Hutt, New Zealand, Institute of Geological and Nuclear Sciences, Institute of Geological and Nuclear Sciences Monograph 13.

[15] Muir, R.J., Bradshaw, J.D., Weaver, S.D., Laird, M.G. (2000), The influence of basement structure on the evolution of the Taranaki Basin, New Zealand, J. of the Geological Society, London, Vol 157, 1179-1185.

[16] New Zealand Petroleum & Minerals (2014), New Zealand Petroleum Basins, Wellington, New Zealand. Ministry of Business, Innovation and Employment.

[17] Peckham, S.D. 2009, Geomorphometry in RiverTools. Developments in Soil Science, 33.

[18] Pilaar, W.F.H, Wakefield, L. L. 1978, Structural and stratigraphic evolution of the Taranaki Basin, offshore North Island, New Zealand. Australian Petroleum Exploration Association journal, 18, 93-101.

[19] Shell BP, 1984; Kapuni Field, Geological summary Kapuni Deep-1, Taranaki, New Zealand. PML38839. Minishtry of Economic Development New Zealand, Unpublished Petroleum Report 1024.

[20] Shell Todd Oil Services Limited. c2015. New Zealand; [accessed 2016 March 21]. http://www.stos.co.nz/index.asp.

[21] Smale, D., Mauk, J.L., Palmer, J., Soong, R., Peter B. 1999, Variations in sandstone diagenesis with depth, time, and space, onshore Taranaki wells, New Zealand. New Zealand J. of Geology and Geophysics, 42, 137-154.

[22] Strahler, A.N. (1952), Hypsometric (area-altitude) analysis of erosional topology, Geological Society of America Bulletin, 63(11): 1117-1142.

[23] Strahler, A.N. (1957), Qantitative analysis of watershed geomorphology, Transactions of the American Geophysical Union, 38(6): 913-920.

[24] Strogen, D.P, Bland, K.J, Nicol, A., King, P.R. (2014), Paleogeography of the Taranaki Basin region during the latest Eocene-Early Miocene and implications for the 'total drowning' of Zealandia, NZ Journal of Geology and Geophysics.

[25] Todd Energy. c2012. Zyber; New Zealand; [accessed 2016 March 21]. http://www.toddenergy.co.nz/.

[26] Walter R. Voggenreiter (1993), Structure and evolution of the Kapuni Anticline, Taranaki Basin, New Zealand: Evidence from the Kapuni 3D seismic survey, *NZ Journal of Geology and Geophysics,* 36:1, 77-94.

VITA

Jarret Taylor Baldwin was born in St. Charles, Missouri. In May of 2010 he graduated from Orchard Farm High school with Magna cum-lade honors. Directly after graduation he enrolled in Missouri University of Science and Technology's Geology and Geophysics program, to which he graduated May of 2014 with his Bachelors of Science. During his undergraduate degree Jarret incorporated himself into several clubs and societies, including the Society of Exploration Geophysics (SEG) and the C.L. Dake Society. In 2013 he was elected as Vice President of SEG. After completion of his Bachelors, Jarret moved on to begin his Master of Science in Geophysics at Missouri University of Science and Technology, to which he graduated in July of 2016. During his busy schedule as a graduate student he was able to uphold his new position as President of SEG which saw the creation of new monthly workshops with sought to aid students in their studies and presentation skills, as well as generate common ground and friendship between undergraduate and graduate students. Additionally Jarret succeeded in completing a semester of teaching assistantship as well as a semester of research assistantship.